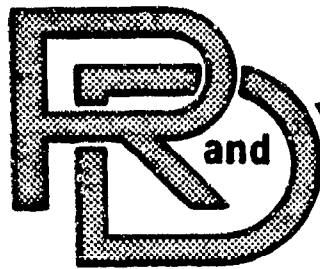


LEVEL II

AD A 056543

12



TARADCOM
LABORATORY
TECHNICAL REPORT

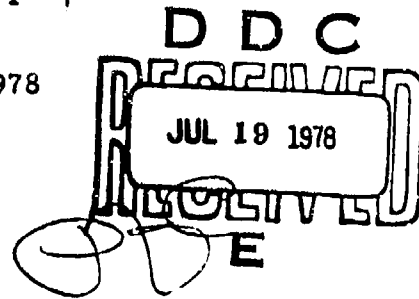
NO. 12347

SHAKE TESTING OF VEHICLES
THROUGH RECORDED
SIMULATION CONTROL SCHEME



VOLUME I

January 1978



by FOSTER-MILLER ASSOCIATES, INC.

A. B. Boghani
K. M. Captain
R. B. Fish

Approved for public release;
distribution unlimited.

U.S. ARMY TANK-AUTOMOTIVE
RESEARCH AND DEVELOPMENT COMMAND
Warren, Michigan 48090

78 07 13 018

AD No. _____
DDC FILE COPY

The findings in this report are not to be construed as an official Department of the Army position, unless so designated by other authorized documents.

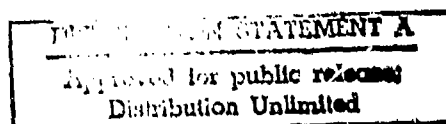
The citation of commercial products in this report does not constitute an official indorsement or approval of such products.

TECHNICAL REPORT NO. 12347

SHAKE TESTING OF VEHICLES
THROUGH RECORDED
SIMULATION CONTROL SCHEME
VOLUME I

A. B. Boghani
K.M. Captain
R. B. Fish

January 1978



Prepared under Contract No. DAAK30-76-C-0004

by

Foster-Miller Associates, Inc.
135 Second Avenue
Waltham, Mass. 02154

for

U. S. Army Tank-Automotive Research and Development Command
Warren, Michigan

78 07 13 018

TABLE OF CONTENTS

	<u>Page</u>
PRINCIPAL NOMENCLATURE	vii
SUMMARY	ix
1. INTRODUCTION AND OBJECTIVE	1
1.1 Implementation Options	3
1.2 Recorded Simulation Control Scheme	8
1.3 Objective and Organization of the Report	10
2. SIMULATION	12
2.1 Model Development	12
2.2 Simulation Results	22
2.3 Simulation Verification	31
3. CONTROL SYSTEM	37
3.1 System Requirements	37
3.2 System Description	39
3.3 System Operation	42
3.4 System Verification	45
4. VERIFICATION	49
5. CONCLUSIONS	55
6. RECOMMENDATIONS	57
APPENDIX A - THE TIRE MODELS	59
APPENDIX B - THE VEHICLE MODEL	74
APPENDIX C - VEHICLE RESPONSE PLOTS	90
REFERENCES	101
DISTRIBUTION LIST	102

ACCESSION for		
TYPE	Write Section	<input checked="" type="checkbox"/>
DDO	Ref Section	<input type="checkbox"/>
UNANNOUNCED		<input type="checkbox"/>
JUSTIFICATION		
.....		
BY		
DISTRIBUTION/AVAILABILITY CODES		
Reg.	AVAIL.	and/or SPECIAL
A		

LIST OF ILLUSTRATIONS

<u>Figure No.</u>		<u>Page</u>
1	TARADCOM Shake Test Facility	2
2	Recorded Simulation Control Scheme	9
3	Formulation of Vehicle Model	17
4	Force Characteristics of Suspension Spring and Damping Models	19
5	Force Characteristics of Frame Stop and Tire Models	20
6	Power Spectral Density of Terrain Profile	23
7	Time History of Tire Force	27
8	Actual and Filtered Ground Profile	29
9	Simulated Vehicle Response - PSD of Vertical Tire Force	33
10	Simulated Vehicle Response - PSD of Fore-and-Aft Tire Force	34
11	Comparison of Simulated Response with Test Data	35
12	Schematic Diagram of the Control System Hardware	40
13	Control System Operation Diagram	43
14	Control Program Flowchart	44
15	Comparison of the Simulation and the Controller Outputs for the Front Axle Displacement	46
16	Comparison of the Simulation and the Controller Outputs for the Middle Axle Displacement	47
17	Comparison of the Simulation and the Controller Outputs for the Rear Axle Displacement	48
18	Simulated Response - Front Wheel Displacement	52
19	Simulated Response - Middle Wheel Displacement	53
20	Simulated Response - Rear Wheel Displacement	54
A-1	Schematic Diagram of Point Contact Tire Model	60
A-2	Schematic Diagram of Rigid Tread Band Tire Model	63
A-3	Determination of Admissible Terrain Contact Point	65
A-4	Schematic Diagram of Fixed Footprint Tire Model	66
A-5	Schematic Diagram of Adaptive Footprint Tire Model	70

LIST OF ILLUSTRATIONS (Cont)

<u>Figure No.</u>		<u>Page</u>
B-1	Freebody Diagram of Hull	76
B-2	Freebody Diagram of Bogie	78
B-3	Hull-Bogie Linkage	79
B-4	Freebody Diagram of Front Suspension	82
B-5	Freebody Diagram of Middle and Rear Suspensions	85
B-6	Freebody Diagram of Unsprung Mass	88
C-1	Simulated Response - CG Acceleration	91
C-2	Simulated Response - Front Wheel Acceleration	92
C-3	Simulated Response - Rear Wheel Acceleration	93
C-4	Simulated Response - Front Wheel Displacement	94
C-5	Simulated Response - Middle Wheel Displacement	95
C-6	Simulated Response - Rear Wheel Displacement	96
C-7	Simulated Response - Vertical Tire Force (Front)	97
C-8	Simulated Response - Vertical Tire Force (Rear)	98
C-9	Simulated Response - Fore-and-Aft Tire Force (Front)	99
C-10	Simulated Response - Fore-and-Aft Tire Force (Rear)	100

LIST OF TABLES

<u>Table No.</u>		<u>Page</u>
1	Shaker Control Implementation Options	4
2	Summary of Basic Tire Models	14
3	Statistical Terrain Characteristics	22
4	Summary of Vehicle Parameter	24
5	Model Parameters for 11.00-18 Tire	26
6	Comparison of Simulation Results with Approximate Analysis	32
7	Control System Hardware	41

PRINCIPAL NOMENCLATURE

A	-	effective contact area
A	-	terrain roughness parameter
a	-	half of bogie length
B	-	effective footprint width
B_{2v}	-	shock absorber damping constant
b	-	lumped damping of point contact model
b'	-	distributed damping of fixed footprint model
b''	-	distributed damping of adaptive footprint model
F_{h2}	-	horizontal force from each of the front tires
F_{h3}	-	horizontal force from each pair of the middle tires
F_{h4}	-	horizontal force from each pair of the rear tires
F_{v2}	-	vertical force from each of the front tires
F_{v3}	-	vertical force from each pair of the front tires
F_{v4}	-	vertical force from each pair of the rear tires
CG	-	hull CG elevation from hull plane
I_b	-	pitch inertia of bogie
I_h	-	pitch inertia of hull
K_2	-	front suspension stiffness
K_3	-	middle and rear suspension stiffness
k	-	lumped stiffness of point contact model
k'	-	distributed stiffness of fixed footprint model
k''	-	distributed stiffness of adaptive footprint model
L	-	equilibrium tire footprint length
L_2	-	distance from front suspension to hull CG

PRINCIPAL NOMENCLATURE (Cont)

- L_3 - distance from bogie connection to hull CG
- M_b - bogie mass
- M_h - hull mass
- M_2 - front unsprung mass, each
- M_3 - middle unsprung mass, each
- M_4 - rear unsprung mass, each
- p_i - tire inflation pressure
- r - tire radius
- S_b - distance from bogie connection to bogie CG
- S_{bs} - distance from bogie connection to rear stop
- S_{fs} - distance from bogie connection to front stop
- S_{34} - distance from bogie connection to hull plane
- V - speed of the vehicle
- Y_b - heave displacement of bogie CG
- Y_o - heave displacement of hull CG
- Y_{w2} - front axle heave displacement
- Y_{w3} - middle axle heave displacement
- Y_{w4} - rear axle heave displacement
- $\delta(\theta)$ - tire deflection at location θ
- θ - angle measured from vertical through wheel center
- Θ - pitch angle of hull, forward pitch positive
- λ - wavelength of irregularity component
- ϕ - pitch angle of bogie
- Ω - reduced frequency ($\Omega = 2\pi/\lambda$)

SUMMARY

Recorded simulation control scheme described in this report is an inexpensive and accurate way of providing realistic inputs to a vehicle being shake tested in the laboratory. The scheme involves simulating operation of the vehicle on the specified terrain to generate axle displacement records, storing the records in memory of a control system, and using them to provide continuous input signals to the vehicle shaker during testing.

The computer simulation developed for the scheme incorporates a terrain-tire-vehicle model, with the option to include any one of the four previously developed tire models: point contact model, rigid tread band model, fixed footprint model and adaptive footprint model. Developed separately from the tire models, the vehicle model considers a three axle military type truck which is of interest to TARADCOM. Comparing the analytical results generated by the terrain-tire-vehicle model with those obtained in field tests demonstrates the ability of the model to simulate the vehicle motion, particularly when employing the adaptive footprint or the fixed footprint models.

The control system developed for storing the axle displacement records and playing them back incorporates a minicomputer, disc memory, input-output peripherals and digital to analog converters. In an illustrative example described in the report, the control system is shown to supply real-time synchronized shaker input signals from the digital displacement records.

Finally the complete scheme is verified by comparing the power spectral densities of the inputs to the vehicle generated by the scheme with those obtained from field tests on the vehicle.

This report includes details of the model and the control system. However, instructions for using the control system and the computer program are available in a separate document, titled "Recorded Simulation Control Scheme - User's Manual".

1. INTRODUCTION AND OBJECTIVE

In recent years, laboratory vibration testing of vehicles has been widely used to help assess structural reliability. In military service, where the dynamic loads are generally higher, vibration testing has become a particularly important tool for reliability evaluation, and has been used with advantage to assess structural integrity, identify critical stress points, and evaluate design improvements (reference 1)*. The basic test procedure consists of shaking a loaded vehicle with hydraulic actuators programmed to simulate typical field service conditions, and monitoring the stresses and deflections of the vehicle structure. A sketch of the shaker facility at the U. S. Army Tank-Automotive Research and Development Command (TARADCOM) is shown in Figure 1. The vehicle is excited by vibratory inputs applied to the wheel spindles, as shown. Because the wheels and tires are removed from the vehicle prior to shake testing, the input excitation signals must correspond, not to the terrain profile, but to the wheel spindle motions occurring in field use. There are two basic ways in which these signals are obtained: either directly from field measurements, or from dynamic computer simulations of an analytical terrain-tire-vehicle model. Where reliable field data are readily available, the former method can be followed. In many situations, however, such data are not easily obtained, and the latter method must then be used.

There are many ways of implementing the computer controlled shake testing (i. e. , using dynamic simulation of the terrain-tire-vehicle model). One such way, recorded simulation control scheme, is described in the report. In this scheme, the vehicle simulation program is used to create axle displacement records which are stored in digital form on a convenient medium, such as a magnetic disc**. The records are then converted to analog input signals and fed repeatedly to the vehicle shaker.

*References are listed at the end of the report.

**An intermediate medium, such as paper tape may also be used, before storing the data on magnetic disc.

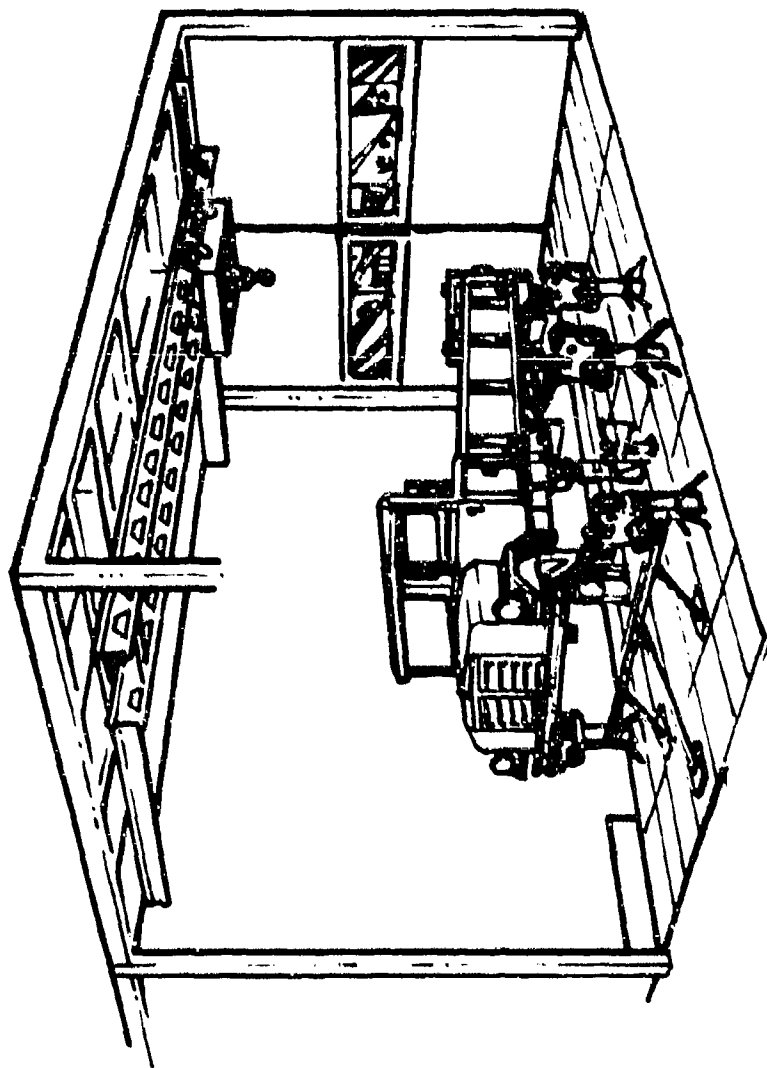


Figure 1. TARADCOM Shake Test Facility

Before describing the recorded simulation control scheme, the implementation options available to operate a vehicle shaker are discussed and advantages of the selected scheme are identified.

1.1 Implementation Options

There are several ways in which the shake tests can be carried out, depending on the method by which the shaker input signals are obtained. In identifying and evaluating the various implementation options for the shaker input, the dominant consideration is that of field correlation, i. e., the reliability with which the input excitation can simulate field service. Other considerations however are also important, and these include such factors as hardware and software requirements, system complexity, operating convenience, etc. The principal implementation schemes that have been or can be used to control the shaker are summarized in Table 1. They are described in further detail and evaluated below.

1.1.1 Direct Field Data Control

This is perhaps the simplest of all the schemes, and does not require any analytical modelling or computation. It consists of recording unsprung mass acceleration (with hub-mounted accelerometers) during vehicle field trials, and then passing the signals through a double integrator to obtain the unsprung mass motion (axle motion) signals that control the shaker. The principal advantage of this method is that it is based on field data with a minimum of signal processing, so that good correlation with field use can be expected. However, there are two drawbacks to this method which are common to all schemes using vehicle field trial data. These are:

- a. Field trial data are needed for every vehicle type, speed, load, and tire pressure of interest.
- b. New concepts and components, including the effects of design parameter changes cannot be conveniently investigated.

Table 1. Shaker Control Implementation Options

Case	No.	Brief	Schematic	System Characteristics		Implementation Options		Remarks	
				Advantages	Disadvantages	Form	Software		Hardware
Field Data Control System	1	Direct Field Data Control		<p>Distances and velocities requirements modest. In all, low processing required. Block connections with field control.</p>	<p>Field trial data needed for every vehicle, land and sea. Vehicle weight, load and speed of interest. Phase relationships of all inputs to be determined. If number of these inputs is large, it may be necessary to use a high speed digital processing facility.</p>	<p>Multi-track data storage. Double integration. One per vehicle.</p>	None	Limited to one vehicle, land trial data is available.	
	2	<p>1. Synthetic Field Data Control</p> <p>2. Analog</p>		<p>Software requirements modest. Analytical models for vehicle and test set available. On-line computer facility not required.</p>	<p>Field trial data needed for every vehicle, land and sea. Phase relationships of all inputs to be determined. If number of these inputs is large, it may be necessary to use a high speed digital processing facility.</p>	<p>Land-based computer. Storage (tapes).</p>	<p>Simulated program package.</p>	<p>Servers of digital computer for processing.</p>	Limited to one vehicle, land trial data is available.
	3	Digital		<p>Software requirements modest. Analytical models for vehicle and test set available. On-line computer facility not required.</p>	<p>Field trial data needed for every vehicle, land and sea. Phase relationships of all inputs to be determined. If number of these inputs is large, it may be necessary to use a high speed digital processing facility.</p>	<p>Digital computer.</p>	<p>Simulated program package. Storage (tapes).</p>	<p>Majority of digital computer for processing.</p>	Limited to one vehicle, land trial data is available.
	4	<p>1. Direct Field Data Control</p> <p>2. Analog</p>		<p>Software requirements modest. Analytical models for vehicle and test set available. On-line computer facility not required.</p>	<p>Field trial data needed for every vehicle, land and sea. Phase relationships of all inputs to be determined. If number of these inputs is large, it may be necessary to use a high speed digital processing facility.</p>	<p>Digital computer.</p>	<p>Simulated program package. Storage (tapes).</p>	<p>Majority of digital computer for processing.</p>	Limited to one vehicle, land trial data is available.
Direct Field Data Control System	5	<p>1. Direct Field Data Control</p> <p>2. Analog</p>		<p>Software requirements modest. Analytical models for vehicle and test set available. On-line computer facility not required.</p>	<p>Field trial data needed for every vehicle, land and sea. Phase relationships of all inputs to be determined. If number of these inputs is large, it may be necessary to use a high speed digital processing facility.</p>	<p>Digital computer.</p>	<p>Simulated program package. Storage (tapes).</p>	<p>Majority of digital computer for processing.</p>	Limited to one vehicle, land trial data is available.
	6	<p>1. Direct Field Data Control</p> <p>2. Analog</p>		<p>Software requirements modest. Analytical models for vehicle and test set available. On-line computer facility not required.</p>	<p>Field trial data needed for every vehicle, land and sea. Phase relationships of all inputs to be determined. If number of these inputs is large, it may be necessary to use a high speed digital processing facility.</p>	<p>Digital computer.</p>	<p>Simulated program package. Storage (tapes).</p>	<p>Majority of digital computer for processing.</p>	Limited to one vehicle, land trial data is available.
	7	<p>1. Direct Field Data Control</p> <p>2. Analog</p>		<p>Software requirements modest. Analytical models for vehicle and test set available. On-line computer facility not required.</p>	<p>Field trial data needed for every vehicle, land and sea. Phase relationships of all inputs to be determined. If number of these inputs is large, it may be necessary to use a high speed digital processing facility.</p>	<p>Digital computer.</p>	<p>Simulated program package. Storage (tapes).</p>	<p>Majority of digital computer for processing.</p>	Limited to one vehicle, land trial data is available.
	8	<p>1. Direct Field Data Control</p> <p>2. Analog</p>		<p>Software requirements modest. Analytical models for vehicle and test set available. On-line computer facility not required.</p>	<p>Field trial data needed for every vehicle, land and sea. Phase relationships of all inputs to be determined. If number of these inputs is large, it may be necessary to use a high speed digital processing facility.</p>	<p>Digital computer.</p>	<p>Simulated program package. Storage (tapes).</p>	<p>Majority of digital computer for processing.</p>	Limited to one vehicle, land trial data is available.

Nevertheless, this method will be attractive for use in situations where test data is already available, or where limited testing of one or two vehicle types is contemplated.

1.1.2 Synthesized Field Data Control

This method consists of synthesizing the shaker signals such that they correspond statistically to the field trial data. It is best used when the statistical characteristics (PSD, etc.) of the field data are already available; otherwise an initial step of statistical processing is required. The basic method of signal synthesis consists of feeding white noise into a filter, so that the output signal, though random, has the PSD specified by the filter*. The filter characteristics are chosen so that the output PSDs correspond to those obtained from field trials. For statistically independent signals, this procedure is relatively straightforward. However, for statistically dependent signals, additional complications are introduced since a greater number of filters is required. This is one of the main difficulties with this method for multi-signal outputs: either a relatively large number of filters must be used, or statistical dependence (phase relationships) between the various signal pairs cannot be assured. For signal pairs whose statistical dependence is known to be weak, the number of filters can be minimized by considering the signals independent. However, since the degree of dependence changes with the terrain and vehicle characteristics, speed, load, etc., significant statistical analysis will be needed to identify, for each case, the outputs that can be synthesized independently.

This implementation scheme is attractive for use primarily in situations where a relatively small number of signals are to be synthesized, and where the statistical characteristics of field trial data are readily available. It will also be attractive for use when existing hardware is suitable.

*The filters and noise sources can be implemented with analog hardware or with digital software, as shown in Table 1.

1.1.3 Direct Simulation Control

Direct simulation control is a method by which the shaker is controlled on-line by a computer. It is a scheme which requires no field trial data, but generates the input signals by means of a dynamic terrain-tire-vehicle simulation. Its implementation is relatively straightforward, but it requires use of an adequate on-line computer during the entire shake test. For facilities with access to an on-line computer, this method can be very attractive because of its simplicity of implementation. Where an adequate on-line simulation cannot be conveniently performed, a modified scheme which retains the basic simplicity can be used. This scheme is described in the following section.

1.1.4 Recorded Simulation Control

This scheme carries out the dynamic vehicle simulation similar to the direct simulation control method, but records the output on a multi-track data recorder (e. g. , on magnetic disc or tape). The records are then played back to control the shaker. Thus by using the recorder, the need for an on-line computer is eliminated. This improvement makes the recorded simulation control scheme particularly attractive for use. The hardware requirements are modest, since the simulation can now be carried out at a batch processing facility. Field trial data is not needed, and a variety of vehicles, types and loading conditions can be conveniently tested using the simulation. No statistical processing is required, and since the shaker signals are generated directly by a time simulation, the statistical dependence of all the signals will be preserved. For the above reasons, the recorded simulation control scheme is well suited to situations where different types of vehicles (including, specifically, multi-axle vehicles) have to be tested under various load and speed conditions, and where parameter and component changes, including new concepts, are to be evaluated.

1.1.5 Synthesized Simulation Control

The synthesized simulation control scheme is essentially similar to the synthesized field data control scheme discussed earlier; the only difference being that the statistical characteristics of wheel motion are obtained by analytical simulation rather than from field trial data. The basic method of synthesizing the signal by feeding white noise through a filter remains unchanged. As before, hardware requirements (filters and noise generators, or a hybrid computer) can be high if statistical dependence is to be preserved. Although field trial data will not be needed, significant computation and/or statistical processing may be required, particularly for multi-axle vehicles. However, the convenience of "hardwired" electronics or computer software* make it particularly attractive for long-term testing of a limited number of vehicle types and load conditions.

1.1.6 System Evaluation

Evaluation and selection of recommended schemes for implementation of TARADCOM must be based on a number of factors, including:

- The ability of the scheme to test vehicles for which field trial data is unavailable.
- The capability of evaluating a variety of vehicle types, including specifically multi-axle trucks with a relatively large number of wheel excitation inputs.
- The hardware and software requirements, and their availability at TARADCOM.
- System complexity, ease of implementation, operating convenience, etc.

*The noise generator and filter system where modeling changes are made by adjusting dial settings or by changing coefficients in a digital computer program.

The first two schemes (direct field data control and synthesized field data control) described in the previous section require vehicle field trial data, and their use at TARADCOM depends upon the availability of such data. The third scheme (direct simulation control), while straightforward in implementation, requires an adequate on-line analog (or hybrid) computer - the availability of which will be a primary factor in deciding upon the use of this scheme at TARADCOM. The fifth scheme, the synthesized simulation control scheme, has the advantage of not requiring test data, and will be convenient to use for long-term testing of a limited number of vehicle types. However, for multi-axle trucks, implementation will be relatively complex and hardware requirements may be high.

The recorded simulation control scheme has many desirable characteristics which make it well suited for implementation. It does not require field trial data. Computation requirements are minimized, since no statistical data processing is necessary. The dynamic vehicle simulation can be carried out off-line at a batch-processing facility, eliminating the need for an on-line computer. The system can conveniently generate multiple signal outputs and, unlike signal synthesis schemes, no special precautions are necessary to preserve the phase relationships of the various wheel excitation inputs. The hardware requirements needed to implement the scheme are modest - the only major item required being a multi-track data storage and retrieval system. Therefore, this scheme is selected for implementation and the rest of the report deals with the details of the scheme in terms of the dynamic vehicle simulation program and a digital controller which performs the data storage and retrieval functions.

1.2 The Recorded Simulation Control Scheme

There are several ways of implementing the recorded simulation control scheme, with the same basic approach of recording the computer generated axle displacement signals and playing them back at the time of shake test. The implementation scheme selected in this effort is shown in Figure 2.

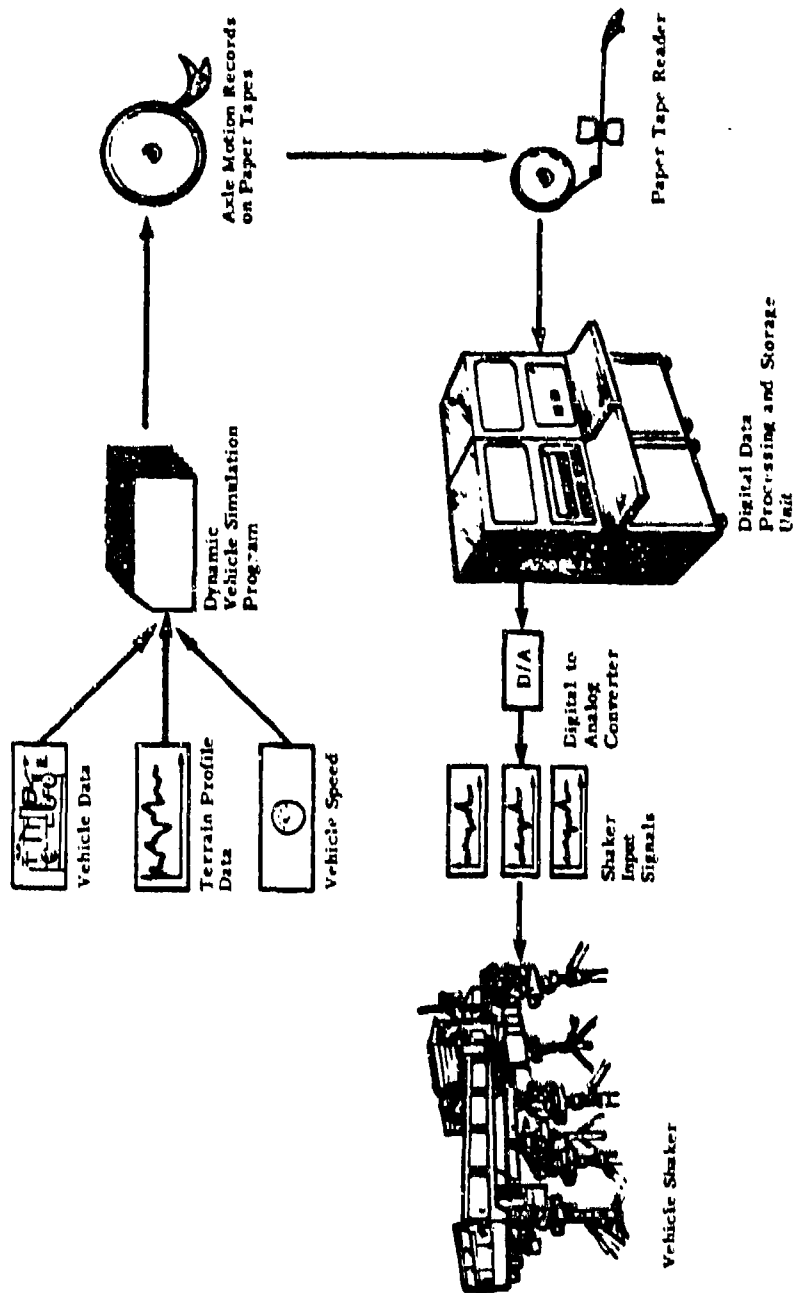


Figure 2. Recorded Simulation Control Scheme

As shown in the figure, the axle motion records are generated by a dynamic vehicle simulation computer program. Data necessary to execute the program include:

- a. Vehicle data (mass, CG location, wheel base, etc.)
- b. Operation data (terrain profile and speed of operation).

The axle displacement records generated by the simulation are stored on paper tapes and transferred to magnetic disc of a digital controller through adequate software. The data stored on the magnetic disc are retrieved at the time of running the shake test and the digital signals are converted to analog signals using a bank of digital-to-analog signal converters. The analog signals are then fed to the shaker through appropriate filters and amplifiers.

The record stored on the disc typically lasts less than a minute in real-time; therefore, the process is repeated until the testing is completed. Also, the simulation program is executed each time the vehicle test parameters (terrain profile, speed, load) are changed, and the axle displacement records on the disc are updated to show the changes.

1.3 Objective and Organization of the Report

Objective of the report is to introduce the recorded simulation control scheme, describe it and demonstrate its effectiveness through an illustrative example. The report describes the scheme in terms of its two steps: (a) generating axle displacement records using the vehicle simulation program, and (b) obtaining input signals for the vehicle shaker from the axle displacement records. The vehicle simulation program incorporates a terrain-tire-vehicle model developed in Chapter 2. There are three components in this model: terrain, tire and vehicle. The terrain model generates a terrain profile from information on its spectral density. The vehicle model developed in this report allows simulation of vehicles similar to the 5-ton M-809 cargo truck. Tire represents an interface between the two models and it is modelled in four different ways (see reference 2):

- a. Point contact model
- b. Rigid tread band model

- c. Fixed footprint model
- d. Adaptive footprint model.

Each component of the overall terrain-tire-vehicle model is developed separately so that it can be used independently in different applications.

Chapter 2 also discussed results obtained from a typical simulation run using a computer program* incorporating the model developed. The simulation results are then compared with corresponding experimental results to formulate guidelines for selecting a tire model and verify the overall model.

The controller needed to store and retrieve the axle displacement records generated by the vehicle simulation is described in Chapter 3. The necessary hardware components and their functions are discussed along with key steps in operation of the controller. Details of the controller operation are, however, not discussed because they are available in the User's Manual (reference 4).

Chapter 4 deals with verification of the complete recorded simulation control scheme through comparison of the spectral densities of the axle displacement signal with those obtained from field data. Finally, conclusions and recommendations are discussed in Chapters 5 and 6.

*The computer program itself is described in a separate document (reference 4).

2. SIMULATION

Development of a reliable model for simulating the vehicle performance was initiated in the first phase of the project (reference 2). It was realized early in the effort that a good model of tire is necessary for accurate performance prediction and therefore in the first phase four different tire models were developed. These models were incorporated in a simple two degree of freedom model and initial simulation results were obtained to provide insight into tire model behavior.

These tire models are now incorporated in a six degree of freedom vehicle model which can simulate the heave-pitch motion of a three axle military type truck. The vehicle has been selected so that the results obtained from the simulation can be compared with the available experimental results. Also, the input signals generated by the scheme can then directly be used to test similar vehicles on the six actuator shaker available at TARADCOM. Because of the non-generalized nature of the vehicle model, modifications are necessary for testing other types of vehicles using the scheme described in the report. However, the terrain and the tire models are developed so that they can be used independently in any application.

The simulation results described in the report are obtained using a computer program which incorporates the model. Details of the computer program are available in the User's Manual (reference 4) and therefore are not repeated here.

2.1 Model Development

The tire, vehicle and terrain models are summarized in the sections that follow. Additional details, including equations, for the tire and vehicle models are presented in the Appendices.

2.1.1 The Tire Model

Four basic tire models were formulated in Phase I, ranging in sophistication from the simple point contact model to the more advanced adaptive footprint model. These models were developed so that the most economical tire simulation can be selected for the task at hand. The models are summarized in Table 2 and described briefly below. Further details can be found in reference 2.

2.1.1.1 The Point Contact Tire Model

The point contact model is represented by a parallel spring-dashpot combination that transmits the support force from the terrain to the vehicle and contacts the ground through a point follower. The spring stiffness is chosen to simulate the effects of inflation pressure and carcass elasticity. The damping provides the energy dissipation caused by carcass deformations. Terrain contact occurs at a single point vertically beneath the wheel center. Dynamic support forces occur due to deflection of the spring and dashpot caused by motion of the wheel spindle relative to the terrain. Fore-and-aft forces are obtained from this model by assuming that the resultant tire force is always normal to the local terrain surface. Whenever the profile surface is inclined to the horizontal, a fore-and-aft force is generated which is related to the vertical force through the tangent of the local surface angle. The tire mass is concentrated at the wheel center, and the terrain follower is free to leave the ground to simulate wheel hop.

2.1.1.2 Rigid Tread Band Tire Model

The rigid tread band tire model is similar to the point contact model, except that the terrain contact point is not constrained to lie vertically beneath the wheel center but is free to move forward or aft depending on the local profile slope. This model is equivalent to a point contact tire with the terrain contact point located at the center of a rigid rolling wheel or circular tread band. In this case, the wheel center sees a motion that is in general different from the terrain profile, due to filtering

Table 2. Summary of Basic Tire Models

Name	Schematic	Characteristics
1. Point Contact Tire Model		<p>(a) Effects of inflation pressure and carcass stiffness represented by single spring-dashpot combination.</p> <p>(b) Effects of finite contact area neglected; i.e., no enveloping capability.</p> <p>(c) Effects of finite tire radius neglected; i.e., terrain contact point vertically below wheel center.</p>
2. Rigid Tread Band Tire Model		<p>(a) Rolling Circular Tread Band.</p> <p>(b) Effects of inflation pressure and carcass stiffness represented by an equivalent radial spring-dashpot combination.</p> <p>(c) Ability to filter small wavelength irregularities due to geometric constraints.</p> <p>(d) Terrain contact point shifted fore or aft of wheel center.</p>
3. Fixed Footprint Tire Model		<p>(a) Contact area independent of tire deflection.</p> <p>(b) Effects of inflation pressure and carcass stiffness represented in terms of linearly distributed stiffness and damping.</p> <p>(c) Ability to envelop small irregularities.</p>
4. Adaptive Footprint Tire Model		<p>(a) Contact area changes with tire deflection and conforms with terrain surface.</p> <p>(b) Effects of carcass stiffness represented in terms of angularly distributed stiffness and damping.</p> <p>(c) Effects of inflation pressure represented by an increase in ground contact pressure independent of tire deflection.</p> <p>(d) Capability to filter and envelop small irregularities.</p>

effects of the rolling wheel. On rough ground, the filtering causes a high attenuation of profile irregularities. For gradual changes in profile elevation, filtering becomes insignificant, and the two models give equivalent results.

As with the point contact model, the support force is transmitted to the vehicle through the parallel spring-dashpot combination that simulates the inflation pressure and carcass forces. Fore-and-aft forces are obtained by assuming that the total tire force always acts normal to the terrain at the contact point. The tire mass is concentrated at the wheel center, and the tread band is free to leave the ground to simulate wheel-hop.

2.1.1.3 Fixed Footprint Tire Model

The fixed footprint tire model interacts with the terrain through a footprint of constant size, independent of the tire deflection. Inflation pressure and carcass forces are simulated by the spring and damper elements distributed uniformly over the contact length. The finite footprint area provides this model with the ability to envelop small irregularities through local deformations within the footprint. In fact, * this model is equivalent to a point contact model in which the local terrain elevation is replaced by the average terrain elevation taken across the footprint length. Like the rigid tread band model, the fixed footprint model also filters the terrain profile, except that the filter characteristics are governed by the footprint length rather than the tire radius. Unlike the rigid tread band model, however, the footprint center is constrained to lie vertically below the wheel center, independent of the local profile slope.

The fore-and-aft tire force is obtained by assuming that the footprint force acts perpendicular to the local profile and the footprint is free to leave the ground to simulate wheel-hop.

*With linear stiffness and damping.

2.1.1.4 Adaptive Footprint Tire Model

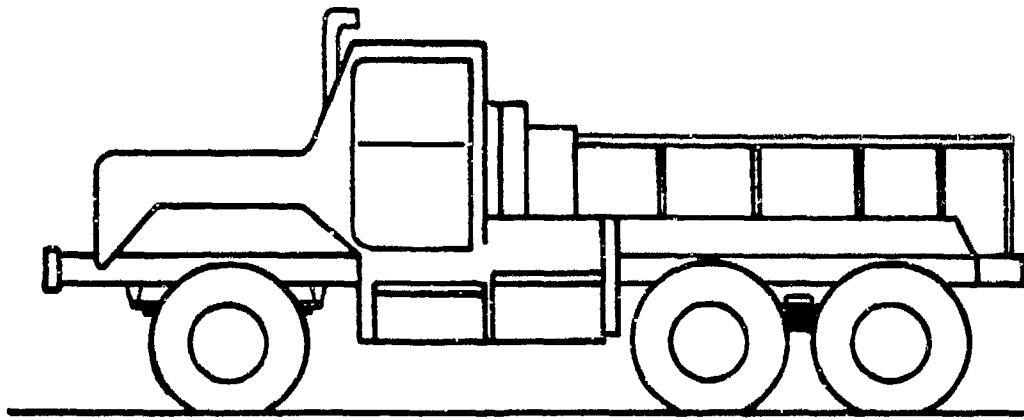
The adaptive footprint tire model consists of a flexible tread band inflated by internal pressure and linked to the wheel center by angularly distributed stiffness and damping which simulate carcass and tread stiffness. As the wheel passes over terrain irregularities, the tread in the footprint region deforms, and gives rise to the pneumatic and carcass components of tire force. The former is given by the inflation pressure acting over the contact area. The latter is found from the resultant of the spring and damping forces in the footprint. In general, the resultant tire force will not be vertical because of the existence of a non-planar footprint, and the calculation of the appropriate components will allow determination of the vertical and fore-and-aft tire force.

Like the fixed footprint model, this model has the ability to envelop small irregularities through local deformations within the footprint. However, the key feature of this model is that the footprint size and orientation relative to the wheel center changes depending on the tire deflection and terrain profile. As with the other models, the tire mass is concentrated at the wheel center and the tire is free to leave the ground to simulate wheel hop.

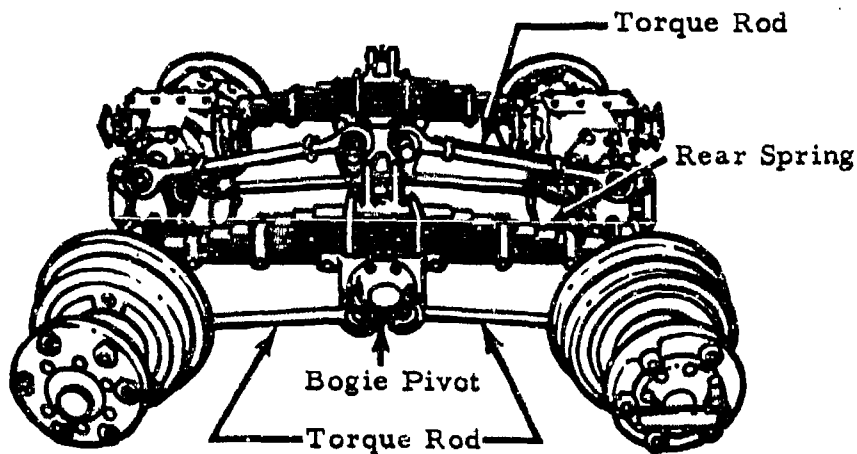
2.1.2 The Vehicle Model

The vehicle model has been formulated to allow simulation of a variety of trucks of interest to the military. The baseline vehicle which guided simulation development and was used to validate the model was the M-809 5 ton, three axle, 6 x 6 cargo truck. This vehicle was selected both because field trial data were available, and because the basic vehicle configuration is representative of a variety of multi-axle military trucks.

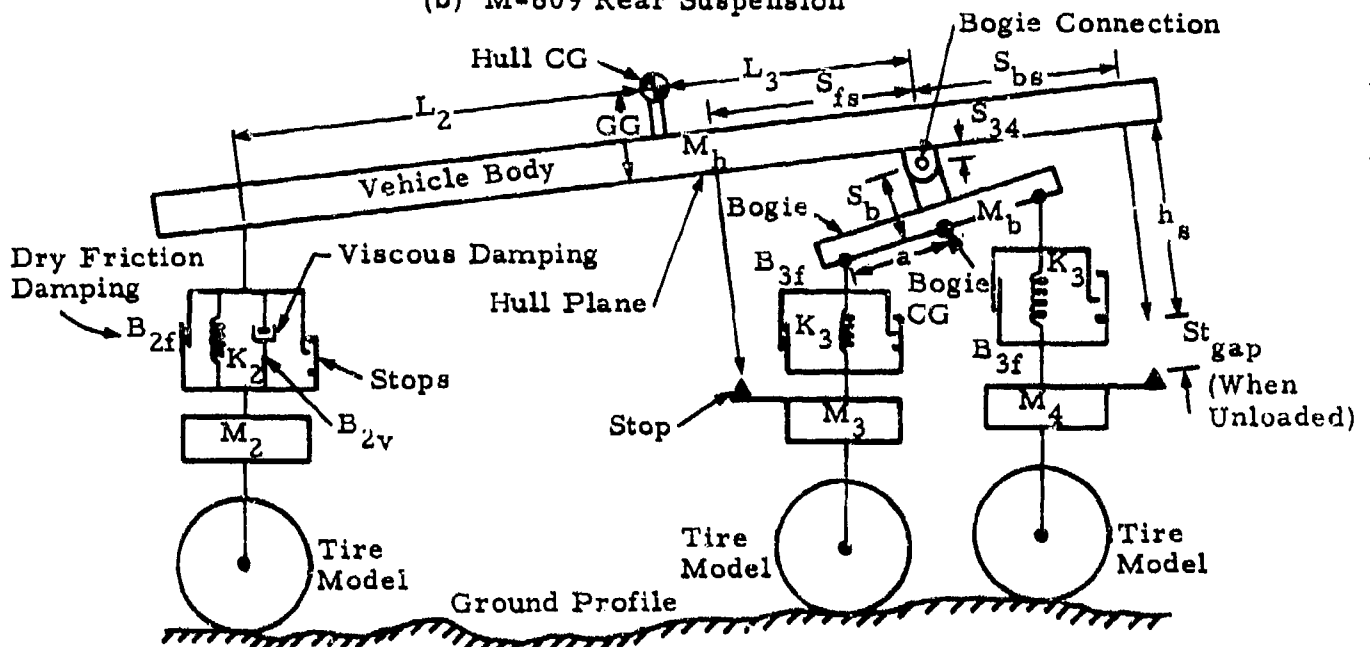
A sketch of the vehicle is shown in Figure 3a. The front wheels are attached to the frame through a semi-elliptical leaf spring and dashpot suspension. The rear suspension (Figure 3b) consists of a pivoted leaf spring assembly (bogie) attached to the chassis through a central shaft (pivot) and connected at the spring ends to the middle and rear wheel spindles. Bounce



(a) M-809 Truck



(b) M-809 Rear Suspension

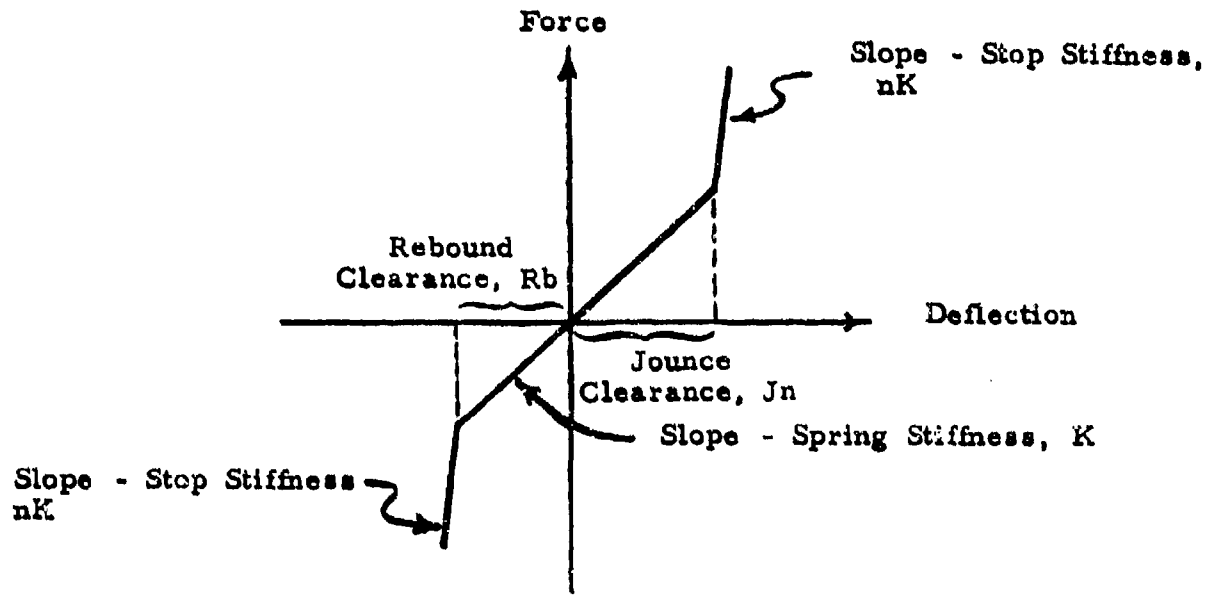


(c) The Model of the Vehicle

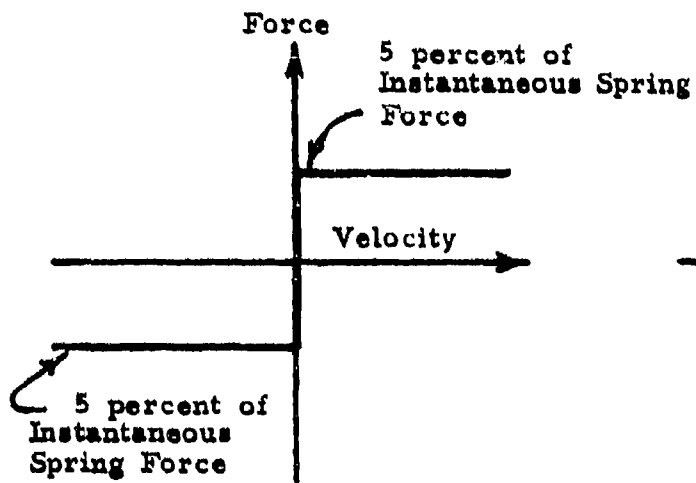
Figure 3. Formulation of Vehicle Model

motion of the rear wheels thus results in two types of suspension motion: flexure of the leaf spring, and rotation of the bogie about the pivot. For symmetrical vibration - i. e., when the rear wheel pair vibrate in phase - the spring is flexed without bogie rotation. For antisymmetrical vibration - i. e., when the rear wheel pair vibrate out of phase - the bogie rotates without spring flexure. In the real case, when the vehicle is going over a bumpy road, both symmetrical and antisymmetrical components will exist, and spring flexure and bogie rotation will occur simultaneously. However, excessive jounce motion of the rear wheels is prevented by stops attached to the main frame.

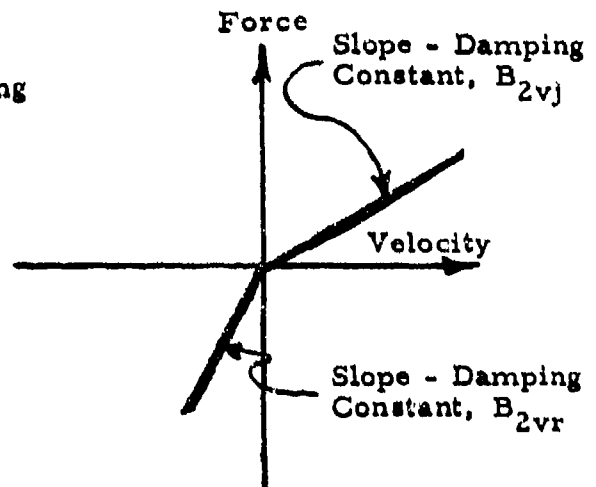
The analytical model for the truck is shown in Figure 3c. The vehicle body is represented by a rigid beam of mass M_h and rotational inertia I_h . The unsprung mass of the front, middle and rear wheels (M_2, M_3, M_4) consists of the effective mass of the tire(s) and the mass of the wheel(s), suspension and other components that move with the wheel. The vertical tire force acts directly on the unsprung mass. The fore-and-aft tire force is transmitted to the vehicle body through suspension elements not shown in the figure. The front suspension leaf spring is modelled as a linear spring (K_2) with a hardening characteristic for large motions (elastic stops), as shown in Figure 4a. When the spring excursion exceeds the jounce or rebound clearance, its stiffness increases by a factor of n (typically, $n = 10$) due to stop contact. Dry friction damping (B_{2f}) is also included in the leaf spring model, as shown in Figure 4b. The dry friction force has a value of 5 percent of the instantaneous spring force (before stop contact), and opposes the velocity. The front shock absorber is modelled as a dashpot with damping coefficient B_{2vj} in jounce and B_{2vr} in rebound, as shown in Figure 4c. The rear suspension bogie assembly is modelled as a rigid beam (mass M_b , rotational inertia I_b) pivoted at the center, with two springs (K_3) attached to the extremities. The beam represents the kinematic configuration and rotational inertia of the bogie during antisymmetrical wheel vibration (i. e., for bogie rotation). The spring elements (K_3) represent each half of the rear leaf spring. As with the front spring, the rear spring is also modelled as a linear spring with elastic stops and dry friction damping (Figures 4a and 4b). No viscous damping is included in the rear suspension model, because of the absence of a shock absorber. Frame mounted stops which prevent excessive rear wheel jounce, and tire stops that limit the maximum tire deflection are also included in the model. The force-deflection characteristics of these elements are shown in Figure 5.



(a) Suspension Spring

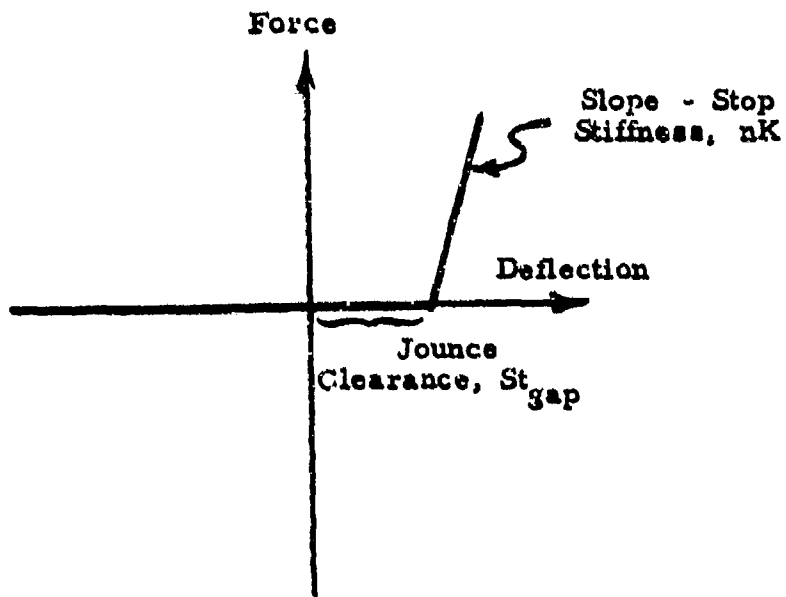


(b) Dry Friction Damping

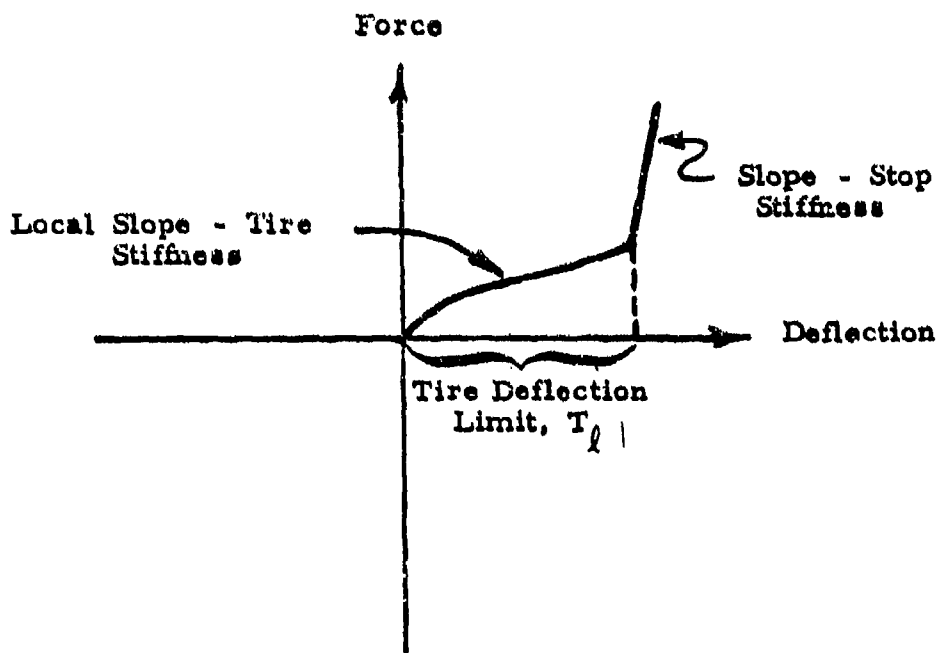


(c) Shock Absorber Damping

Figure 4. Force Characteristics of Suspension Spring and Damping Models



(a) Rear Wheel Frame Stops



(b) Tire

Figure 5. Force Characteristics of Frame Stop and Tire Models

The vehicle model described above has been developed primarily for the initial bounce-pitch simulations needed to verify the tire models and carry out the demonstration shake tests. Subsequently, the roll mode can be included by providing separate left and right wheel inputs and including vehicle body roll inertia.

2.1.3 The Terrain Model

The terrain model developed for the simulation consists of a series of profile elevation coordinates whose values are determined statistically, and can represent several types of unimproved roads of varying degrees of roughness (reference 2). This terrain model has been chosen primarily to make the verification runs of the vehicle simulation program, and for the initial shake tests. Subsequently, the analytically obtained terrain coordinates can be replaced conveniently with real terrain data.

A 500 foot length of profile has been generated and used for the model validation runs. An rms roughness of 1 inch was chosen for the simulated profile, so that its power spectral density (PSD) generally agrees with Aberdeen Proving Grounds test track data (reference 3), for which the M-809 truck trial results were available. The statistical terrain characteristics are summarized in Table 3. The PSD of the profile is shown in Figure 6.

As shown in the figure, the PSD is plotted as a function of a reduced frequency $\Omega (= 2\pi/\lambda)$, where λ is the wavelength of the irregularity component. This frequency can be converted to frequency in Hz by multiplying by $V/2\pi$. Corresponding PSD is obtained by multiplying the PSD shown by $2\pi/V$.

The straight line on the figure represents the analytically specified PSD. The points were found by computing the PSD from the actual elevation coordinates. The low frequency scatter is due in part to the reduced number of complete cycles available for calculating the mean square values, and can be reduced by increasing the profile length. The dynamic simulation results and experimental comparison are presented in the sections that follows.

Table 3. Statistical Terrain Characteristics

rms Roughness, y_{rms}	1 inch
PSD Relationship, $S_{y_0}(\Omega)$	A/Ω^2
Amplitude Probability Distribution	Gaussian
Upper Cutoff Wavelength, λ_1	57 feet
Lower Cutoff Wavelength, λ_2	0.177 feet
Vehicle Speed, V	18 mph
Excitation Frequency Range	0.46 - 150 Hz

2.2 Simulation Results

The terrain, tire and vehicle models described previously were integrated into a dynamic bounce-pitch simulation suitable for obtaining the shaker input signals. Three programs have been developed: program GRND which generates the terrain profile, program TIRE which determines the vehicle motion time history, and program SPEC which computes the PSDs of vehicle motion. These programs, and their method of use, is described in detail in a separate document (reference 4). A test case simulation using these programs was carried out to verify the models and provide the necessary data for the initial demonstration shake tests. The simulations were carried out for an M-809 truck moving at 18 mph over a 500 foot long track of 1 inch rms roughness. The parameters of the tire and the vehicle used for the simulation are summarized in Table 4. Table 5 shows additional tire parameters which are required for the more sophisticated tire models.

A short extract of the time history of tire force obtained with each of the tire models is shown in Figure 7. Examination of the force response of the point contact tire shows that it is significantly higher than that of the other models, and has a greater high frequency content. Another characteristic seen from the time simulation is that wheel hop (zero tire force) is important. In the 10 foot section of record shown, the point contact model spends almost 60 percent of the time out of ground contact. The other two

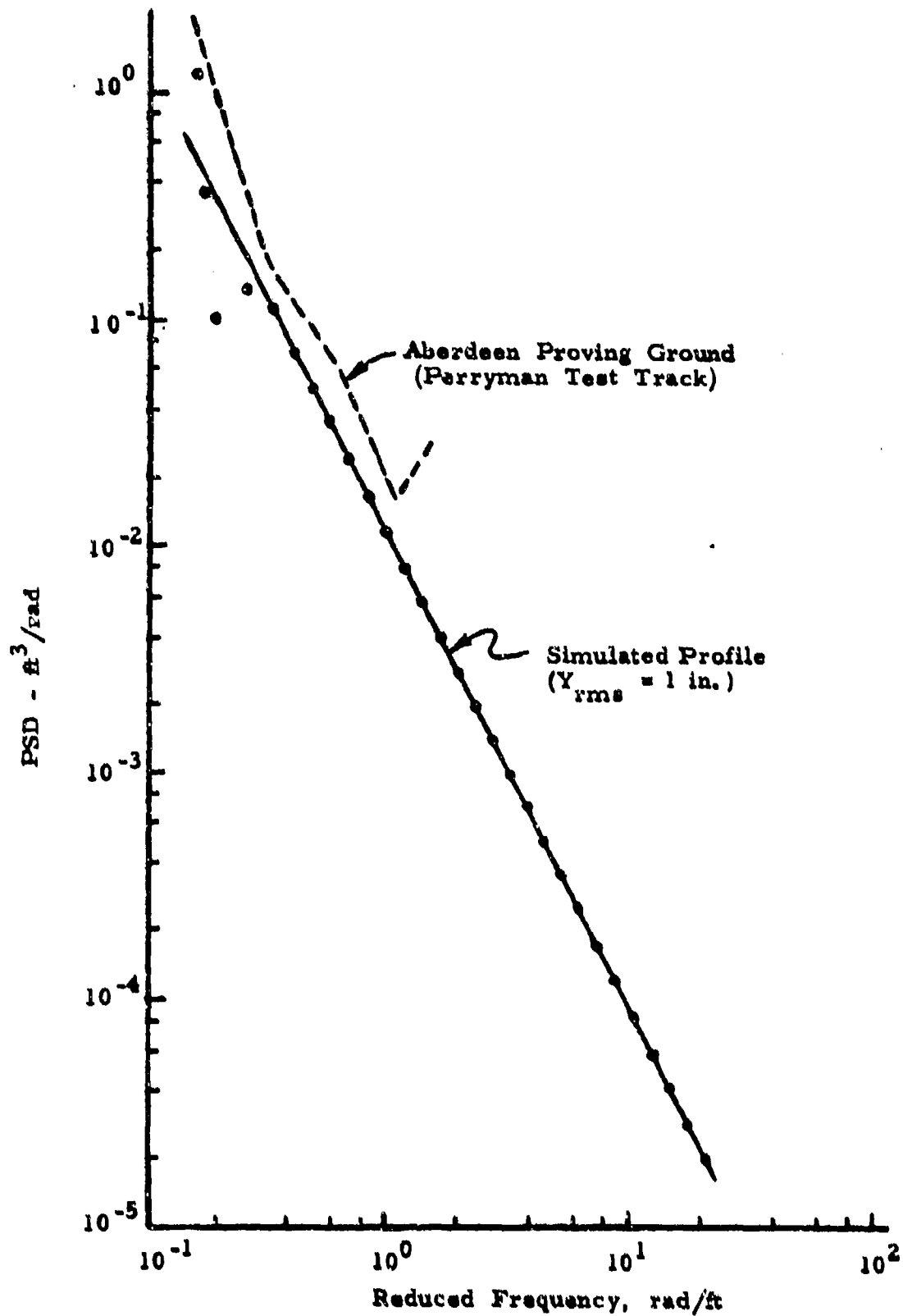


Figure 6. Power Spectral Density of Terrain Profile

models (rigid tread band and fixed footprint) also show wheel hop, although in decreasing amounts. Although the adaptive footprint simulation is free of wheel hop for the 10 foot section shown, the wheel hop condition is closely approached on two occasions. The reason for the reduction in wheel hop with the more advanced models is that they filter the short wavelength irregularities, and hence attenuate the high frequency excitation which causes wheel hop. The filtered ground profiles for the rigid tread band and fixed footprint tire models are shown in Figure 8 along with the actual profile for comparison. The reduction in high frequency content, especially for the fixed footprint model is readily apparent.

Table 4. Summary of Vehicle Parameters

Vehicle Type - M-809, 5 ton, 6 x 6 cargo truck Tire - Goodyear 11.00-18, Military NDCC			
Vehicle Body Parameters	Symbol	Value	Unit
Mass of Hull	M_h	718.6	Slugs
Mass of Bogie	M_b	6.0	Slugs
Front Unsprung Mass (each side)	M_2	40.6	Slugs
Middle Unsprung Mass (each side)	M_3	42.1	Slugs
Rear Unsprung Mass (each side)	M_4	43.6	Slugs
Pitch Inertia of Hull (about cg)	I_h	34924	Slug·ft ²
Pitch Inertia of Bogie (about pivot)	I_b	3.0	Slug·ft ²
Front Suspension to Hull CG Length	L_2	12.5	ft
Bogie Pivot to Hull CG Length	L_3	2.4	ft
Hull CG Height	CG	0	ft
Offset, Bogie Pivot to Hull Plane	S_{34}	0	ft
Offset, Bogie Pivot to Bogie CG	S_b	0	ft
Bogie Pivot to Front Stop Length	S_{fs}	2.2	ft
Bogie Pivot to Rear Stop Length	S_{bs}	2.2	ft
Half Bogie Length	a	2.2	ft

Table 4. Summary of Vehicle Parameters (Cont)

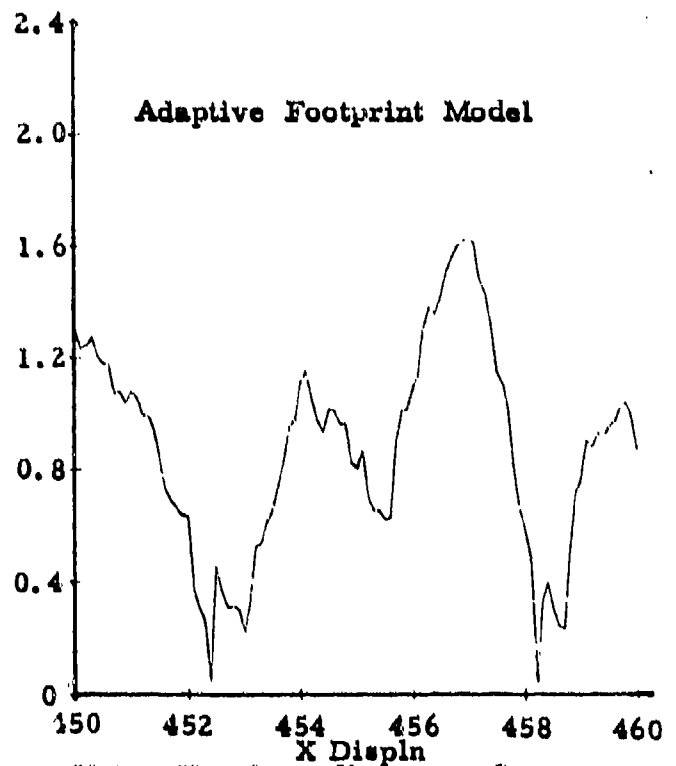
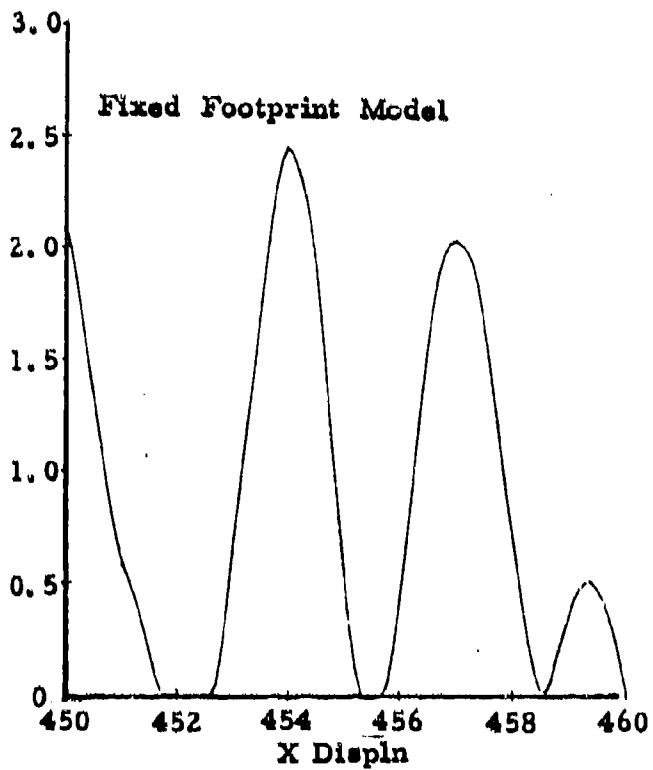
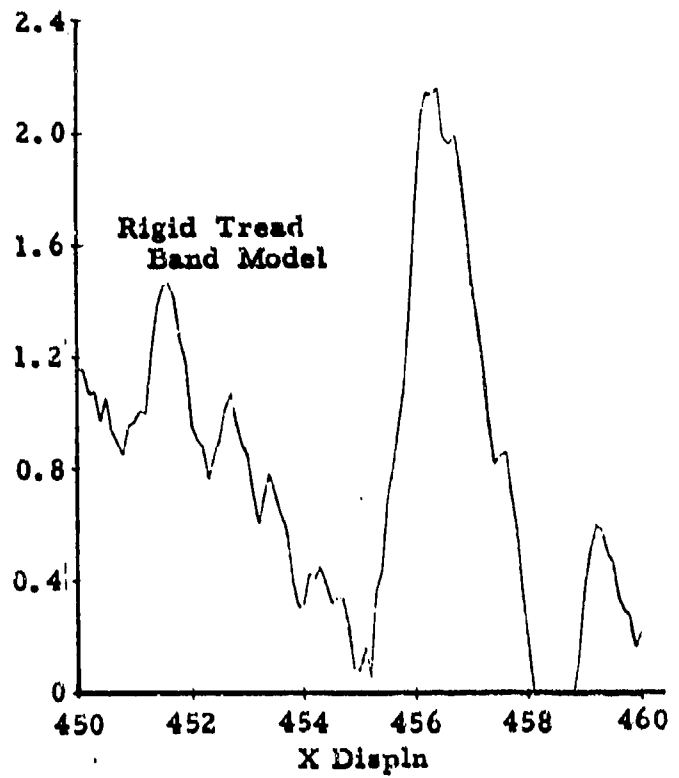
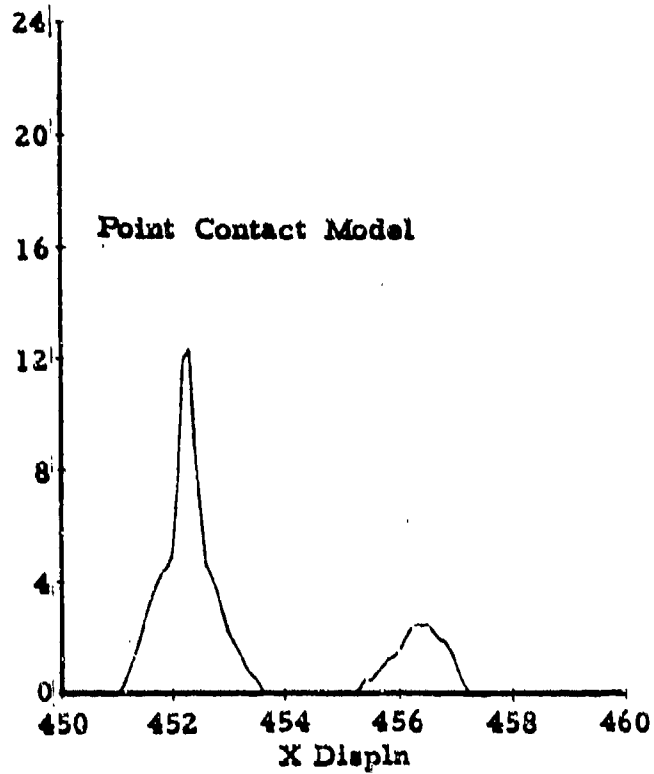
Vehicle Body Parameters (Cont)	Symbol	Value	Unit
Stop Length	h_s	0.25	ft
Stop Clearance (Unloaded)	St_{gap}	0.39	ft
Suspension Parameters	Symbol	Value	Unit
<u>Front Suspension (each)</u>			
Stiffness	K_2	29976	lb/ft
Viscous Damping Coefficient (Jounce)	B_{2vj}	185	lb·sec/ft
Viscous Damping Coefficient (Rebound)	B_{2vr}	600	lb·sec/ft
Jounce Travel (Unloaded)	Jn_2	0.5	ft
Rebound Travel (Unloaded)	Rb_2	0.5	ft
Dry Friction Coefficient	B_{2f}	*	
<u>Middle and Rear Suspension (each)</u>			
Stiffness	K_3	87000	lb/ft
Jounce Travel (Unloaded)	Jn_3	0.7	ft
Rebound Travel (Unloaded)	Rb_3	0.7	ft
Dry Friction Coefficient	B_{3f}	*	
Tire Parameters	Symbol	Value	Unit
Stiffness	k	39000	lb/ft
Damping	b	31	lb·sec/ft
Radius	r	1.67	ft
Contact Length	L	1.03	ft
Effective Width	B	0.52	ft
Inflation Pressure	P_1	30	psi
Tire Deflection Limit	T_f	0.4	ft

*Selected such that the dry friction damping force is equal to 5 percent of the spring force, with direction opposing the velocity.

Table 5. Model Parameters for 11.00-18 Tire

Parameters	Point Contact Model	Rigid Tread Band Model	Fixed Footprint Model	Adaptive Footprint Model
Mass	80 lbs	80 lbs	80 lbs	80 lbs
Stiffness	$k = 39000 \text{ lb/ft}$	$k = 39000 \text{ lb/ft}$	$k' = 38000 \text{ lb/ft}^2$	$k'' = 29500 \text{ lb/ft}^3$
Damping	$b = 31 \text{ lb-sec/ft}$	$b = 31 \text{ lb-sec/ft}$	$b' = 30 \text{ lb-sec/ft}^2$	$b'' = 57.9 \text{ lb-sec/ft}^3$
Radius	*	$r = 1.67 \text{ ft}$	*	$r = 1.67 \text{ ft}$
Contact Length	*	*	$L = 1.03 \text{ ft}$	*
Effective Contact Area	*	*	*	$A = 77 \text{ in.}^2$
Inflation Pressure	*	*	*	$P_i = 30 \text{ psi}$
Deflection Limit	$T_f = 0.4 \text{ ft}$	$T_f = 0.4 \text{ ft}$	$T_f = 0.4 \text{ ft}$	$T_f = 0.4 \text{ ft}$

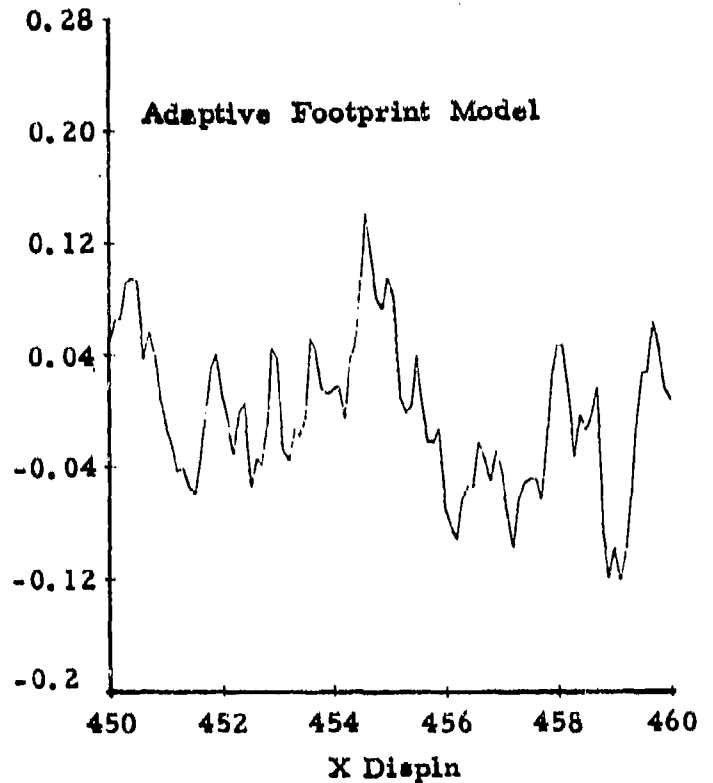
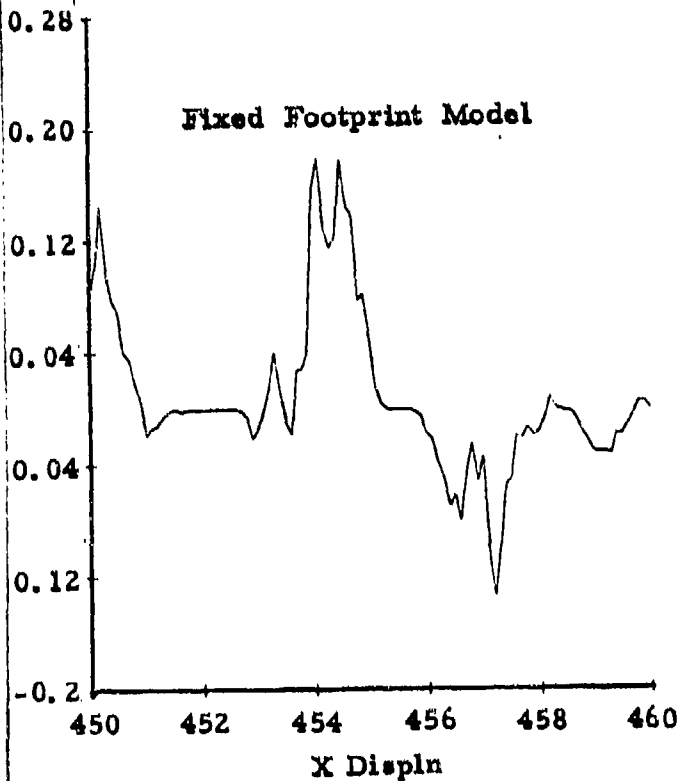
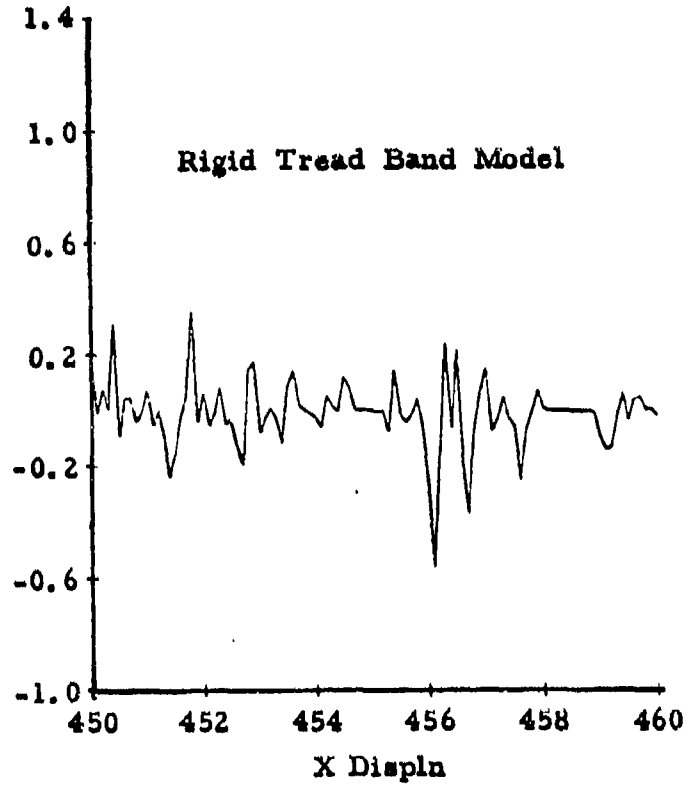
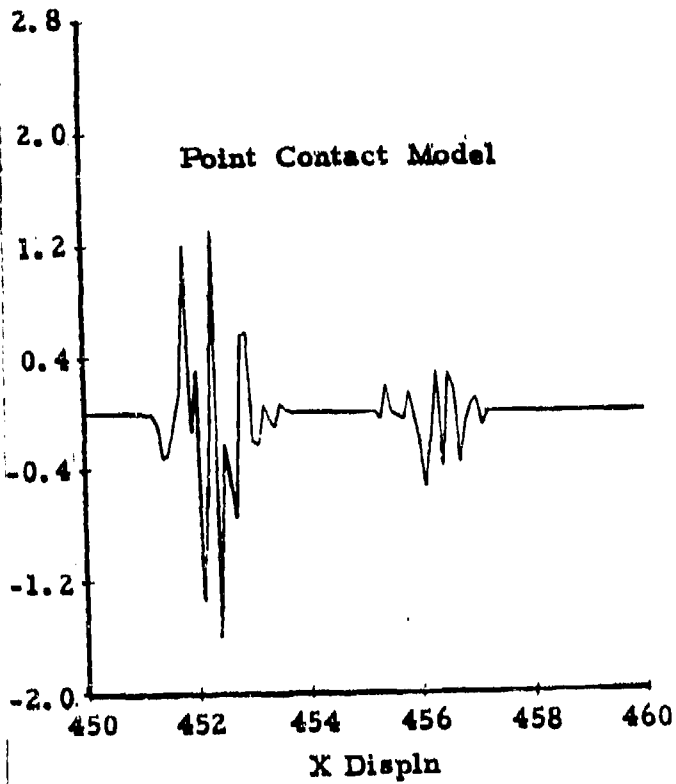
*Not needed as an independent model parameter.



Note: X axis - distance, ft
Y axis - force/equilibrium force

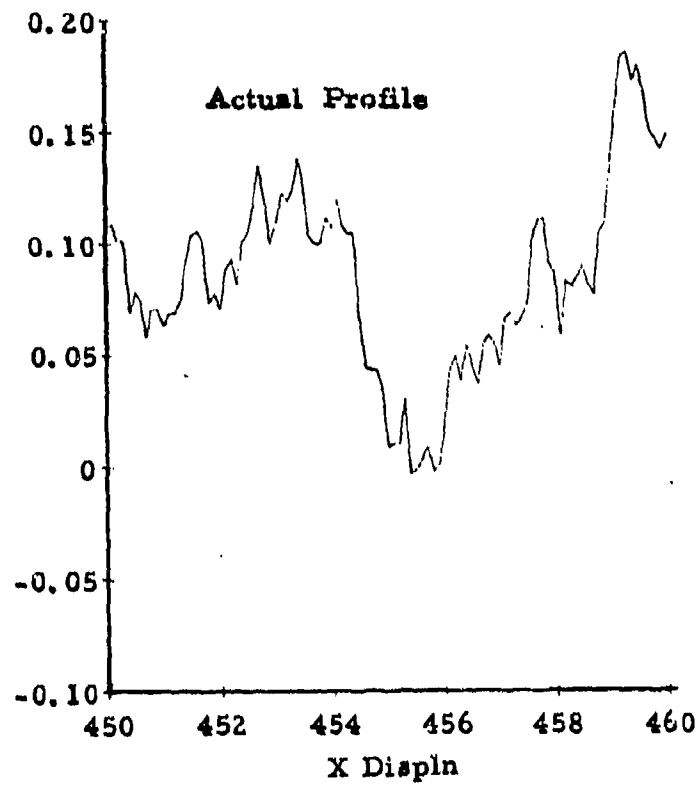
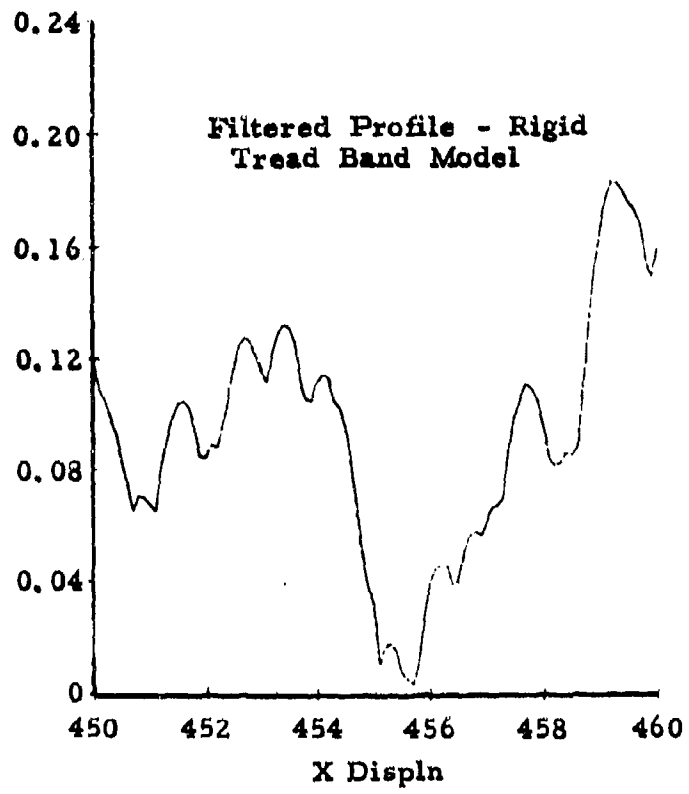
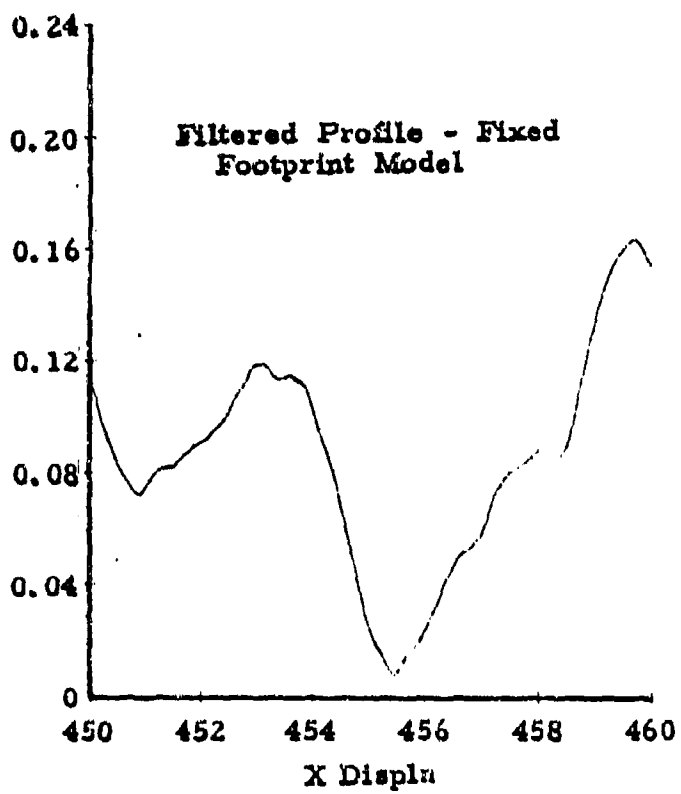
(a) Vertical Force

Figure 7. Time History of Tire Force



(b) Fore-and-aft Force Note: X axis - distance, ft
 Y axis - force/equilibrium force

Figure 7. Time History of Tire Force (Cont)



Note:
 X axis - distance, ft.
 Y axis - elevation, ft.

Figure 8. Actual and Filtered Ground Profile

Additional conclusions regarding the tire models can be drawn from the PSDs of the time functions. The PSDs of tire force are shown in Figures 9 and 10. Figure 9 shows the PSD of vertical tire force obtained with each tire model. There are three distinct peaks that can be observed. The first peak, at about 0.5 rad/ft corresponds to the vehicle body bounce/pitch natural frequency.* The second peak, occurring at about 1.5 rad/ft, corresponds to the bogie pitch natural frequency caused by antisymmetric (out-of-phase) vibration of the two rear axles. The third peak, occurring at about 2.5 rad/ft, corresponds to the conventional unsprung mass natural frequency.

As an initial check of the program formulation, the above natural mode frequencies have been compared with those found from a simplified approximate analysis. The approximate expressions for natural frequency (ω_n) are obtained by choosing the appropriate stiffness (K) and inertia (M) and then determining $\omega_n = \sqrt{K/M}$ as follows.

$$\text{Body Bounce,} \quad \omega_{nb} \approx \sqrt{2 \left(\frac{K_2 k}{K_2 + k} + \frac{4K_3 k}{K_3 + 2k} \right) / M_h} \quad (1)$$

$$\text{Body Pitch,} \quad \omega_{np} \approx \sqrt{2 \left(\frac{K_2 k}{K_2 + k} L_2^2 + \frac{4K_3 k}{K_3 + 2k} L_3^2 \right) / I_h} \quad (2)$$

$$\text{Bogie Pitch,} \quad \omega_{np}^1 \approx \sqrt{2k/M_4} \quad (3)$$

* Since body bounce and pitch natural frequencies for the M809 truck are very close together, two separate peaks are not always observed.

$$\text{Front Wheel Bounce, } \omega'_{\text{nbf}} \approx \sqrt{(K_2+k)/M_2} \quad (4)$$

$$\text{Rear Wheel Bounce, } \omega'_{\text{nbr}} \approx \sqrt{(K_3+2k)/M_4} \quad (5)$$

These expressions, evaluated from Table 4, are summarized in Table 6. As can be seen, the simulation results are in close agreement with the approximate analysis, which serves as an initial check of the program formulation.

The simulation results (Figures 9 and 10) show that the simpler tire models generally overestimate the transmitted tire force. Although at low frequencies all models give similar results, the differences become apparent in the middle and upper frequency ranges of interest. For instance, point contact model predictions at the higher frequencies can be up to an order of magnitude greater than those of the more advanced models. The rigid tread band model also gives generally higher force estimates, specially for the fore-and-aft force. The fixed footprint and adaptive footprint simulations, however, are in good agreement with each other, and give the lowest force predictions, because of their ability to envelop small irregularities through local footprint deformations.

Similar conclusions regarding the various tire models can be reached by examining the other simulation results (CG acceleration, wheel acceleration, etc.). These results confirm that the adaptive footprint and fixed footprint tire models agree closely, and predict lower accelerations than the rigid tread band and point contact models. For reference, all the principal simulation results are presented in Appendix C.

2.3 Simulation Verification

The basic objective in developing the present terrain-tire-vehicle simulation is to provide a means of generating realistic shake test input signals. Therefore, before carrying out the tests, it is necessary to verify the model predictions with field trial data so that the shake test

Table 6. Comparison of Simulation Results with Approximate Analysis

Natural Mode	Natural Frequency (Hz)	
	Bounce-Pitch Computer Simulation	Approximate Analysis
Body Pitch, ω_{np}	2.2	2.1
Body Bounce, ω_{nb}	2.2	2.6
Bogie Pitch, ω'_{np}	6.7	6.8
Front Wheel Bounce, ω'_{nbf}	6.7	6.6
Rear Wheel Bounce, ω'_{nbr}	11	10

results can be accepted with confidence. This verification has been carried out using data obtained with the M-809 truck during field trials at the Aberdeen Proving Grounds (reference 3). The unsprung mass (rear wheels) acceleration has been chosen for comparison, since it is directly related to the wheel motions from which the shaker signals are derived.

The results showing the PSD of this parameter for the point contact, fixed footprint and adaptive footprint tire models are shown in Figure 11 along with the experimentally determined PSD. As can be seen, the point contact model significantly overestimates the acceleration over the entire frequency range. The adaptive footprint model, however, shows much better agreement, and in the middle and high frequency bands - of particular importance to fatigue simulation in the shake tests - the simulation data closely follow the experimental results. The fixed footprint model also shows good agreement with field data, although at the natural frequency peak, it somewhat overestimates the force. The rigid tread band model, though providing better predictions than the point contact model, tends to overestimate the force in the middle and upper frequency range, as shown in Appendix C.

REAR TIRE FORCE (VERTICAL)

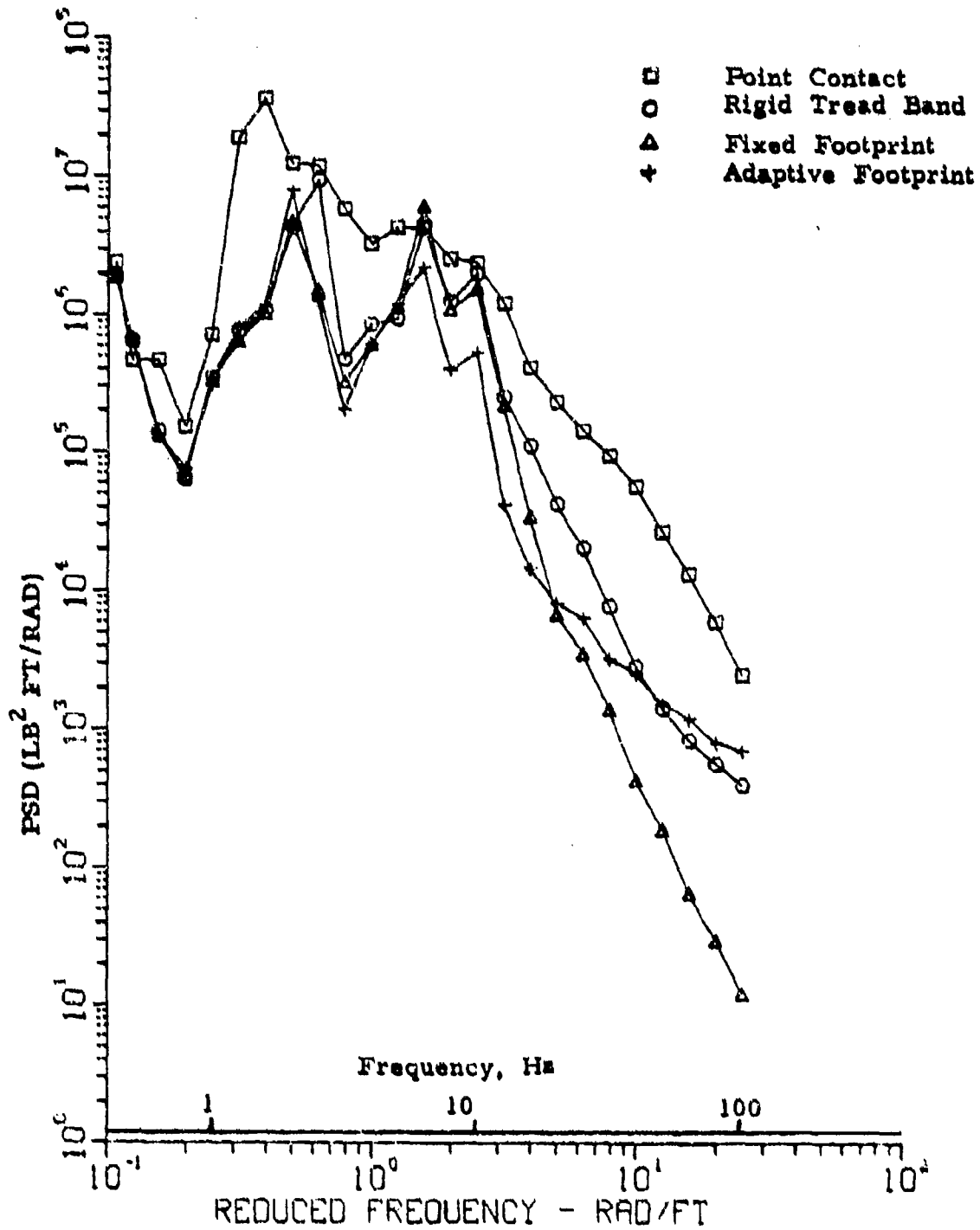


Figure 9. Simulated Vehicle Response - PSD of Vertical Tire Force

REAR TIRE FORCE (FORE-AND-AFT)

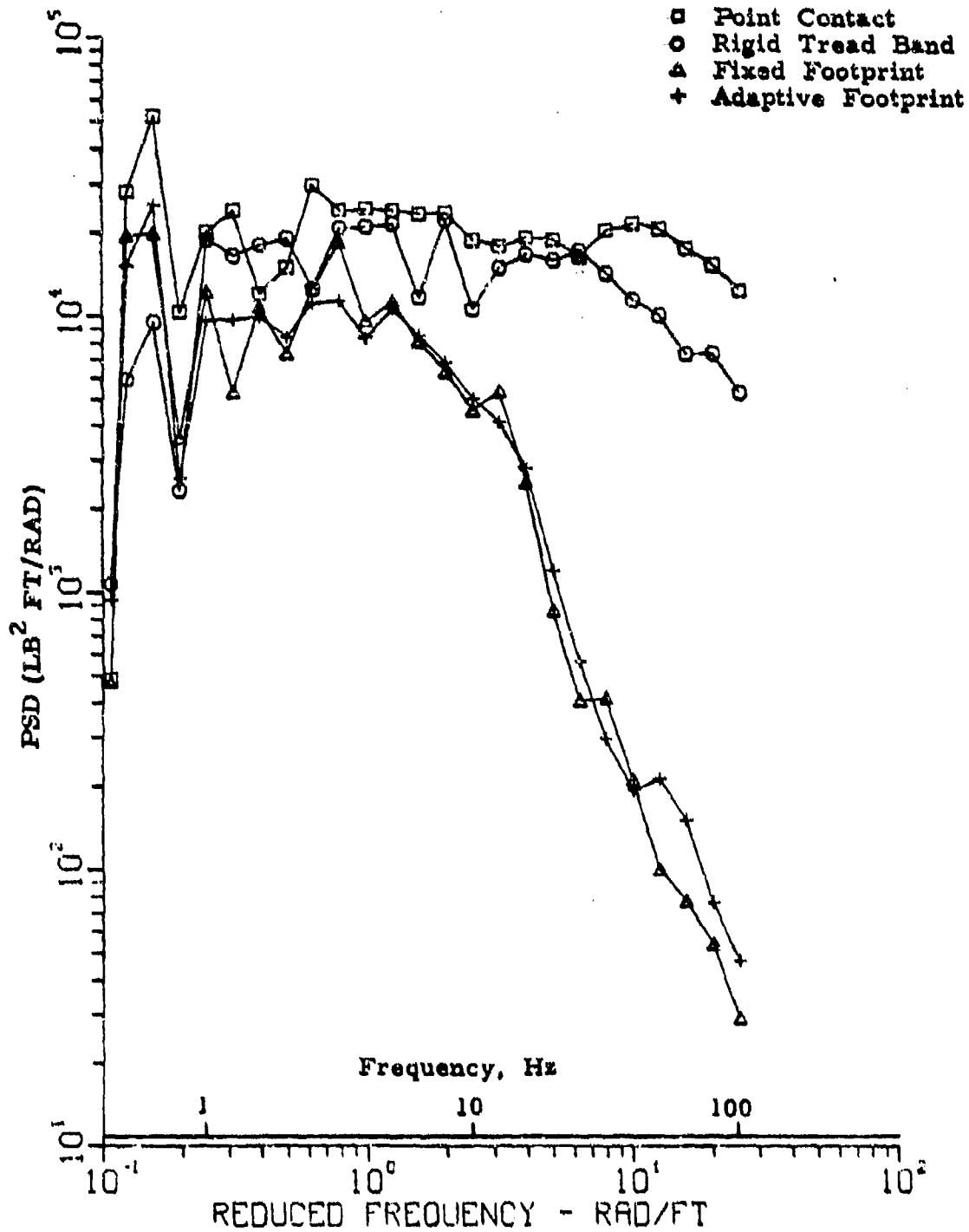


Figure 10. Simulated Vehicle Response - PSD of Fore-and-Aft Tire Force

REAR AXLE ACCLN

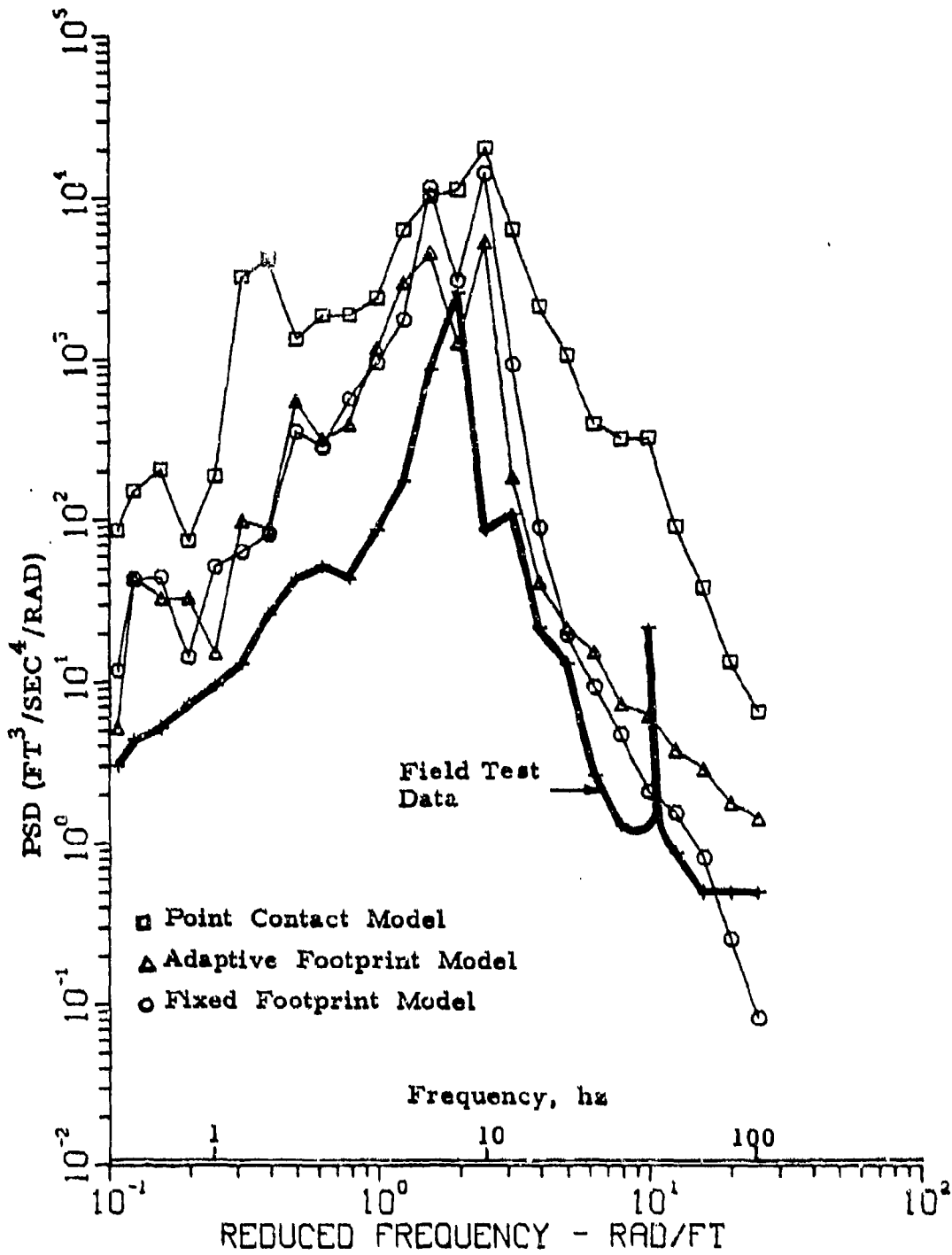


Figure 11. Comparison of Simulated Response with Test Data

These results confirm the initial conclusions of the first phase of this effort, namely, that the adaptive footprint tire model has superior capabilities for predicting the transmitted tire forces, and can be used with advantage for vehicle simulation and shake testing. The results also confirm that the fixed footprint tire model - though predicting slightly higher forces in the middle frequency band - provides a viable alternative for simulations in which computation requirements are to be minimized. *

*As explained in Appendix A, the fixed footprint model (with linear stiffness and damping) is equivalent to a point contact model moving over a filtered profile. Profile filtering can thus be carried out off-line, and the dynamic simulations can then proceed using the simple relationships of the point contact model.

3. CONTROL SYSTEM

The recorded simulation control scheme has been described in terms of two steps. The first step, obtaining axle displacement records from a vehicle simulation program, was described in the last chapter. This chapter describes how the axle displacement records are used to produce input signals for the vehicle shaker.

There are several subtasks involved in performing the second step. The tasks of reading the axle displacement records, storing them in an easily retrievable form and supplying them to the shaker at a correct rate demand a sophisticated control system. The control system used in this effort is described in the following pages. Detailed procedures for operating the control system, however, are not described in this report since they are best discussed in the User's Manual (reference 4).

3.1 System Requirements

To be suitable for the application, the control system must meet several requirements. The controller must be able to synchronize the shaker input signals to real-time, otherwise, the vehicle will not experience the inputs in the same time frame as it does in the field use. To be able to supply the data in real-time, the axle displacement records must have a time scale stored along with the displacement values and a clock should interface with the controller to ensure that the displacement values are transferred at the stored time values. For this application, a high frequency clock should be used so that the accuracy of the stored time data is preserved.

The data transfer rate requirement is closely coupled to the previous requirement, because the real-time capability can be achieved only if the transfer rate is adequate. Data transfer rate depends on time step between the two consecutive displacement values, which in turn is derived from the maximum frequency content the signal should have. The time step, which is fixed while running the vehicle simulation to create the axle displacement records, should be such that the displacement signal up to 100 Hz can be reconstructed from the digital records. This requires that a time step of

about 5 milliseconds should be used*. The displacement data at this time step are stored in 16 bit format and supplied to three channels (front, middle and rear axle), giving a system requirement for a minimum data transfer rate of about 9600 bits per second (Baud). If the upper limit on the frequency content of the input signal is increased or if the data is stored in 32 bit floating point format instead of 16 bit format, the transfer rate will be higher than 9600 bits per second.

The control system should have a capability of repeating the axle displacement records during the test. Computing and storage requirements generally limit the record length to less than a minute** (it is 18 seconds for the example used in the report). At the end of the record, the system should be able to start from the beginning without a significant loss of time.

The next requirement to be met by the control system is adequate data storage. For the 18 second record used in the illustrative example, a 150 thousand, 16 bit word, storage medium is needed to include axle displacement information along with the corresponding time reference.

The final requirement for the control system is a provision for converting the stored digital data to analog input signals for the shaker. Digital to analog converters with bipolar (signed) outputs and at least 11 bit (0.05 percent) accuracy would be adequate. The digital to analog conversion rate should also be high enough to meet the required data transmission rate.

The requirements outlined above eliminate from consideration the use of magnetic tape or core memory of a digital computer, because the magnetic tape cannot be rewound fast enough to meet the requirement for repeating the record, and the core memory of a computer generally does not have a large enough capacity to store the data.

*The smallest frequency that can be discriminated from a digital record with time step T is about $1/2T$ Hz.

**The length of the record should be such that the spectral content of the profile is preserved. See reference 2 for details.

The requirements, then, are best met by a digital or hybrid computer with a magnetic disc storage unit. The data handling and timing capabilities of a digital computer are ideal for the storage and transmission of a large volume of data as required by this system. A minicomputer, with adequate core memory to run the control software, interfaced with a disc storage unit, a digital clock, and a bank of digital to analog converters constitutes the controller, the actual hardware of which is described in the next section.

3.2 System Description

The control system selected for implementing the recorded simulation control scheme is an EAI (Electronic Associates, Inc.) 590 hybrid computer system shown schematically in Figure 12.

As shown in the figure, the central part of the system is a Pacer 100 minicomputer with a 16K, 16 bit word, core memory. The digital computer is connected through a hybrid interface to an EAI 580 analog computer which incorporates the digital to analog converters (D/A), analog to digital converters (A/D), sense and control lines, and a 1 MHz digital clock timer. The digital computer is also connected to a 2.2 million word (16 bit) disc storage unit through a direct memory access channel (DMAC). Input-output to the control system is achieved through a high speed paper tape reader/punch, a teletype and a line printer. Specifications of these hardware components are summarized in Table 7.

The above system meets the requirements outlined in the previous section quite well. The clock has an effective frequency of 42 KHz (after taking into account 24 μ sec required by the read and set subroutines controlling the clock), which is adequate for synchronizing time of the input signal to about 0.5 percent of the corresponding value. The D/A converters have a setup and transfer time of 252 μ sec for the three channels, therefore, the maximum transmission rate is close to 4 KHz, which is about ten times faster than required. The reset time for the system after reaching the end of the record is about 0.25 second, which is considered adequate. Data storage capacity of the disc is 2.2 million words as compared to the required capacity of 150 thousand words.

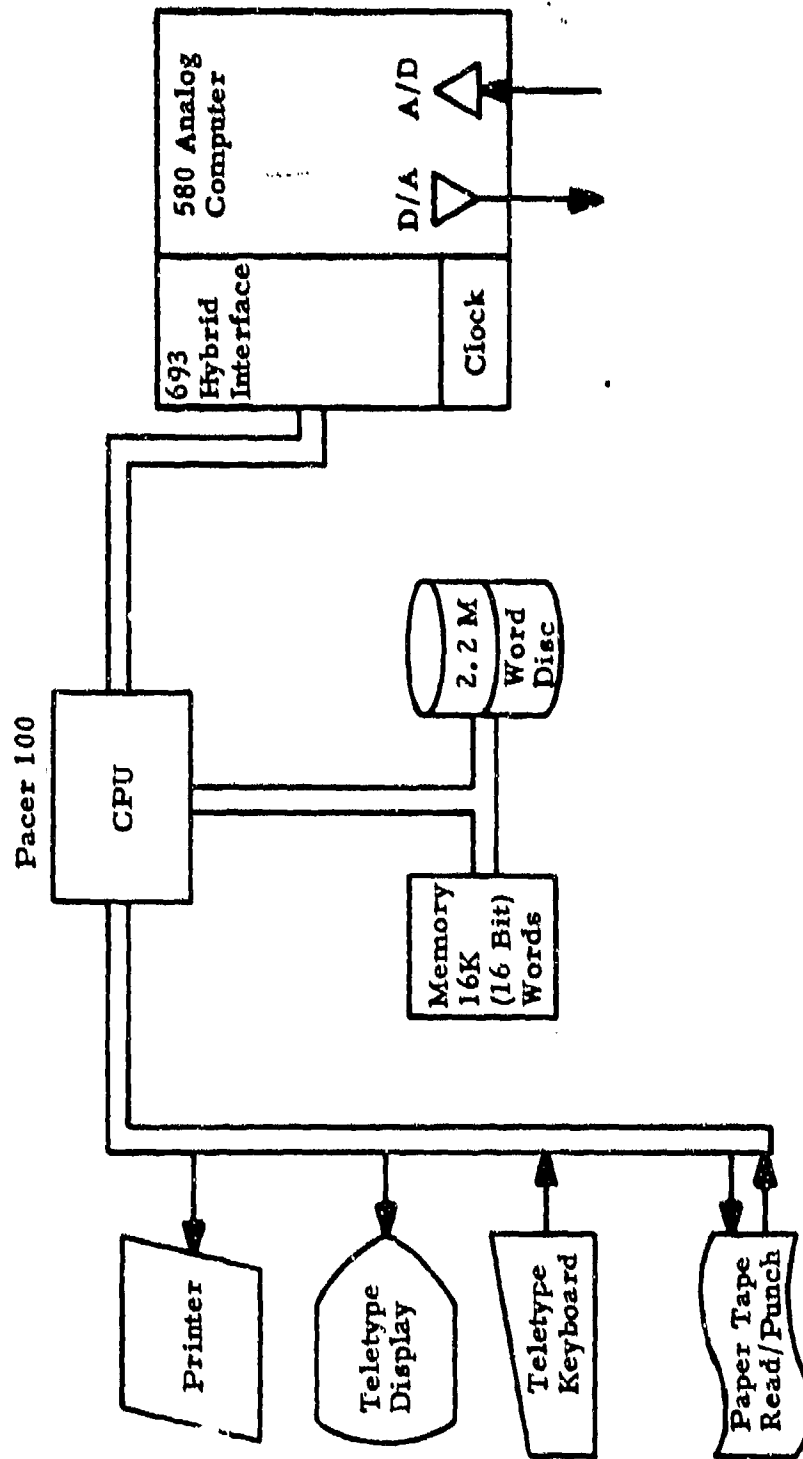


Figure 12. Schematic Diagram of the Control System Hardware

Table 7. Control System Hardware

PACER 100 Computing System

- 16,384 16-bit words of core memory
- Hardware multiply divide
- Priority interrupt system
- Memory protect system
- Power fail/auto restart system
- Five universal controller positions
- 1 Microsecond memory cycle

Direct Memory Access Channel (DMAC)

- Provides for I/O concurrent with computation on cycle stealing basis
- 1 Million words/second

Interval Timer/Real Time Clock

- Provides a high resolution 16 bit real-time clock
- Timer update signal source for four PACER interval timers

Disc Cartridge Controller and One Dual Disk Drive on DMAC

- Provides 1.1 million words of storage on one fixed platter
- Provides 1.1 million words of storage on one removable platter

Hybrid Device Interface 693

- Parallel processor control
- Logical control, sensing and interrupts
- Coefficient device setting
- Data monitoring/display
- Eight channels D/A multiplication (15 bit)
- 15 Channels A/D conversion (13 bit)

Input/Output Devices

- High speed paper tape reader, 300 characters/sec.
- High speed paper tape punch, 120 characters/sec.
- Teletypewriter station (console device), ASR 33
- Line printer, 80 column
- CPU control front panel

Table 7. Control System Hardware (Cont)

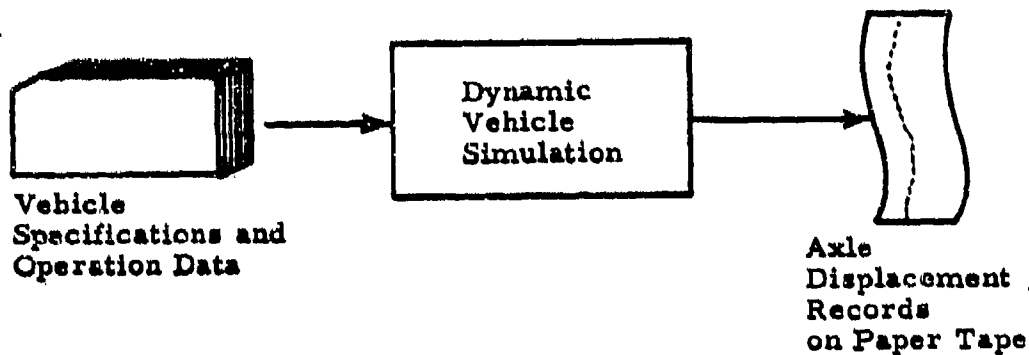
Software Systems

- MHDOS, moving head disc operating system
- FORTRAN IV compiler
- Assembler
- BTE, basic text editor
- CIG, core image generator
- HOI, hybrid operations interpreter
- COP, control options processor
- FIU, file interactive utility
- RTL, run time library
- HLR, hybrid linkage routines
- Applications software packages

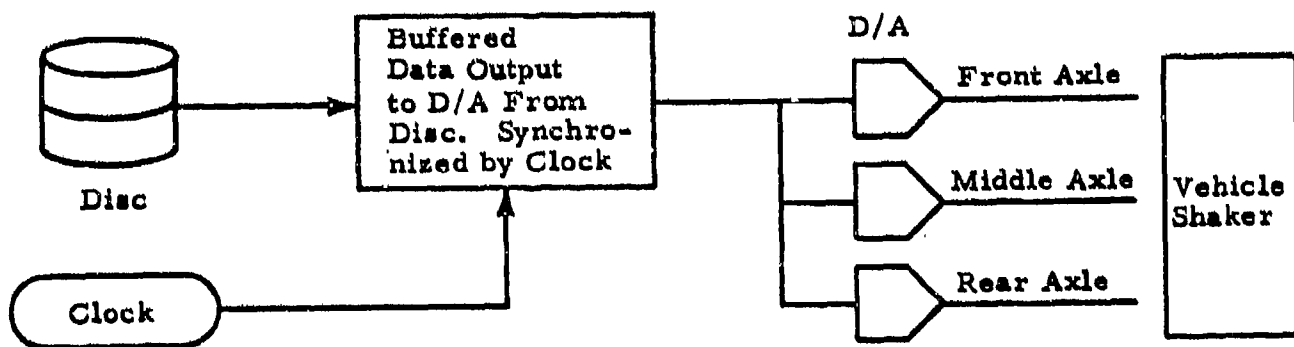
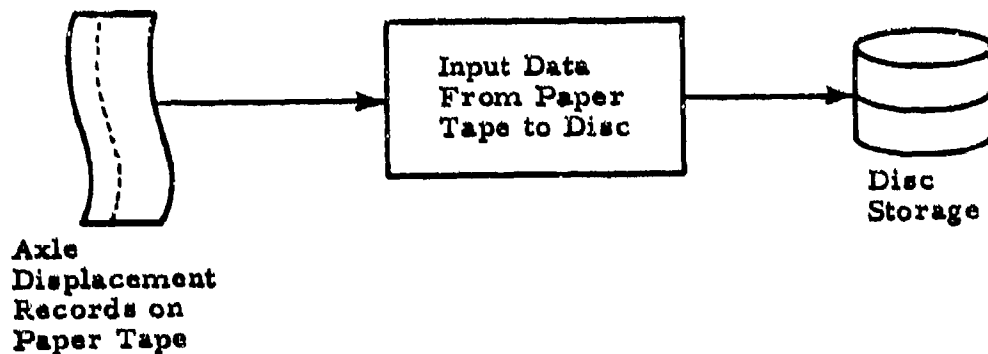
Thus the control system meets all the requirements for the recorded control scheme application. The data transfer rate and the storage capacity are significantly more than those presently required. But, then, room is available for expansion if higher frequency input signals or longer record lengths are required.

3.3 System Operation

The control system reads and stores the axle displacement records generated by the vehicle simulation program. The records are transferred to a buffer and converted to time synchronized analog shaker input signals during a vehicle test. This simple description of the system operation is illustrated by Figure 13. The operation described in the figure requires several steps by the user, such as loading the program into memory, opening and positioning the data file, and initiating execution. A complete description of the operation is presented in the User's Manual (reference 4) and therefore not repeated here. An outline of the operation is, however, shown in Figure 14 and described below.



(a) Task Performed by Vehicle Simulation



(b) Task Performed by Control System

Figure 13. Control System Operation Diagram

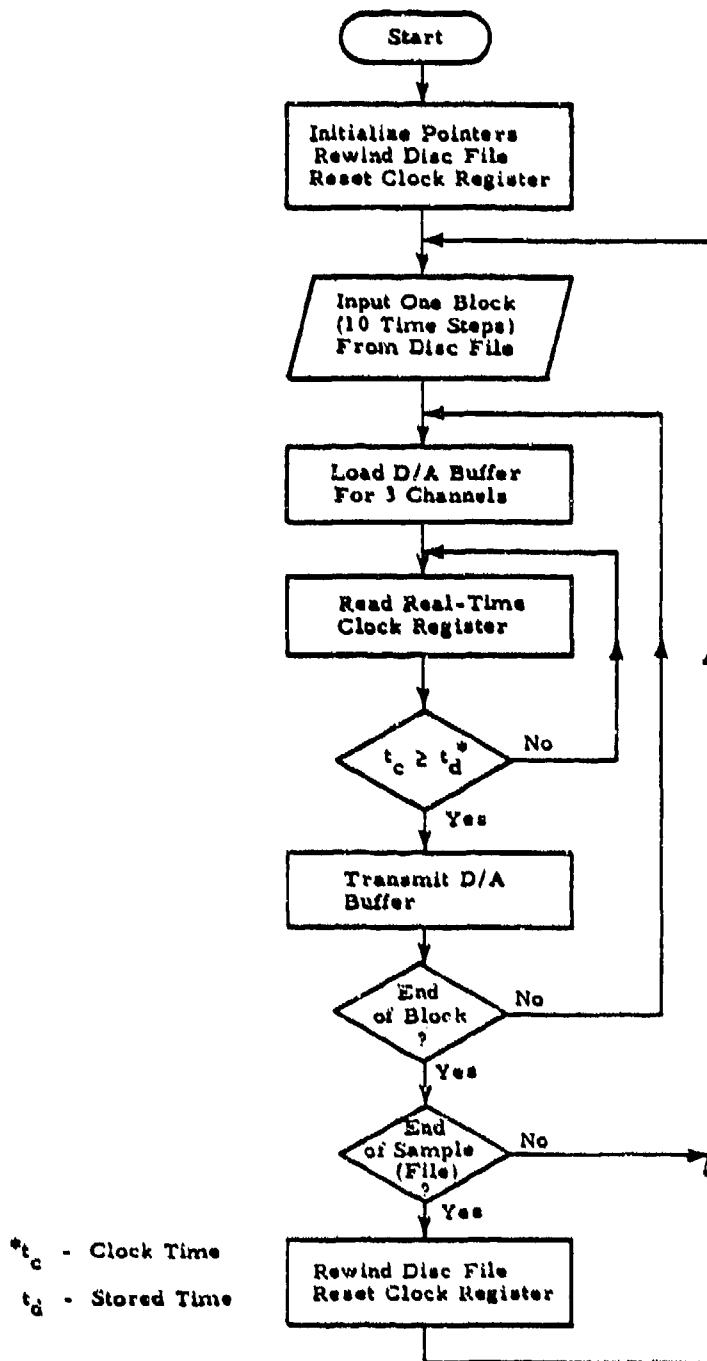


Figure 14. Control Program Flowchart

The operation is initiated by transferring the axle displacement data from the paper tape in blocks of ten time steps to 88 word records on disc. This format of storing data results in the highest rate of data transfer.

The execution begins by setting the control pointers, initializing program parameters and activating the hybrid interface. The clock is reset and a data block containing ten time steps is transferred from the disc to a buffer in core memory. The clock time is then compared with the stored time value. If the clock time is less than the stored time, the system waits until it becomes equal and then transfers the data in the D/A buffer to D/A output. At the end of each block of ten time steps, more data is retrieved from the disc to reside in the buffer.

At the end of each block, the system checks for the end of the axle displacement record. If end of the record is reached, the disc is rewound, the clock register is reset and the process is repeated.

3.4 System Verification

Performance of the control system in generating shaker input signals from axle displacement records is demonstrated by Figures 15, 16, and 17. In these figures, the plots of the three axle displacement records obtained from the vehicle simulation are compared with the outputs of the respective D/A channels. For a conversion factor of 10 volts equals 1 foot, the plots are identical in each case, thereby verifying the system performance.

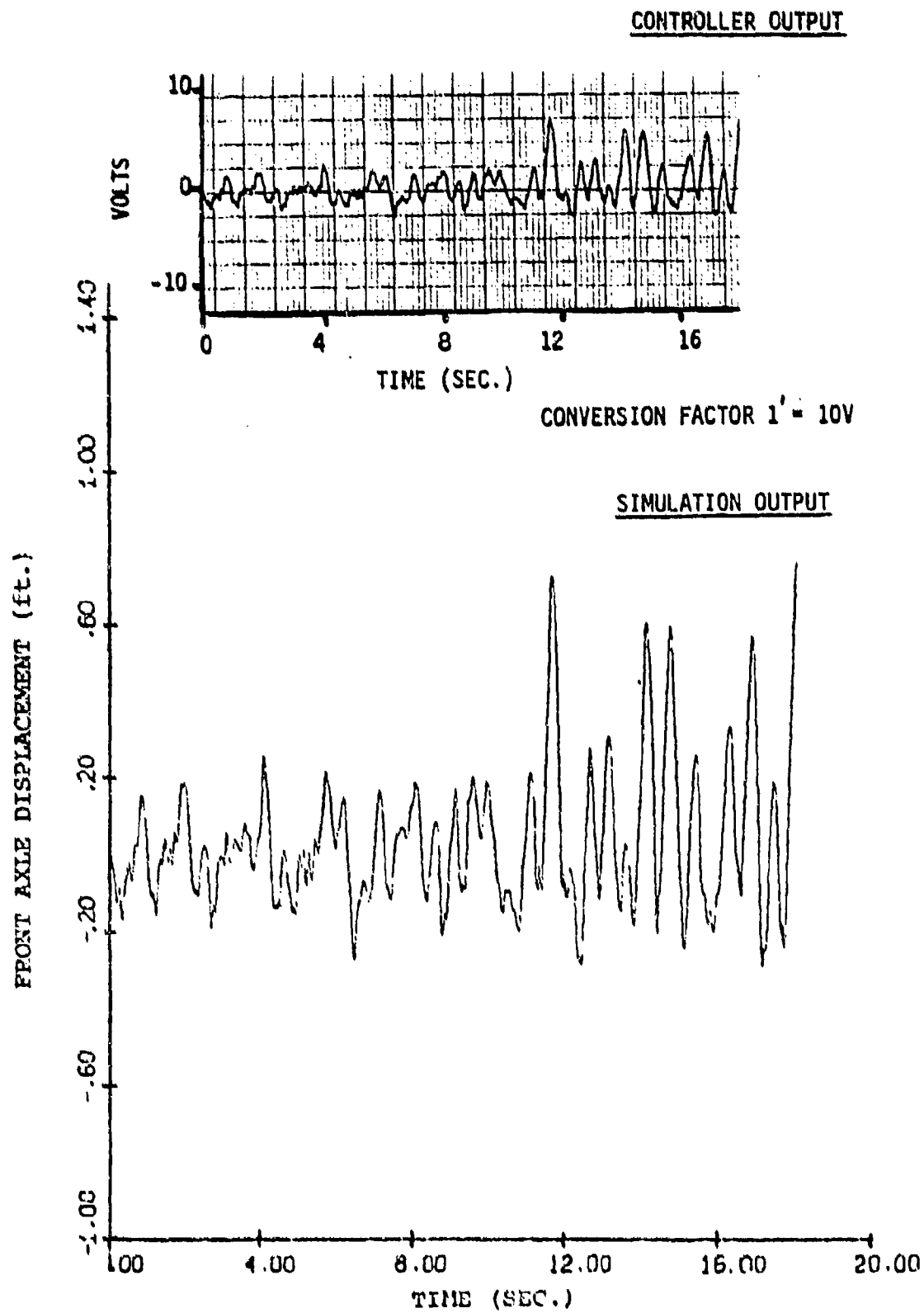
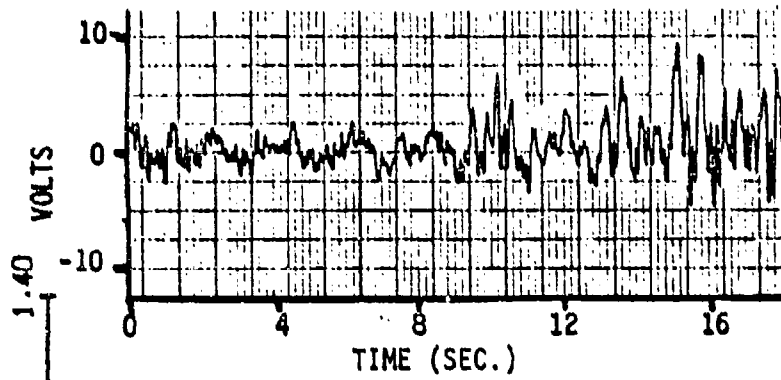


Figure 15. Comparison of the Simulation and the Controller Outputs for the Front Axle Displacement

CONTROLLER OUTPUT



CONVERSION FACTOR
1' = 10V

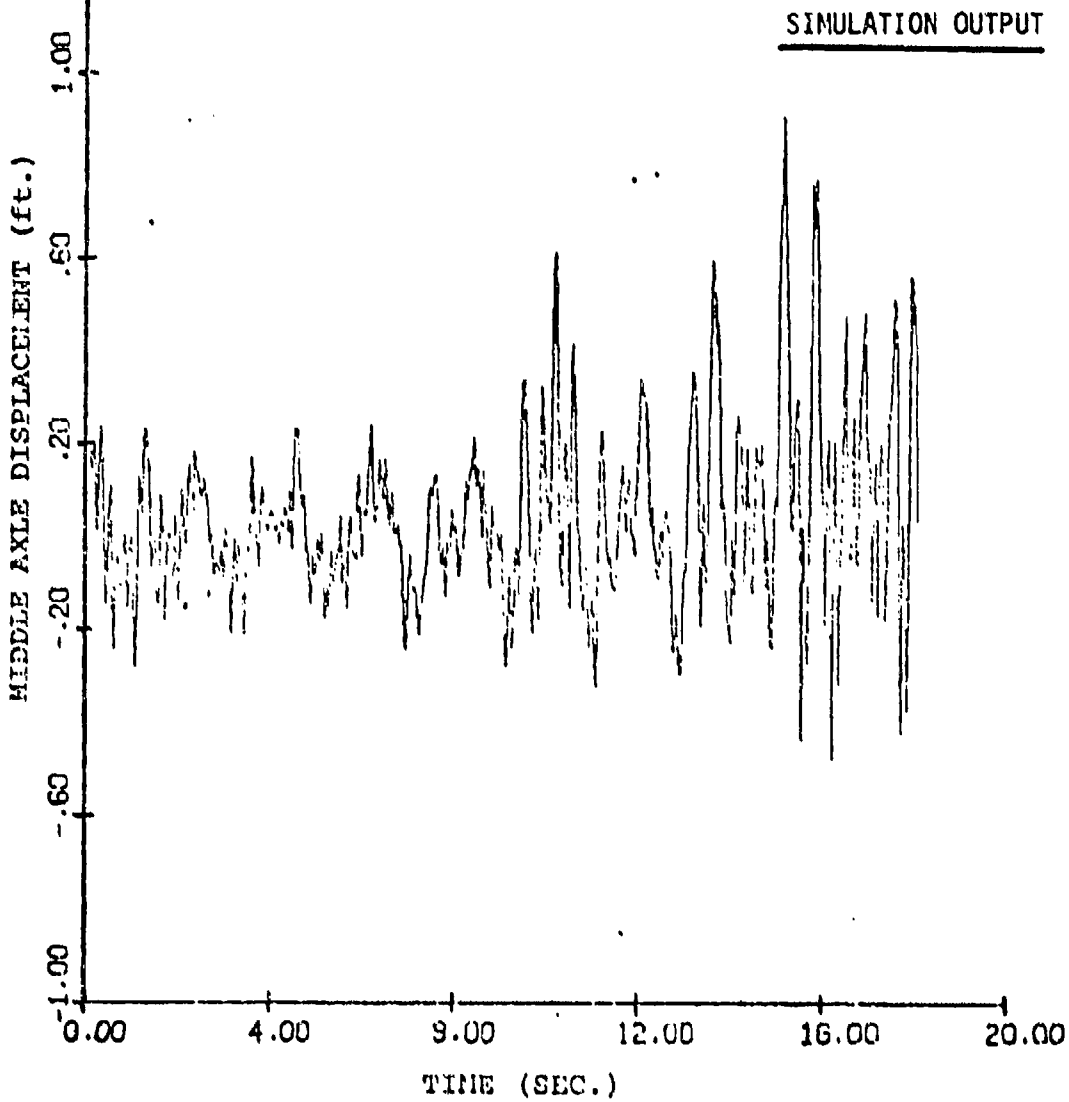


Figure 16. Comparison of the Simulation and the Controller Outputs for the Middle Axle Displacement

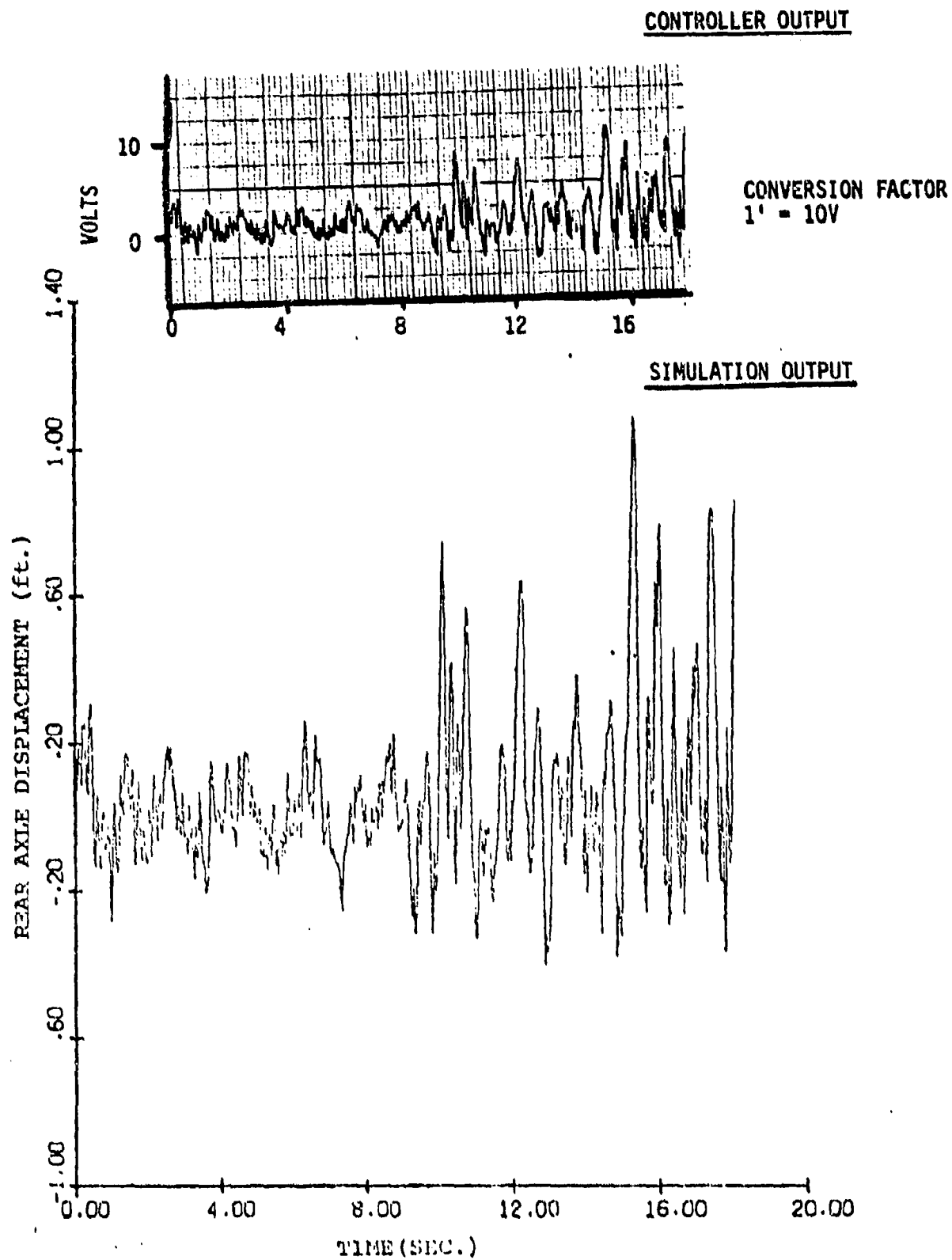


Figure 17. Comparison of the Simulation and the Controller Outputs for the Rear Axle Displacement

4. VERIFICATION

One of the dominant considerations in evaluating merits of a method for testing vehicles in laboratory is correlation of the inputs to the vehicle generated by the test method with those experienced in field environment. Translated to the present application, this means that the axle displacement inputs produced by the recorded simulation control scheme should match the axle displacements experienced by the vehicle for similar conditions in the field environment.

In case of random signals, as those being considered, correlation is best expressed by similarity of the spectral densities. Earlier in the report the spectral densities of the rear axle acceleration, generated by the vehicle simulation program employing various tire models, were compared with the corresponding data obtained in the field test. The axle displacement spectral densities for the same test are now compared to determine if the vehicle experiences similar inputs during both the shake test and field test.

In monitoring the vehicle response during the field test, accelerometers were used to measure axle acceleration spectral densities. These data have to be converted to axle displacement spectral densities before they can be compared with the corresponding input signals generated by the control system. Also, the measured spectral densities have to be plotted against the reduced frequency (Ω), and not frequency in Hertz, because that is the scale used in the analytical results. These transformations are achieved through the following equations.

$$S_{\text{accln}}(f) \left| \begin{array}{l} \text{in} \\ \text{ft/sec}^2 \end{array} \right. = S_{\text{accln}}(f) \left| \begin{array}{l} \text{in} \\ g \end{array} \right. g^2$$

$$S_{\text{accln}}(\Omega) = S_{\text{accln}}(f) \frac{v}{2\pi}$$

$$S_{\text{displn}}(\Omega) = \frac{S_{\text{accln}}(\Omega)}{\omega^4}$$

where

- f = frequency in Hz
- ω = frequency in rad/sec
- Ω = reduced frequency in rad/ft
- V = vehicle velocity in ft/sec
- g = acceleration due to gravity
- S = spectral density

The spectral densities of the front, middle and rear axle ($S_{\text{displn}}(\Omega)$) thus obtained from the field data are then plotted along with the corresponding spectral densities of the axle displacement records produced by the recorded simulation control scheme, as shown in Figures 18, 19 and 20. The figures show that the spectral densities of the axle displacements obtained from the field tests are in good agreement with those generated by the control scheme. Just as discussed in Section 2, employing adaptive footprint model and fixed footprint model generally result in more accurate representation of the field environment than that obtained using point contact or the rigid tread band model.

For all three axle displacements, the agreement amongst the models and the field data is poorest in the low frequency range. In that range, the spectral densities are calculated based on only a small number of complete cycles. Therefore, there is a scatter in the model predictions. If the profile length is increased, the scatter will reduce and the models will agree better with the test data.

For the front axle displacement results, the adaptive tire model is able to duplicate the field test data quite accurately up to about 20 Hz. At higher frequencies the field data has higher power content than that predicted analytically. This is partially due to noise in the signal recording system.

In Figure 19, the advantages of employing either the fixed footprint model or the adaptive footprint model become more apparent. Using these models produces axle displacement signals which duplicate the field axle displacements quite accurately, whereas using the point contact model overestimates the spectral density by a factor of 10^3 in the 10-30 Hz range. Similar conclusions can be drawn from the results shown in Figure 20. (A spike in the field data signal in this case at about 60 Hz may be due to the noise in the spectral density generating system.)

A generally good agreement between the analytical and the field test results, shown in the figures, proves that the scheme is able to provide the vehicle with realistic inputs. Thus, the scheme meets its development objective.

FRONT AXLE DISPLN

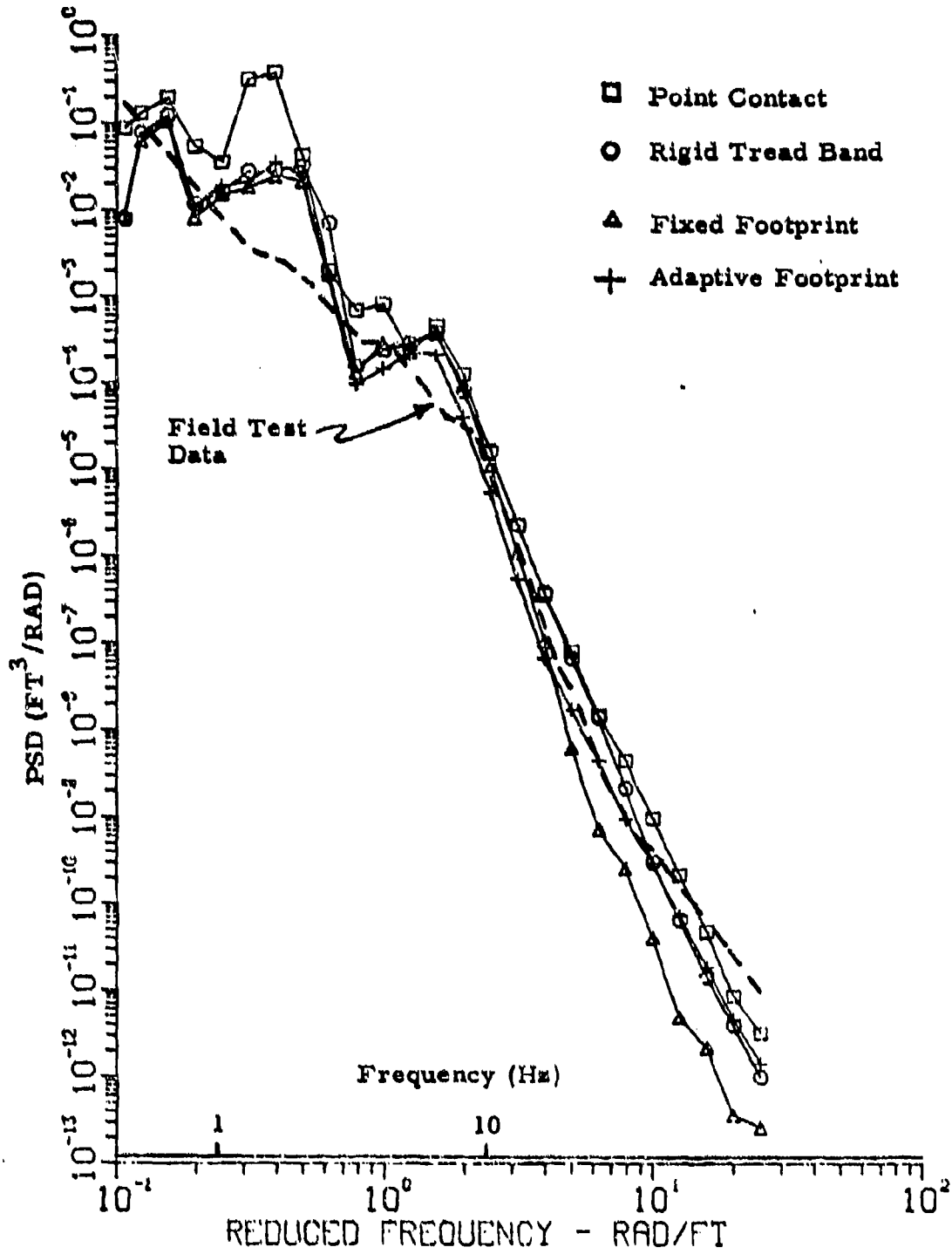


Figure 18. Simulated Response - Front Wheel Displacement

MIDDLE AXLE DISPLN

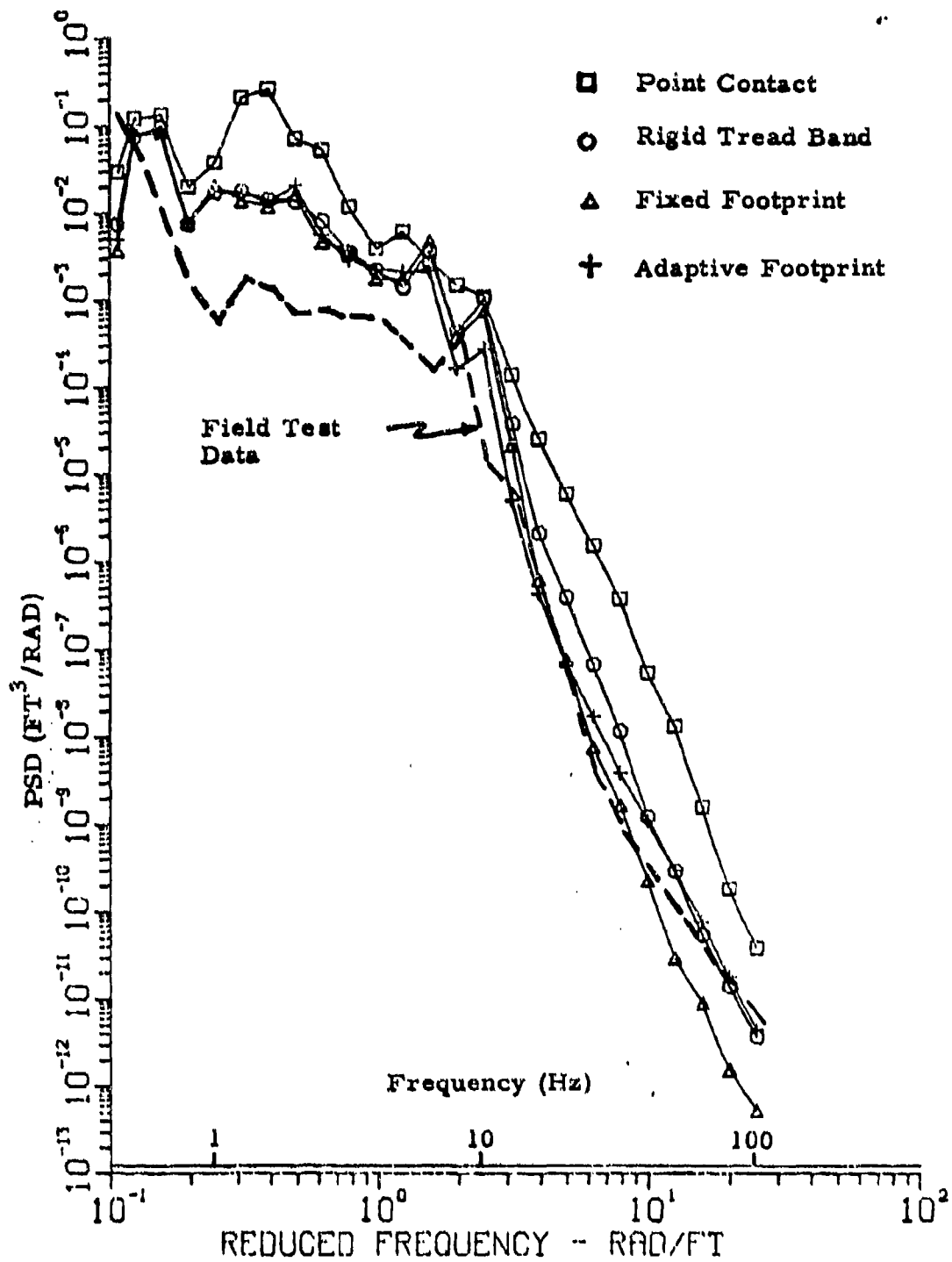


Figure 19. Simulated Response - Middle Wheel Displacement

REAR AXLE DISPLN

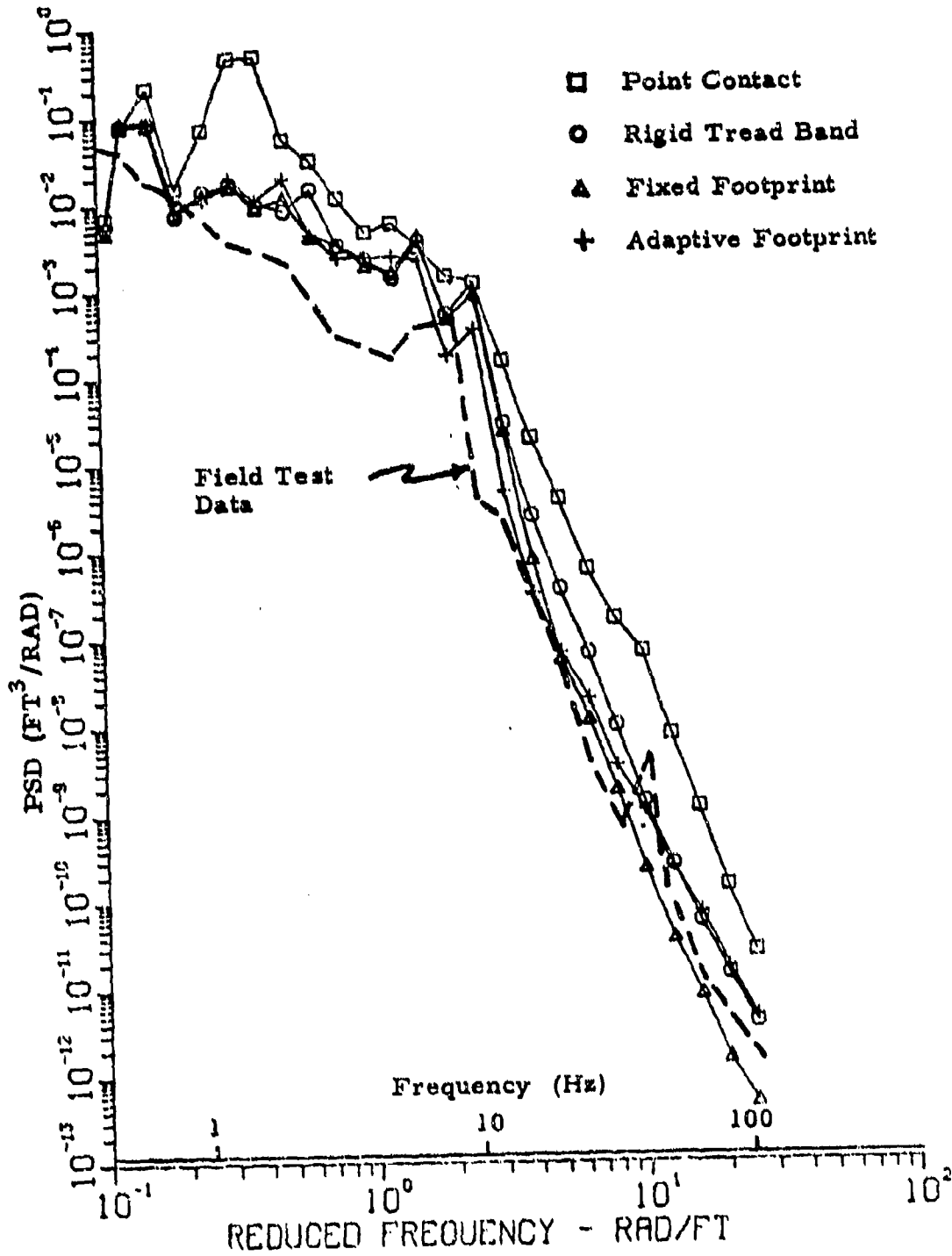


Figure 20. Simulated Response - Rear Wheel Displacement

5. CONCLUSIONS

The recorded simulation control scheme is developed to provide a method of testing vehicles in laboratory without requiring field data. For a particular vehicle, the scheme involves simulating vehicle operation over a terrain of interest at a given speed. The simulation generates records of axle displacements which can be played back to provide the vehicle shakers with realistic inputs. Of the two steps involved in the recorded simulation control scheme, the first step, i. e. producing axle displacement records, uses a terrain-tire-vehicle computer program. The second step is performed by a control system which stores the axle displacement records and converts them to time-synchronized analog signals during a shake test.

The vehicle simulation program incorporates four different models of tires. Applicability of these tire models is explored by comparing the simulation results with those obtained during field testing of an M-809 cargo truck. The comparison shows that the adaptive footprint model provides superior tire force predictions, due to its ability to envelop ground irregularities through local footprint deformations. Vehicle simulations using the adaptive footprint model are well able to predict the principal natural frequencies of vehicle vibration, and the simulated response agrees closely with field trial data, particularly in the middle and upper frequency range. Since many shake test failures are caused by high-frequency stress reversal (fatigue), the adaptive footprint model is particularly well-suited for simulating fatigue failures in the laboratory.

The fixed footprint model, while not as advanced as the adaptive footprint model, also provides improved force predictions. Since this model can be simulated by an equivalent point contact model in series with a filter (see Appendix A), it will be a viable alternative for simulations in which the computational requirements are to be minimized. The simpler tire models (i. e., the point contact and rigid tread band models) generally overestimate the tire forces, particularly at high frequencies (i. e., typically in the 5-50 Hz region), and their use will be governed by this limitation.

The control system performs its function adequately. The system is able to store the axle displacement records obtained from the vehicle simulation program on a magnetic disc and, at the time of shake test, produces continuous analog input signals by repeating the limited length records. These analog signals are synchronized perfectly to the real time and there is no detectable difference between the analog output and the digital input to the control system.

The axle displacement signals obtained are compared to the corresponding signals recorded in a field test. Both signals show similar spectral densities, thereby proving that the recorded simulation scheme is able to provide adequate control to the vehicle shaker.

6. RECOMMENDATIONS

The recorded simulation control scheme described in this report can be used in many ways to improve performance of vehicles. The scheme can be employed, for example, to carry out a study of fatigue failures of vehicle components by shake testing the vehicle for extensive periods of time. The tests can be repeated for different terrains and speeds and, from the test results, modifications to prevent such failures can be suggested.

A study to select optimum tires for a particular application can be performed using the control scheme. In such a study, data for candidate tires can be obtained from manufacturers and performance of the vehicle incorporating those tires can be determined using the vehicle simulation program and the shake test facility. A comparison criteria, such as the maximum speed at which the driver motion becomes unacceptably large, can evaluate performance of various tires and the optimum tire can be selected.

The recorded simulation control scheme can also be used to carry out a parametric analysis of vehicles. Effects of changing various parameters, such as the suspension spring rates, damping coefficients, center of gravity location, etc., on vehicle performance can be predicted by the computer simulation program and verified by the shake test facility. Such a parametric analysis can be helpful in designing new vehicles or modifying the existing ones.

The recorded simulation scheme itself can be modified to expand its capabilities. For example, the core memory incorporated in the present control system, which is sufficient to perform record storing and input signal supplying steps of the scheme, can be increased, so that the vehicle simulation program can be executed on the control system and the intermediate step of preparing axle displacement records on paper-tapes (or some such medium) can be eliminated. The control system can also be

modified to record outputs of various transducers monitoring performance of the vehicle. These records can then be processed to obtain statistical information, such as spectral densities and cross-correlation of the variables describing vehicle performance.

The vehicle simulation program can be expanded to include roll motion of the vehicle. Also, the fore-and-aft forces generated by the simulation can be used in vehicle testing if the vehicle shaker is suitably modified.

A final suggestion for future work is to develop synthesized simulation control (described in Chapter 1) because this scheme eliminates the task of storing the axle displacement records. Also, by using random signal generators, biases which are present in the stored records are removed. However, developing such a scheme may need significant software and/or hardware development. Meanwhile, the recorded simulation control scheme can provide an improved method for laboratory testing of vehicles.

APPENDIX A

THE TIRE MODELS

Details of the four tire models are presented in the following:

A-1. Point Contact Tire Model

The schematic diagram of the point contact tire model is shown in Figure A-1. The terrain elevation coordinate y_0 is measured positive upwards from the mean line and is a function of the distance x . The wheel center motion coordinate y_1 is measured positive upwards from the initial equilibrium position; i. e., with the tire statically loaded under the vehicle weight and $y_0 = 0$. F_v and F_h are the vertical and horizontal components of footprint force. F_y and F_x are the tire forces transmitted to the vehicle suspension. The principal assumptions of the analysis are:

1. The tire mass is concentrated at the wheel center.
2. Terrain contact occurs at a single point vertically below the wheel center.
3. The total footprint force acts normal to the terrain surface at the contact point.
4. When in contact, forces between the follower and the ground must be compressive. When the contact force becomes zero, the follower leaves the ground (wheel hop).

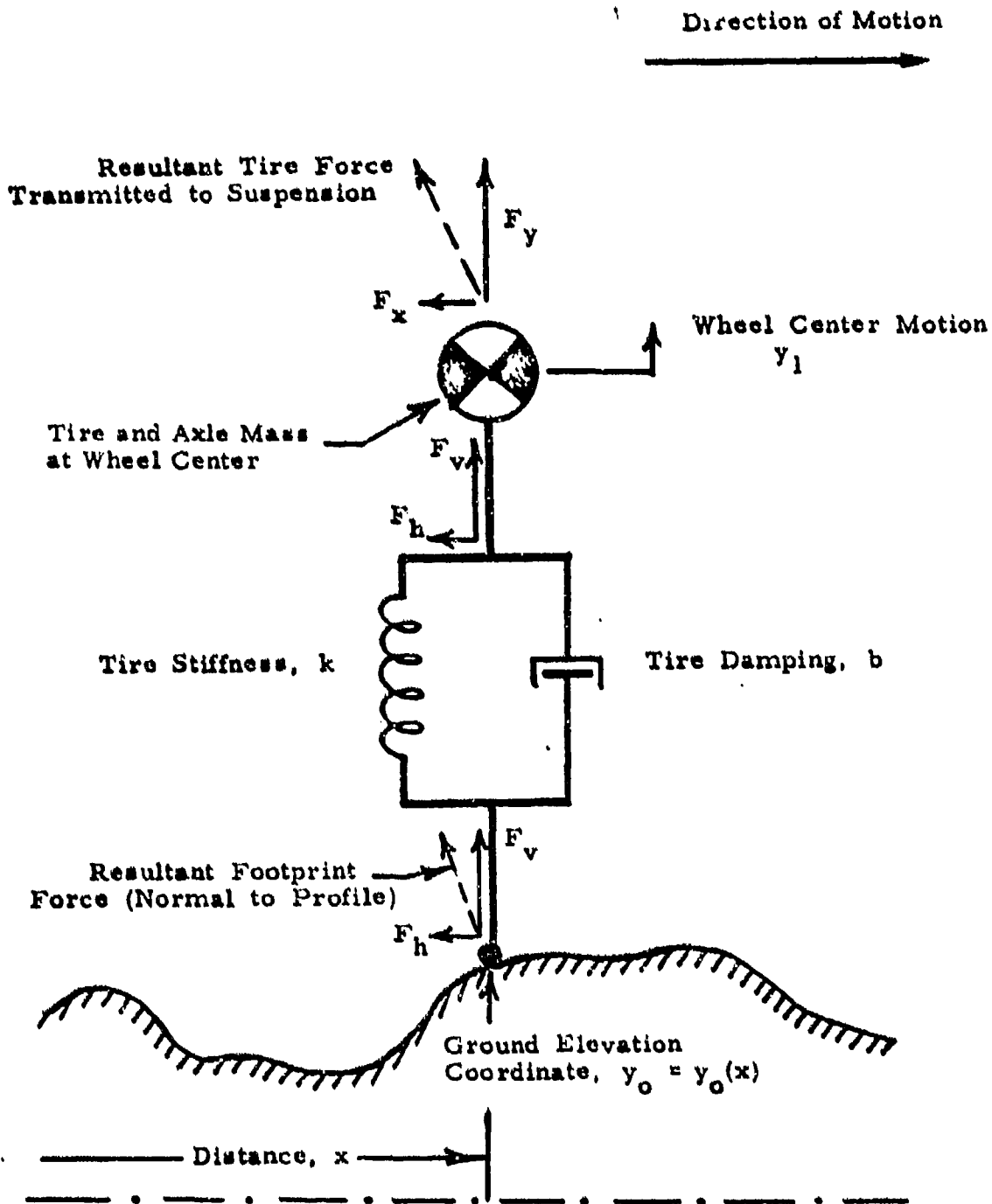


Figure A-1. Schematic Diagram of Point Contact Tire Model

5. The tire force-deflection characteristics are represented, in general, by nonlinear stiffness k and damping b . In general, k and b can be functions of the tire deflection and deflection rate.

For arbitrary vertical displacements and velocities y_0 , y_1 , \dot{y}_0 , \dot{y}_1 the total spring-damper force is

$$F = \int_0^{y_{st} + y_0 - y_1} k dy + \int_0^{\dot{y}_0 - \dot{y}_1} b d\dot{y} \quad (A-1)$$

where y_{st} is the static deflection of the tire under the equilibrium load W , and \dot{y}_0 is the time rate of change of profile elevation seen by the follower due to tire motion. y_{st} and \dot{y}_0 are found from

$$\int_0^{y_{st}} k dy = W \quad (A-2)$$

$$\dot{y}_0 = V(dy_0/dx) \quad (A-3)$$

where V is the forward velocity (dx/dt) and (dy_0/dx) is the slope of the ground at the contact point.

The vertical footprint force F_v will be equal to F when the follower is in ground contact ($F > 0$) or zero when the follower is out of contact ($F \leq 0$)

$$\left. \begin{array}{l} F_v = F \quad ; \quad F > 0 \\ F_v = 0 \quad ; \quad F \leq 0 \end{array} \right\} \quad (A-4)$$

Since the resultant footprint force acts normal to the terrain, the fore-and-aft force component F_h is related to the vertical component F_v as follows.

$$F_h/F_v = dy_o/dx \quad (A-5)$$

Equations (A-1) to (A-5) determine the footprint forces F_v and F_h . The tire forces transmitted to the vehicle suspension, F_y and F_x , are determined from the equations below.

$$F_y = F_v - m\ddot{y}_1 \quad (A-6)$$

$$F_x = F_h \quad (A-7)$$

A-2. Rigid Tread Band Model

The schematic diagram of the rigid tread band model is shown in Figure A-2. Comparison with the point contact model of Figure A-1 shows that it is equivalent to a point contact model traversing a modified terrain profile $\bar{y}_o(x)$ obtained from the tread band center motion. Therefore, the analysis and equations for the point contact model shown in the previous section remain unchanged,* and it is only necessary to find the modified profile $\bar{y}_o(x)$ in terms of the original terrain profile $y_o(x)$ and the tread band radius r .

Because of the presence of the circular tread band, the terrain contact point will in general be shifted a distance \bar{x} fore or aft of the wheel center as illustrated in Figure A-2. From geometry, the tread band center height \bar{y}_o at any location x , is given by

$$y_o(x) = y_o(x + \bar{x}) + \sqrt{r^2 - \bar{x}^2} \quad (A-8)$$

*The criterion for wheel hop also remains unchanged, i. e., when the contact force goes to zero, the wheel leaves the ground.

Direction of Motion

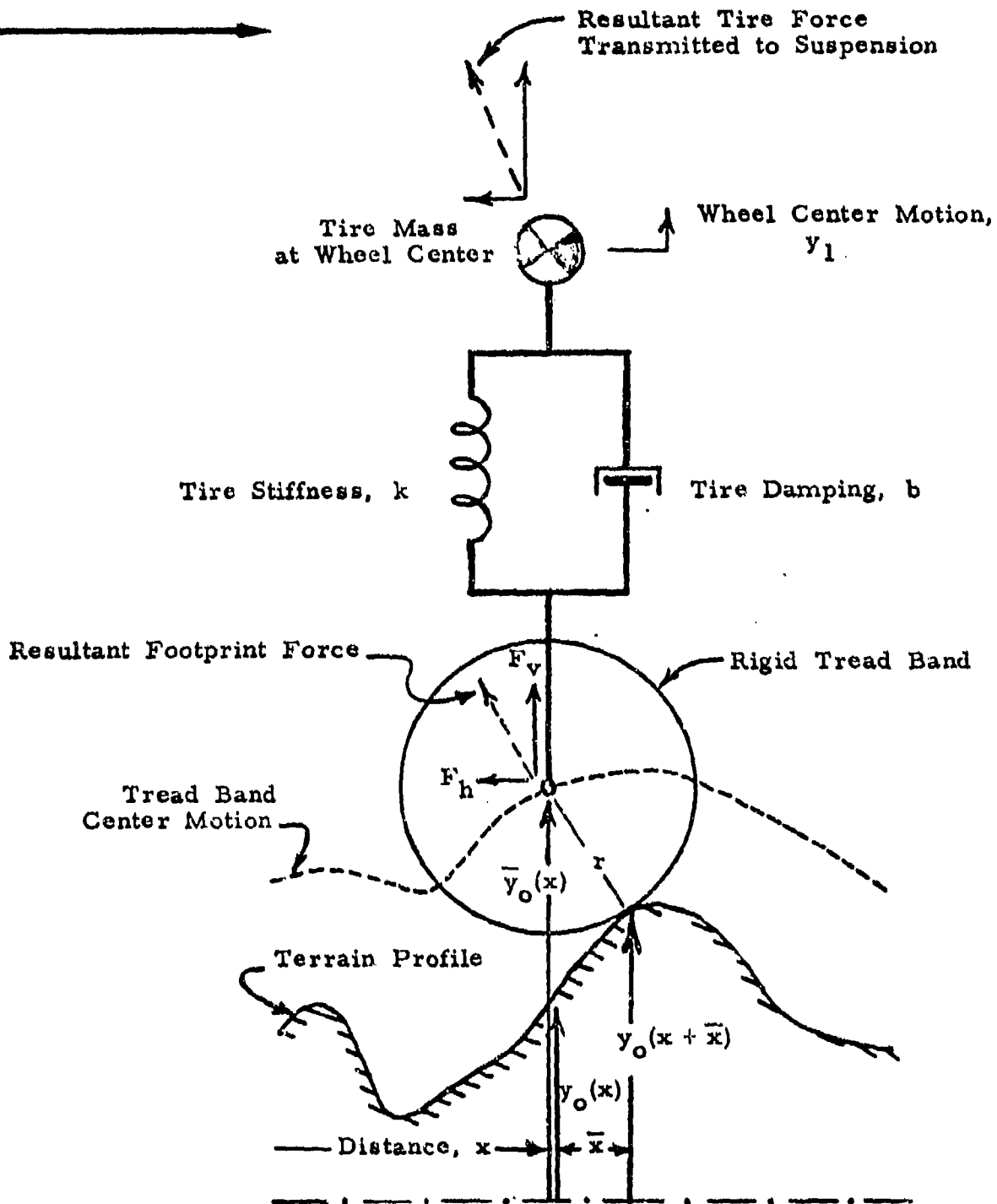
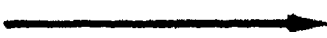


Figure A-2. Schematic Diagram of Rigid Tread Band Tire Model

The criterion for determining \bar{x} is that, at the contact point, the slope of the tread band and the terrain profile must be equal. The terrain profile slope at the contact point is $d[y_0(x + \bar{x})]/d\bar{x}$. The slope of the tread band at this point is $-d(\sqrt{r^2 - \bar{x}^2})/d\bar{x}$. Equating these two slopes, the condition that must be satisfied at the contact point is

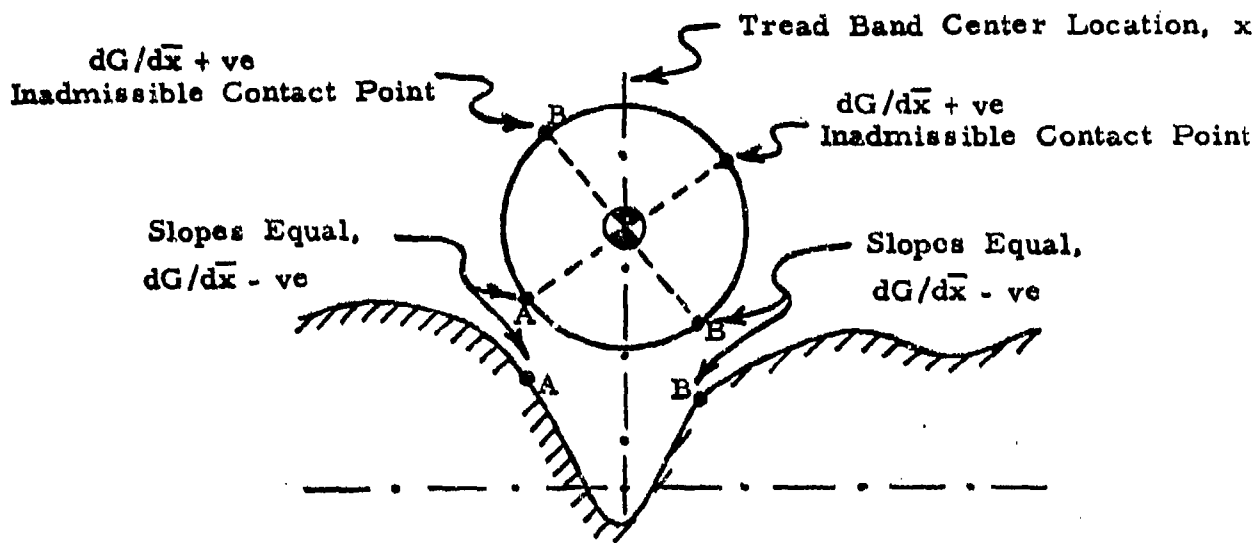
$$G = \frac{d}{d\bar{x}} \left[y_0(x + \bar{x}) + \sqrt{r^2 - \bar{x}^2} \right] = 0 \quad (A-9)$$

Solution of the above equation determines the contact offset distance \bar{x} in terms of the tire location x and radius r . In general, the roots of Equation (A-9) will give two values of \bar{x} corresponding to diametrically opposite points having equal slope, as shown in Figure A-3. Physically, contact can only occur in the lower half of the tread band, and for this point $dG/d\bar{x}$ will be negative. Solutions of Equation (A-9) can also give multiple pairs of \bar{x} values implying that the slope condition can be satisfied at several points on the lower half of the tread band. In such cases, the highest value of $y_0(x)$ found from Equation (A-8) will represent the physically realizable condition. The other values can only be satisfied through tread band deformations as illustrated in Figure A-3. A section of modified profile obtained as described above through wheel center filtering is included in Figure 7. The original profile from which the modified profile was derived is also included in this figure.

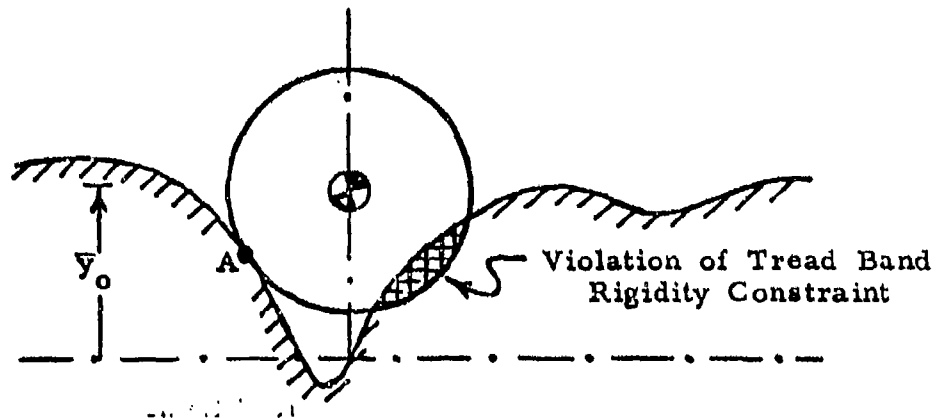
Thus Equations (A-8) and (A-9) along with the criteria for selecting the physically admissible root allow determination of the tread band center motion $\bar{y}_0(x)$, which along with Equations (A-1) through (A-7) constitute the rigid tread band analytical model.

A-3. Fixed Footprint Model

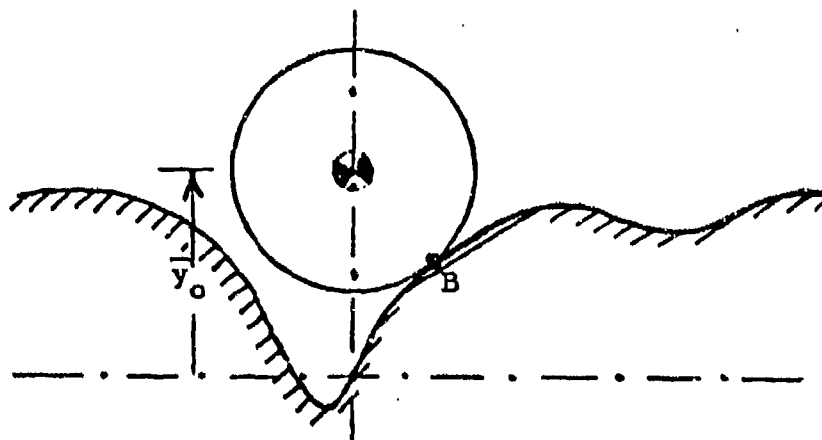
The schematic diagram for the fixed footprint model is shown in Figure A-4. In this model, terrain contact occurs over a finite footprint length L , and the tire stiffness and damping is uniformly distributed over the contact length. The principal assumptions of the



(a) Physical Representation of Roots of Equation (A-7)



(b) Inadmissible Contact



(c) Admissible Contact

Figure A-3. Determination of Admissible Terrain Contact Point

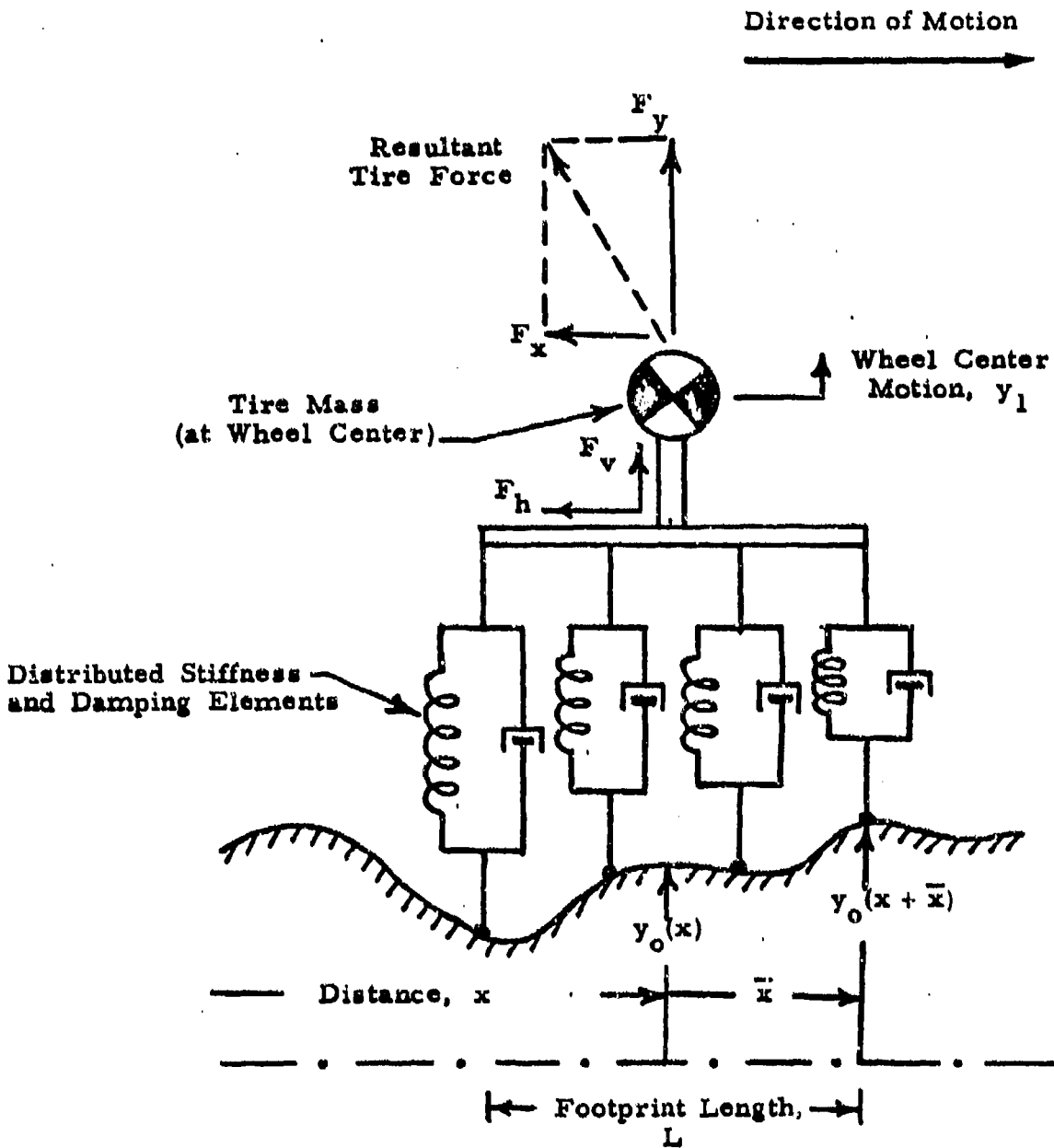


Figure A-4. Schematic Diagram of Fixed Footprint Tire Model

analysis are summarized below.

1. The tire mass is concentrated at the wheel center.
2. Terrain contact occurs through a footprint of fixed size, independent of tire deflection.
3. The footprint center is constrained to lie vertically below the wheel center.
4. The footprint force components act normal to the local terrain surface.
5. When in contact, the resultant footprint pressure force must be compressive, and all parts of the footprint must contact the ground. When this force becomes zero, the complete footprint leaves the ground.
6. The tire fore-deflection characteristics are represented, in general, by nonlinear stiffness and damping uniformly distributed over the footprint.

For arbitrary vertical displacements and velocities $y_0(\bar{x})$, y_1 , $\dot{y}_0(\bar{x})$, \dot{y}_1 the total force in the distributed spring-damper elements is

$$\begin{aligned}
 F = & \int_{-L/2}^{+L/2} \int_0^{y_{st} + y_0(\bar{x}) - y_1} k' dy d\bar{x} \\
 & + \int_{-L/2}^{+L/2} \int_0^{\dot{y}_0(\bar{x}) - \dot{y}_1} b' d\dot{y} d\bar{x} \quad (A-10)
 \end{aligned}$$

where y_{st} is the (uniform) static deflection of the footprint under the equilibrium load W , $y_o(\bar{x})$ is the profile elevation as a function of the footprint length coordinate \bar{x} , and $\dot{y}_o(\bar{x})$ is the time rate of change of profile elevation at any location \bar{x} within the footprint due to tire forward motion. y_{st} and $\dot{y}_o(\bar{x})$ are found from

$$\int_0^{y_{st}} k' L dy = W \quad (A-11)$$

$$\dot{y}_o(\bar{x}) = V \frac{d y_o(\bar{x})}{d\bar{x}} \quad (A-12)$$

where V is the forward velocity and $dy_o(\bar{x})/d\bar{x}$ is the local slope of the ground at the footprint location \bar{x} .

As discussed in Section A-1, for the point contact model, the footprint force F_v is given by

$$\left. \begin{aligned} F_v &= F & ; & \quad F > 0 \\ F_v &= 0 & ; & \quad F \leq 0 \end{aligned} \right\} \quad (A-13)$$

and

$$F_h/F_v = \frac{d y_o(x)}{dx} \quad (A-14)$$

Equations (A-10) to (A-14) determine the footprint forces F_v and F_h for the fixed footprint tire model. The tire forces transmitted to the vehicle, F_y and F_x , are determined from the basic tire model equations, Equations (A-6) and (A-7).

$$F_y = F_v - m\ddot{y}_1$$

$$F_x = F_h$$

For the special case of linear stiffness and damping, the fixed footprint tire model is equivalent to a point contact model having the same total stiffness and damping (i. e., $k = k'L$, $b = b'L$) and travelling over a modified terrain profile such that each point on the modified profile is the mean value of the original profile taken over the footprint, i. e.,

$$\bar{y}_o(x) = \frac{1}{L} \int_{-L/2}^{+L/2} y_o(x + \bar{x}) d\bar{x} \quad (A-15)$$

This is equivalent to reducing the amplitude of every Fourier component of the original profile by a factor of $\text{Sin}(\pi L/\lambda)/(\pi L/\lambda)$ where λ is the wavelength of the component considered. A section of filtered profile obtained as described above is included in Figure 7. The original profile from which this was derived is also shown in the figure.

A-4. Adaptive Footprint Model

The schematic diagram for the adaptive footprint tire model is shown in Figure A-5. In this model, terrain contact occurs over a footprint of finite length, which is dependent on tire deflection. Tire stiffness and damping is uniformly distributed over the angular segment that includes the contact zone. The principal assumptions of the analysis are summarized below.

1. The tire mass is concentrated at the wheel center.
2. Every tread element deforms independently of its neighbors and contacts the terrain in the footprint zone. The tire retains its original shape outside the footprint.

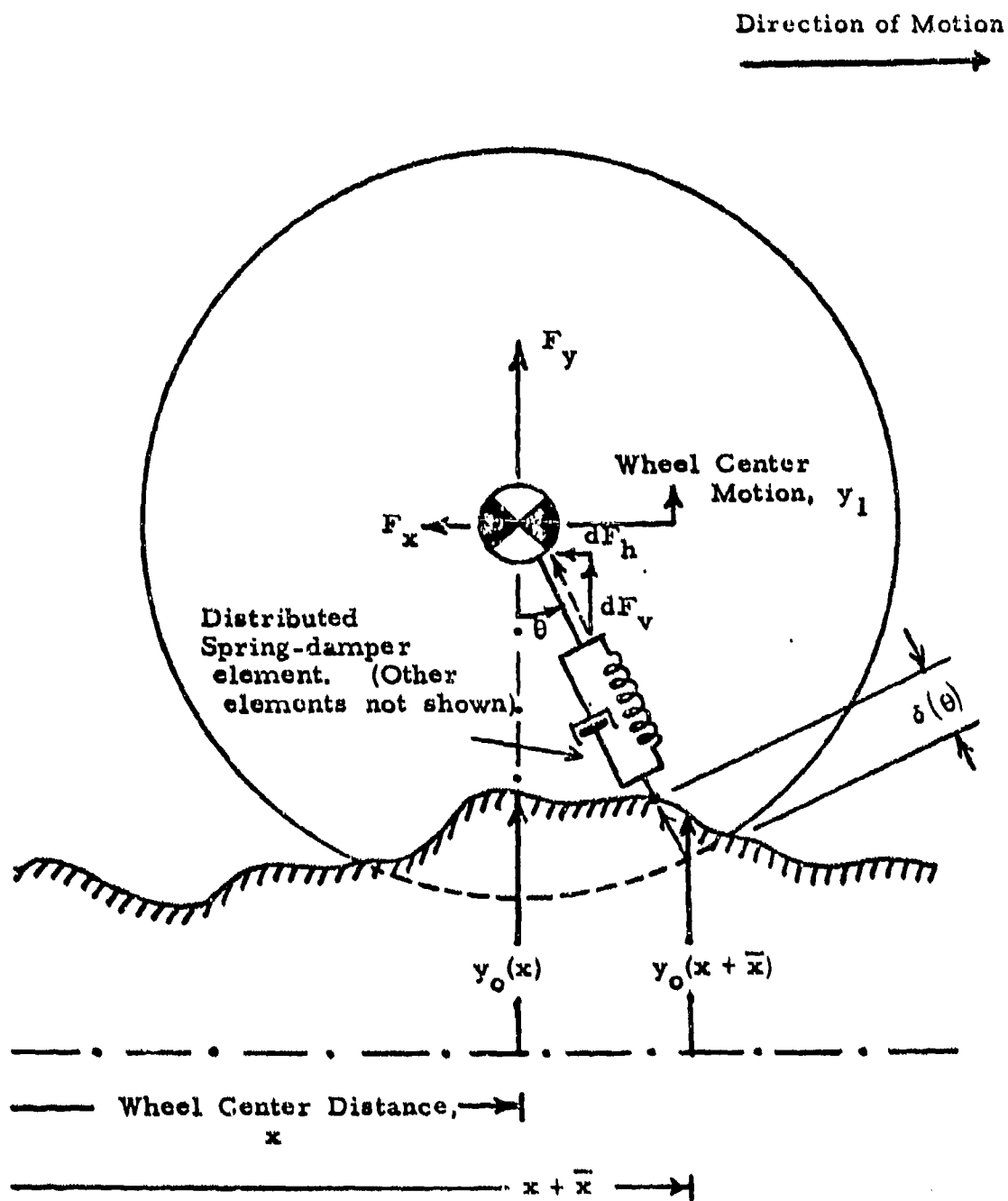


Figure A-5. Schematic Diagram of Adaptive Footprint Tire Model

3. The tire force-deflection characteristics are represented as follows:

- (a) By a constant inflation pressure p_i acting over the footprint area.
- (b) By distributed nonlinear radial stiffness k'' and damping b'' to simulate carcass load contributions. As in the other models, k'' and b'' can be functions of the tire deflection and deflection rate.

For arbitrary vertical displacements $y_o(\bar{x})$, y_1 , $\dot{y}_o(\bar{x})$, \dot{y}_1 , the force components dF_h and dF_v due to deflection of a tread element oriented at an angle θ to the vertical (initial distance \bar{x} from the wheel center) is given by

$$\left. \begin{aligned}
 dF_v(\theta) &= dF_c \cos\theta + \frac{p_i B r d\theta}{\sqrt{1 + \left[\frac{dy_o(\bar{x})}{d\bar{x}}\right]^2}} & dF_c > 0 \\
 dF_v(\theta) &= 0 & dF_c \leq 0
 \end{aligned} \right\} \text{(A-16)}$$

$$\left. \begin{aligned}
 dF_h(\theta) &= dF_c \sin\theta + \frac{p_i B \left[dy_o(\bar{x})/d\bar{x}\right] r d\theta}{\sqrt{1 + \left[\frac{dy_o(\bar{x})}{d\bar{x}}\right]^2}} & dF_c > 0 \\
 dF_h(\theta) &= 0 & dF_c \leq 0
 \end{aligned} \right\} \text{(A-17)}$$

where

$$dF_c = \left[\int_0^{\delta(\theta)} k'' dy + \int_0^{\dot{\delta}(\theta)} b'' d\dot{y} \right] d\theta \quad (A-18)$$

and

$$\bar{x} = r \sin \theta \quad (A-19)$$

In Equations (A-16) and (A-17), the first term represents the carcass force contribution, and the second gives the inflation pressure force. In these equations

- B - effective footprint width
- $\frac{dy_o(\bar{x})}{d\bar{x}}$ - local slope of terrain profile at contact point
- $\delta(\theta)$ - radial deflection of tread element oriented at angle θ from vertical
- $\dot{\delta}(\theta)$ - radial velocity of tread element due to tire motion.

The radial deflection $\delta(\theta)$ is the sum of the initial deflection $\delta_{st}(\theta)$ due to the equilibrium load W , and the deflection due to terrain irregularity $y_o(\bar{x})$ and wheel center motion y_1

$$\delta(\theta) = \delta_{st}(\theta) + \left[y_o(x+\bar{x}) - y_1 \right] / \cos \theta \quad (A-20)$$

and

$$\dot{\delta}(\theta) = \left\{ v \left[\frac{dy_o(x+\bar{x})}{d\bar{x}} \right] - \dot{y}_1 \right\} / \cos \theta \quad (A-21)$$

The initial radial deflection $\delta_{st}(\theta)$ at location θ under the static vehicle weight is found from solution of the following three simultaneous equations

$$\int_{-\theta_0}^{+\theta_0} \int_0^{\delta_{st}(\theta)} \cos \theta k'' dy d\theta + p_i A = W \quad (A-22)$$

$$\theta_0 = \cos^{-1} \left(\frac{r - y_{st}}{r} \right) \quad (A-23)$$

$$\delta_{st}(\theta) = \frac{y_{st} - r(1 - \cos \theta)}{\cos \theta} \quad (A-24)$$

where y_{st} is the equilibrium tire deflection at the footprint center ($\theta = 0$), and A is the effective contact area at equilibrium.

The effective tire width B is equal to the effective area divided by the footprint length,

$$B = A/2r \sin \theta_0 \quad (A-25)$$

Finally, the total vertical and horizontal components of footprint force, F_v and F_h , can be obtained by integrating Equations (A-16) and (A-17) over the lower half of the tire, where terrain contact is possible

$$F_v = \int_{\theta = -\pi/2}^{\theta = +\pi/2} dF_v(\theta) \quad (A-26)$$

$$F_h = \int_{\theta = -\pi/2}^{\theta = +\pi/2} dF_h(\theta) \quad (A-27)$$

The forces transmitted to the vehicle suspension, F_y and F_x , can then be found from Equations (A-6) and (A-7) as before.

APPENDIX B
THE VEHICLE MODEL

The vehicle model includes all the vehicle components excluding the tires. The tire model is derived separately (see Appendix A) and the general tire model variables are converted to the vehicle model variables as shown in Table B-1. The vehicle model consists of the following elements: the hull, the bogie, the front suspension, the middle suspension, the rear suspension, the front unsprung mass, the middle unsprung mass and the rear unsprung mass. These models are described below.

B-1 The Vehicle Body

The vehicle body or hull is shown in Figure B-1. It is acted upon by horizontal and vertical forces from the front suspension, bogie convection and frame mounted stops as shown. The forces are assumed to act in the horizontal and vertical directions in an inertial frame of reference, and not in the vehicle reference frame.

Two variables, incremental vertical displacement of the hull CG (Y_o), measured from initial equilibrium condition, and the hull pitch angle (Θ) defines the position of the hull at any instant.

The equations of motion about the CG are as follows.

$$M_h \ddot{Y}_o = - M_h g + 2 (F_{y2} + F_{y34} + F_{fs} + F_{bs}) \quad (1)$$

$$\begin{aligned} I_h \ddot{\Theta} = & 2 F_{y34} [L_3 \cos \Theta + (S_{34} + GG) \sin \Theta] \\ & + 2 F_{fs} [(L_3 - S_{fs}) \cos \Theta + GG \sin \Theta] \\ & + 2 F_{bs} [(L_3 + S_{bs}) \cos \Theta + GG \sin \Theta] \\ & + 2 F_{x34} [(S_{34} + GG) \cos \Theta - L_3 \sin \Theta] \\ & - 2 F_{y2} (L_2 \cos \Theta - GG \sin \Theta) - F_{x2} (L_2 \sin \Theta + GG \cos \Theta) \quad (2) \end{aligned}$$

Table B-1. Conversion of General Tire Variables to the Vehicle Model Variables

General Tire Variable	Vehicle Model Variables		
	Front Tires	Middle Tires	Rear Tires
F_y	F_{y2}	F_{sy3}	F_{sy4}
F_x	F_{x2}	F_{sx3}	F_{sx4}
F_v	F_{v2}	$F_{v3/2}$	$F_{v4/2}$
F_h	F_{h2}	$F_{h3/2}$	$F_{h4/2}$
m	M_2	M_3	M_4
y_1	Y_{w2}	Y_{w3}	Y_{w4}

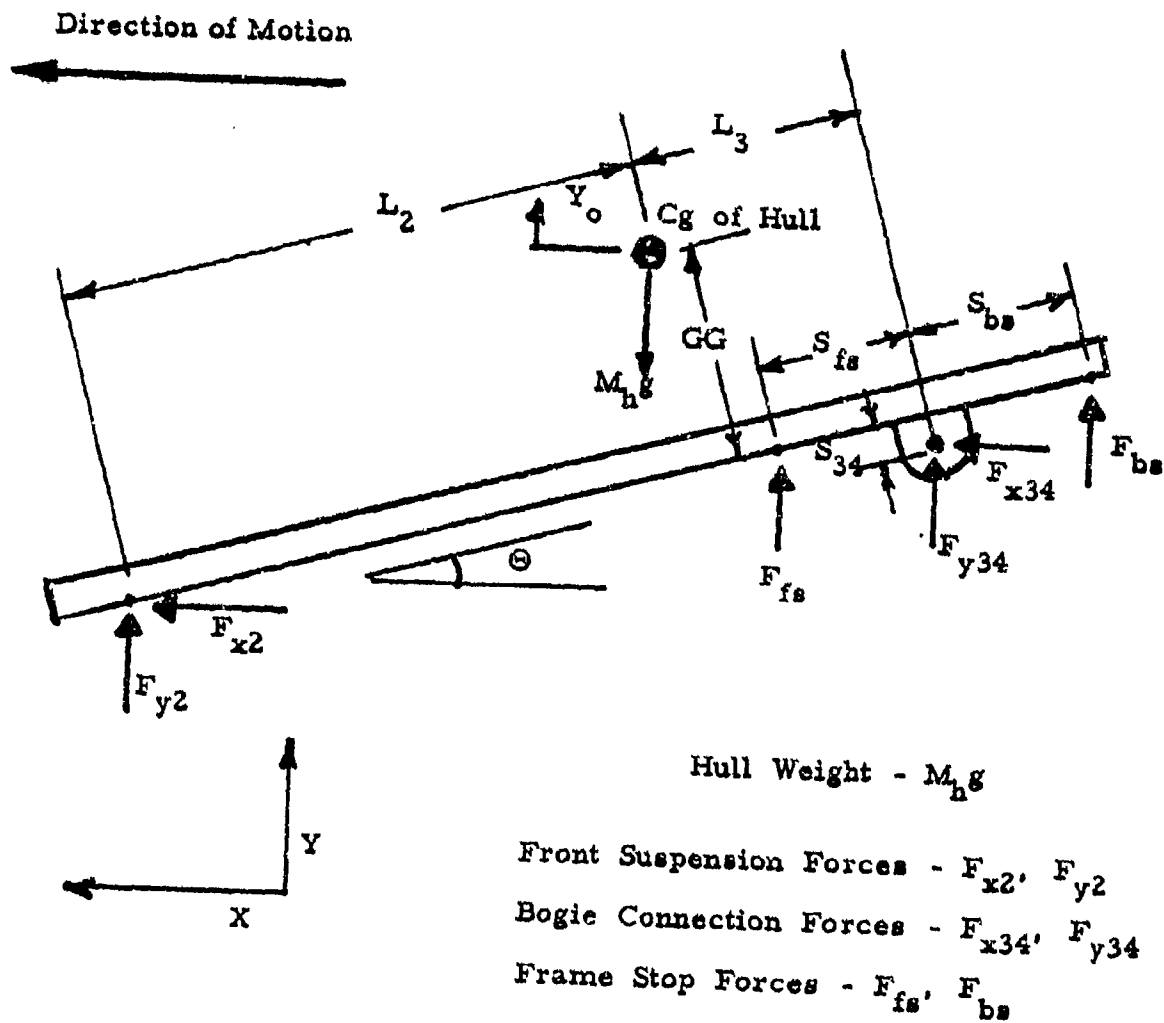


Figure B-1. Freebody Diagram of Hull

The factor of 2 in the above equations appears because identical forces act on the right and left side of the vehicle, and the forces shown in Figure B-1 (except the weight) are for one side only.

B-2 Bogie

The bogie is pivoted to the hull, so that it can rotate relative to the hull. The bogie-hull connection is considered to be a frictionless pin-joint, transmitting only forces and no torques.

The bogie mass and inertia includes those of the leaf springs and pivot. The middle and rear axle masses are included in the unsprung mass, and not in the bogie mass.

The freebody diagram (inertial reference frame) of the bogie is shown in Figure B-2.

The variables which define the bogie position are the vertical displacement of the bogie CG measured from the initial equilibrium condition, (Y_b), and the bogie pitch angle (ϕ). The equations of motion for vertical motions and rotation about the CG are

$$M_b \ddot{Y}_b = - M_b g + 2 (F_{sy3} + F_{sy4} - F_{y34}) \quad (3)$$

$$I_b \ddot{\phi} = 2 (F_{sy4} a \cos \phi + F_{sx4} a \sin \phi + F_{y34} S_b \sin \phi - F_{x34} S_b \cos \phi - F_{sy3} a \cos \phi - F_{sx3} a \sin \phi) \quad (4)$$

From a horizontal force balance,

$$F_{x34} = F_{sx3} + F_{sx4} \quad (5)$$

Because the bogie pivot is attached to the hull, the bogie CG acceleration (\ddot{Y}_b) can be expressed in terms of \ddot{Y}_o , $\ddot{\Theta}$ and $\ddot{\phi}$. From Figure B-3,

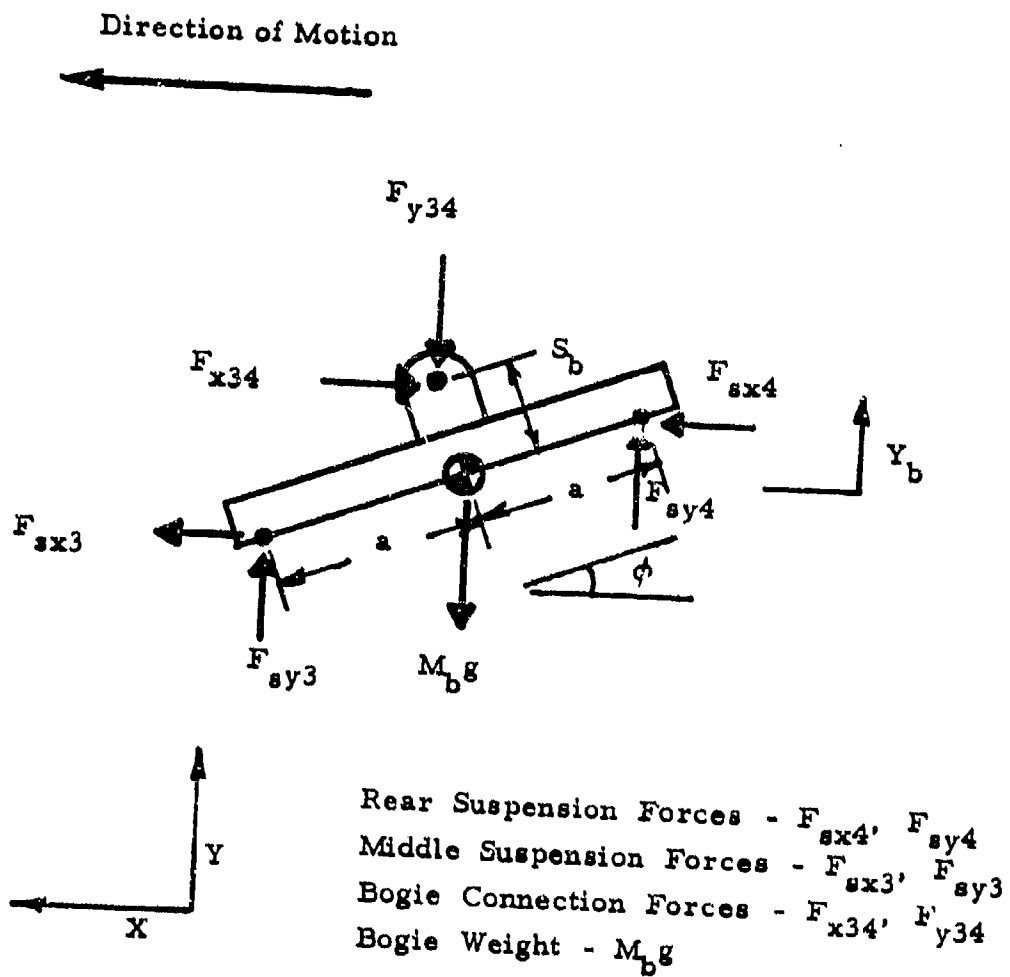


Figure B-2. Freebody Diagram of Bogie

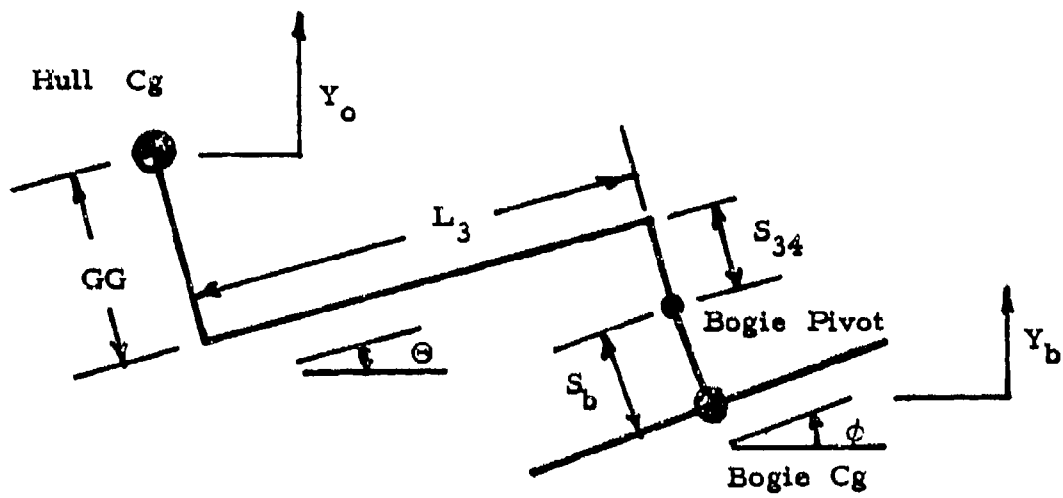


Figure B-3. Hull-Bogie Linkage

$$Y_b = Y_o + L_3 \sin \Theta (GG + S_{34}) (1 - \cos \Theta) + S_b (1 - \cos \phi) \quad (6)$$

Differentiating Equation (6) twice

$$\begin{aligned} \ddot{Y}_b &= \ddot{Y}_o + L_3 (-\dot{\Theta}^2 \sin \Theta + \ddot{\Theta} \cos \Theta) \\ &+ (S_{34} + GG) (\dot{\Theta}^2 \cos \Theta + \ddot{\Theta} \sin \Theta) \\ &+ S_b (\dot{\phi}^2 \cos \phi + \ddot{\phi} \sin \phi) \end{aligned} \quad (7)$$

The bogie force F_{y34} can be determined by solving Equations (1) to (4) along with Equation (7) simultaneously. This gives

$$F_{y34} = \frac{\left(\frac{2XD}{M_b} - \frac{XA}{M_h} - \frac{2XG \cdot XC}{L_h} - \frac{2XH \cdot XF}{L_b} - XI \right)}{\left(\frac{2XG \cdot XB}{L_h} + \frac{2XH \cdot XE}{L_b} + \frac{2}{M_h} + \frac{2}{M_b} \right)} \quad (8)$$

where

$$XA = -M_h g + 2(F_{y2} + F_{fs} + F_{bs})$$

$$XB = L_3 \cos \Theta + (S_{34} + GG) \sin \Theta$$

$$XC = F_{fs} [(L_3 - S_{fs}) \cos \Theta + GG \sin \Theta] + F_{bs}$$

$$\begin{aligned} &[(L_3 + S_{bs}) \cos \Theta + GG \sin \Theta] - F_{x34} [(S_{34} + GG) \cos \Theta \\ &- L_3 \sin \Theta] - F_{y2} (L_2 \cos \Theta - GG \sin \Theta) - F_{x2} \end{aligned}$$

$$(L_2 \sin \Theta + GG \cos \Theta)$$

$$\begin{aligned}
XD &= F_{sy3} + F_{sy4} - \frac{M_b}{2} g \\
XE &= S_b \sin \phi \\
XF &= F_{sy4} a \cos \phi + F_{sx4} a \sin \phi - F_{x34} S_b \cos \phi \\
&\quad - F_{sy3} a \cos \phi - F_{sx3} a \sin \phi \\
XG &= L_3 \cos \Theta + S_{34} \sin \Theta + GG \sin \Theta \\
XH &= S_b \sin \phi \\
XI &= -L_3 \dot{\Theta}^2 \sin \Theta + S_{34} \dot{\Theta}^2 \cos \Theta + S_b \dot{\phi}^2 \cos \phi \\
&\quad + GG \dot{\Theta}^2 \cos \Theta
\end{aligned}$$

B-3 The Suspension

There are two pairs of leaf springs connecting the chassis to the axles. The front pair support the front axle, and along with shock absorbers form the front suspension. The rear leaf springs support the middle and the rear axles and form the middle and the rear suspensions. There are no shock absorbers in the middle and rear suspensions. The suspension spring and damping characteristics are shown in Figure 4.

B-3.1 The Front Suspension

The front suspension, shown schematically in Figure B-4, consists of the leaf spring, modelled as a linear spring with elastic stops in parallel with dry friction damping, and a shock absorber. The forces on the suspension are as follows:

$$F_{y2} = F_{k2} + F_{b2f} + F_{b2v} + F_{stop 2} \quad (9)$$

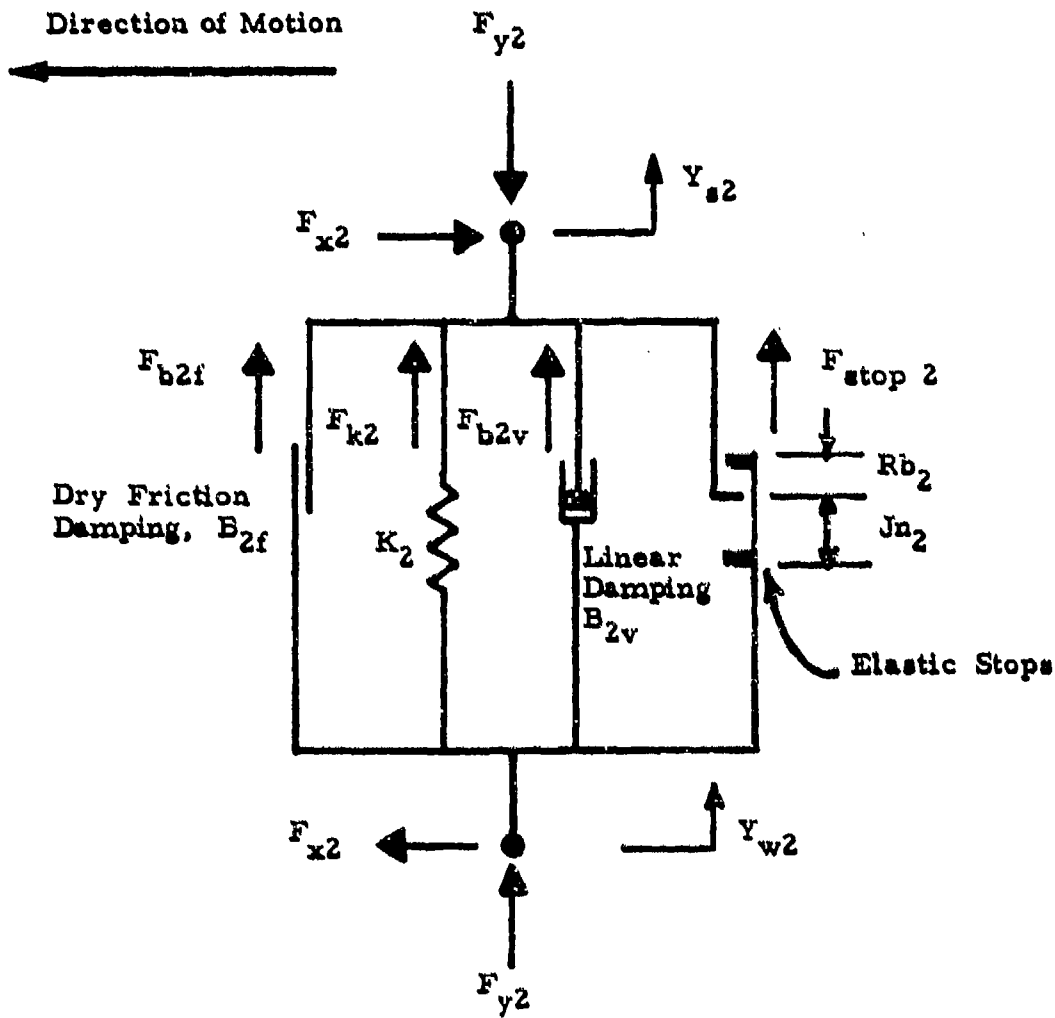


Figure R-4. Freebody Diagram of Front Suspension

F_{k2} - spring shiffness force

$$F_{k2} = K_2 \delta_2 \quad (10)$$

where

$$\delta_2 = Y_{sp2} + Y_{w2} - Y_{s2} \quad (11)$$

Y_{sp2} - equilibrium suspension displacement

$$Y_{sp2} = \frac{M_h g L_3}{2 K_2 (L_2 + L_3)} \quad (12)$$

$$Y_{s2} = Y_o - L_2 \sin \Theta \quad (13)$$

F_{b2f} - dry friction force

$$F_{b2f} = F_{rsf} K_2 |Y_{w2} - Y_{s2}| \frac{\dot{\delta}_2}{|\dot{\delta}_2|} \quad (14)$$

where

F_{rsf} - dry friction factor

(assumed to be 0.05)

$$\dot{\delta}_2 = \dot{Y}_{w2} - \dot{Y}_{s2} \quad (15)$$

$$\dot{Y}_{s2} = \dot{Y}_o - L_2 \cos \Theta \dot{\Theta} \quad (16)$$

F_{b2v} - shock absorber force

$$F_{b2v} = B_{2v} \dot{\delta}_2 \quad (17)$$

where

$$B_{2v} = B_{2vj} \text{ for } \dot{\delta}_2 > 0$$

$$= B_{2vr} \text{ for } \dot{\delta}_2 \leq 0$$

$F_{\text{stop } 2}$ - stop force

$$F_{\text{stop } 2} = \begin{cases} (Y_{w2} - Y_{s2} - J_{n2}) nK_2; & Y_{w2} - Y_{s2} \geq J_{n2} \\ 0 & -Rb_2 < Y_{w2} - Y_{s2} < J_{n2} \\ -(Y_{s2} - Y_{w2} - Rb_2) nK_2; & Y_{s2} - Y_{w2} \geq Rb_2 \end{cases} \quad (18)$$

It should be noted that the dry friction force given by Equation (14) is approximate; a more advanced model requires simultaneous solution of several equations and has not been included in this initial formulation.

B-3.2 The Middle and Rear Suspensions

The middle and rear suspensions, formed by the bogie leaf springs are identical. Figure B-5 shows the schematic diagram of these suspensions.

For the middle suspension, the forces are

$$F_{sy3} = F_{k3} + F_{b3f} + F_{\text{stop } 3} \quad (19)$$

F_{k3} - spring stiffness force

$$F_{k3} = K_3 \delta_3 \quad (20)$$

where

$$\delta_3 = Y_{sp3} + Y_{w3} - Y_{s3} \quad (21)$$

Y_{sp3} - equilibrium suspension displacement

$$Y_{sp3} = \left(\frac{M_h g}{4} \cdot \frac{L_2}{(L_2 + L_3)} + \frac{M_h g}{4} \right) 1/K_3 \quad (22)$$

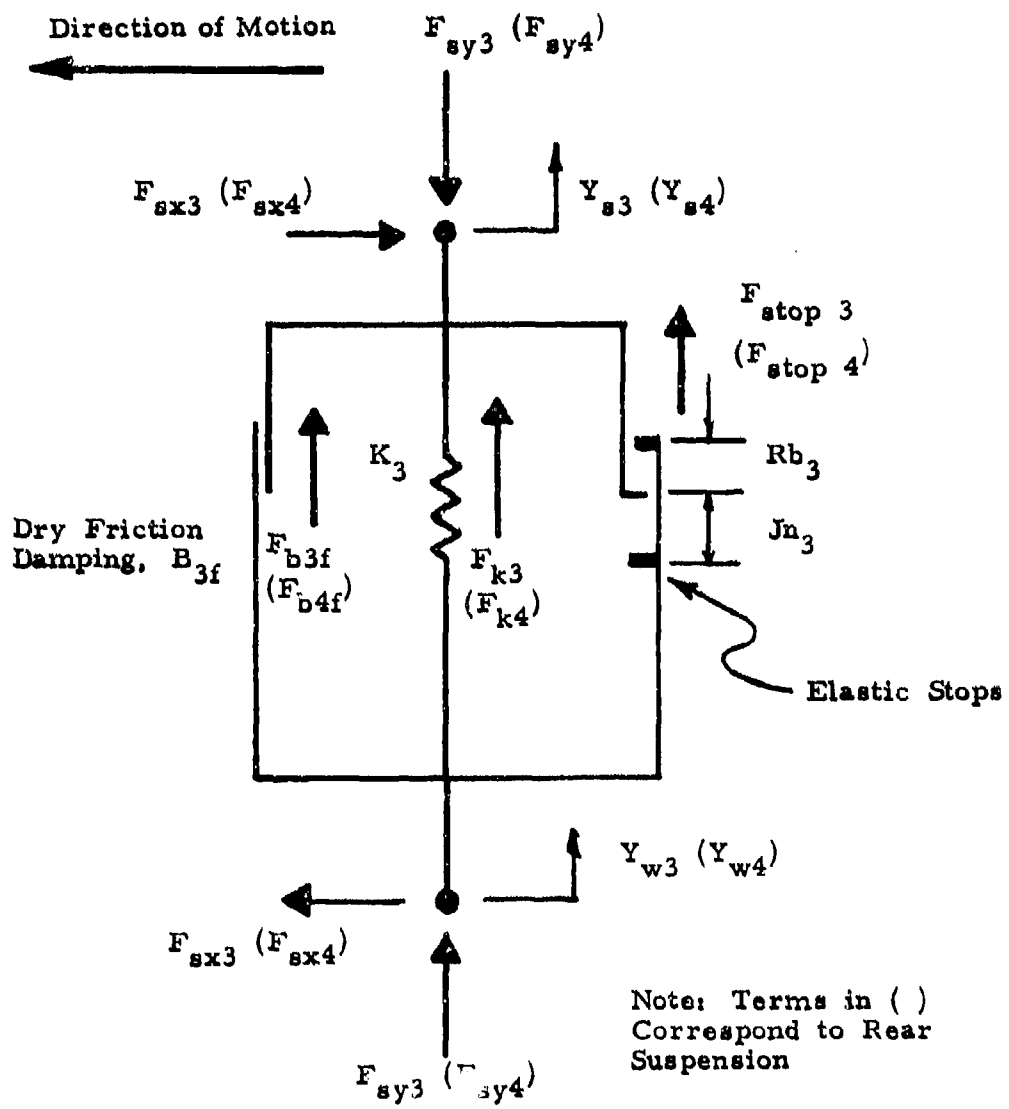


Figure B-5. Freebody Diagram for Middle and Rear Suspensions

$$Y_{s3} = Y_b - a \sin \phi \quad (23)$$

$$Y_b = Y_o + L_3 \sin \Theta + S_{34} (1 - \cos \Theta) + S_b (1 - \cos \phi) \quad (24)$$

F_{b3f} - dry friction force

$$F_{b3f} = F_{rsf} K_3 |Y_{w3} - Y_{s3}| \frac{(\dot{\delta}_3)}{|\dot{\delta}_3|} \quad (25)$$

where $\dot{\delta}_3 = \dot{Y}_{w3} - \dot{Y}_{s3} \quad (26)$

$$\dot{Y}_{s3} = \dot{Y}_b - a \cos \phi \dot{\phi} \quad (27)$$

$$\dot{Y}_b = \dot{Y}_o + L_3 \cos \Theta \dot{\Theta} \quad (28)$$

$$+ S_{34} \sin \Theta \dot{\Theta} + S_b \sin \phi \dot{\phi}$$

$F_{stop 3}$ - stop force

$$F_{stop 3} = \begin{cases} (Y_{w3} - Y_{s3} - Jn_3) nK_3; & Y_{w3} - Y_{s3} \geq Jn_3 \\ 0 & -Rb_3 < Y_{w3} - Y_{s3} < Jn_3 \\ -(Y_{s3} - Y_{w3} - Rb_3) nK_3; & Y_{s3} - Y_{w3} \geq Rb_3 \end{cases} \quad (29)$$

Similarly for the rear suspension, the forces are

$$F_{sy4} = F_{k4} + F_{b4f} + F_{stop 4} \quad (30)$$

$$F_{k4} = K_3 \delta_4 \quad (31)$$

$$\delta_4 = Y_{sp4} + Y_{w4} - Y_{s4} \quad (32)$$

$$Y_{sp4} = \left[\frac{M_b g L_2}{4(L_2 + L_3)} + \frac{M_b g}{4} \right] 1/K_3 \quad (33)$$

$$Y_{s4} = Y_b + a \sin \phi \quad (34)$$

$$F_{b4f} = F_{rsf} K_3 |Y_{w4} - Y_{s4}| \dot{\delta}_4 / |\dot{\delta}_4| \quad (35)$$

$$\dot{\delta}_4 = \dot{Y}_{w4} - \dot{Y}_{s4} \quad (36)$$

$$\dot{Y}_{s4} = \dot{Y}_b + a \cos \phi \dot{\phi} \quad (37)$$

$$F_{stop 4} = \begin{cases} (Y_{w4} - Y_{s4} - Jn_3) nK_3; & Y_{w4} - Y_{s4} \geq Jn_3 \\ 0 & -Rb_3 < Y_{w4} - Y_{s4} < Jn_3 \\ -(Y_{s4} - Y_{w4} - Rb_3) nK_3; & Y_{s4} - Y_{w4} \geq Rb_3 \end{cases} \quad (38)$$

B-4 The Unsprung Mass

The front unsprung mass (each side) consists of the mass of half the axle and one front tire, while the middle and the rear unsprung mass (each side) consist of the mass of half the axle and two tires (because the rear axles have dual tires).

B-4.1 Front Unsprung Mass

The free body diagram of the front unsprung mass is shown in Figure B-6(a). The equations of motion in the vertical and horizontal directions are

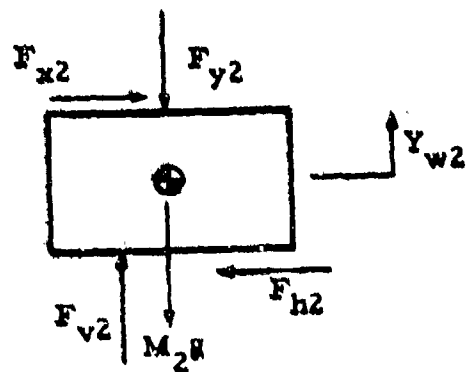
$$M_2 \ddot{Y}_{w2} = -M_2 g + F_{v2} - F_{y2} \quad (39)$$

$$F_{x2} = F_{h2} \quad (40)$$

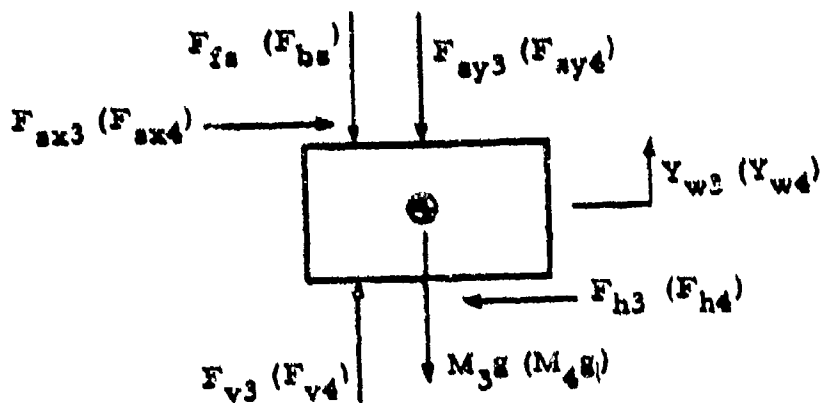
Tire Forces $\left\{ \begin{array}{l} F_{v2}, F_{v3}, F_{v4} \\ F_{h2}, F_{h3}, F_{h4} \end{array} \right.$

Suspension Forces $\left\{ \begin{array}{l} F_{x2}, F_{ax3}, F_{ax4} \\ F_{y2}, F_{ay3}, F_{ay4} \end{array} \right.$

Unsprung Weight M_2g, M_3g, M_4g



(a) Front Unsprung Mass



Note: Terms in () correspond to rear unsprung mass.

(b) Middle and Rear Unsprung Mass

Figure B-6. Freebody Diagram of Unsprung Mass

Acceleration terms are absent in Equation (40) because constant forward velocity has been assumed.

B-4.2 Middle and Rear Unsprung Mass

The free body diagram of the middle and rear unsprung mass is shown in Figure B-6(b).

The equations for the middle unsprung mass are:

$$M_3 \ddot{Y}_{w3} = -M_3 g + F_{v3} - F_{sy3} - F_{fs} \quad (41)$$

$$F_{sx3} = F_{h3} \quad (42)$$

Similarly the equations for the rear unsprung mass are

$$M_4 \ddot{Y}_{w4} = -M_4 g + F_{v4} - F_{sy4} - F_{bs} \quad (43)$$

$$F_{sx4} = F_{h4} \quad (44)$$

Stop forces F_{fs} and F_{bs} are determined as follows:

$$G_b = S_{bs} (\Theta - \phi) + St_{gap} - \delta_4 \quad (45)$$

$$G_f = S_{fs} (\Theta - \phi) + St_{gap} - \delta_3 \quad (46)$$

then

$$\begin{aligned} F_{fs} &= 0 & G_f &> 0 \\ &= -K_{stop} G_f K_3 & 0 &\leq G_f \leq h_s \\ &= -H_{stop} (G_f + h_s) K_3 + K_{stop} K_3 h_s & G_f &> h_s \end{aligned} \quad (47)$$

$$\begin{aligned} F_{bs} &= 0 & G_b &> 0 \\ &= -K_{stop} G_b K_3 & 0 &\leq G_b \leq h_s \\ &= -H_{stop} (G_b + h_s) K_3 + K_{stop} K_3 h_s & G_b &> h_s \end{aligned} \quad (48)$$

Where K_{stop} is the stop stiffness factor for bogie-stop and h_{stop} is the stop stiffness factor for bogie-hull

APPENDIX C

VEHICLE RESPONSE PLOTS

A complete set of PSDs of vehicle response obtained from the M-809 truck simulation are shown in Figures C-1 to C-10. The following symbols are keyed to the various curves.

Square	Point Contact Tire Model
Circle	Rigid Tread Band Tire Model
Triangle	Fixed Footprint Tire Model
Cross	Adaptive Footprint Tire Model

Power Spectral Densities of Vehicle Force, Motion and Acceleration for M-809 Truck (Speed - 18 mph, Terrain Roughness - 1"rms)

Cg Acceleration	C-1
Front Axle Acceleration	C-2
Rear Axle Acceleration	C-3
Front Axle Displacement	C-4
Middle Axle Displacement	C-5
Rear Axle Displacement	C-6
Vertical Tire Force (Front)	C-7
Vertical Tire Force (Rear)	C-8
Fore-and-aft Tire Force (Front)	C-9
Fore-and-aft Tire Force (Rear)	C-10

CG ACCLN

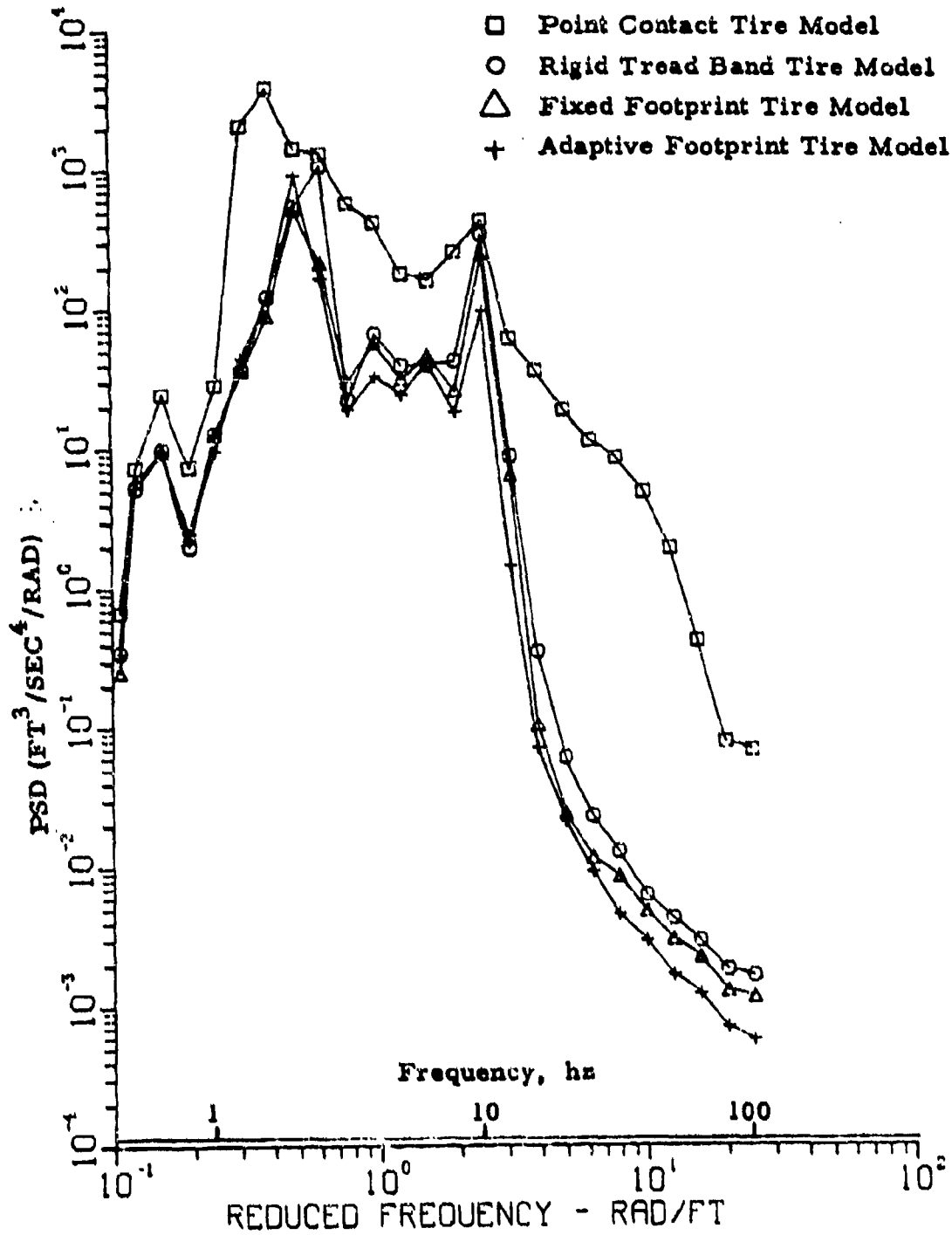


Figure C-1. Simulated Response - CG Acceleration

FRONT AXLE ACCLN

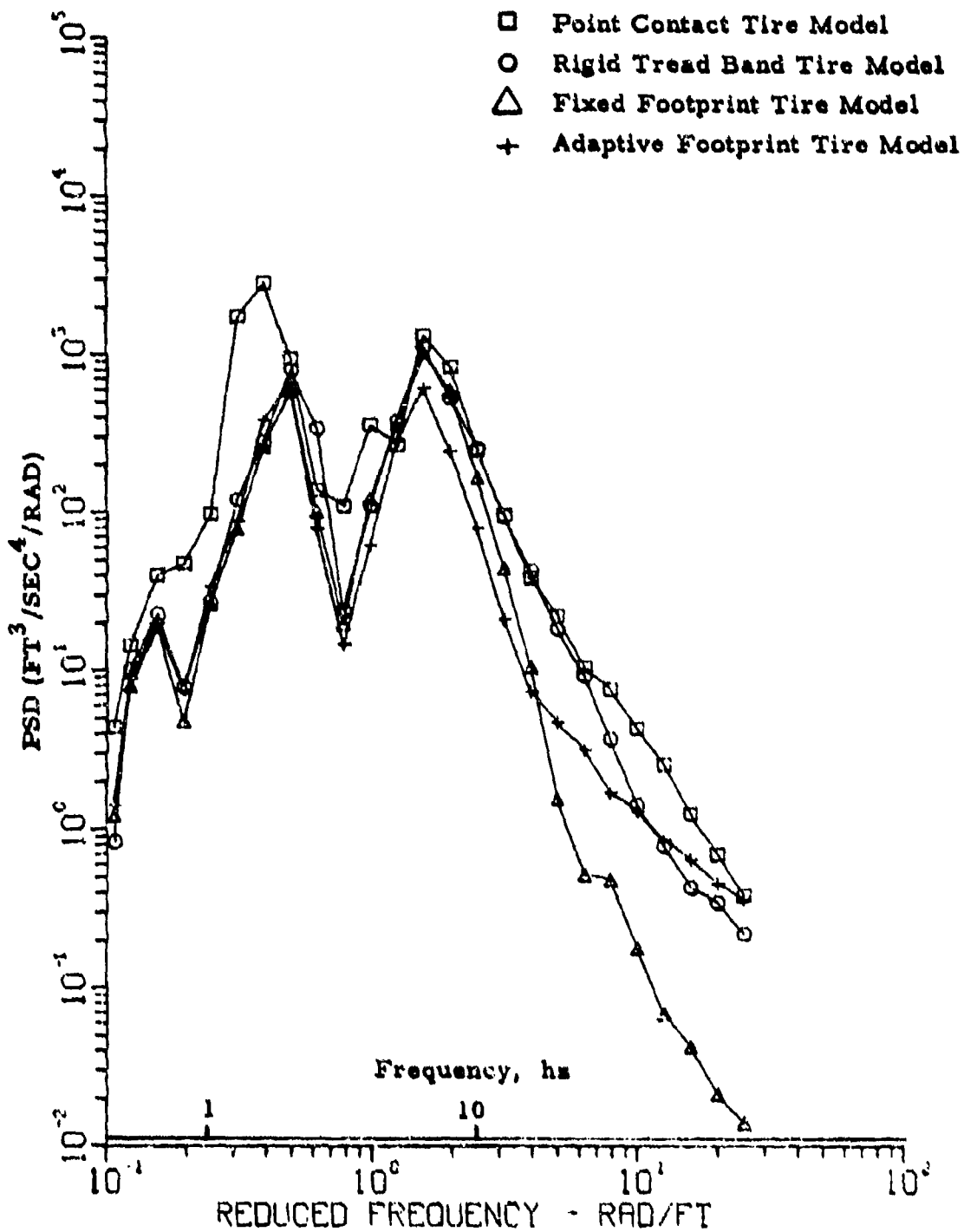


Figure C-2. Simulated Response - Front Wheel Acceleration

REAR AXLE ACCLN

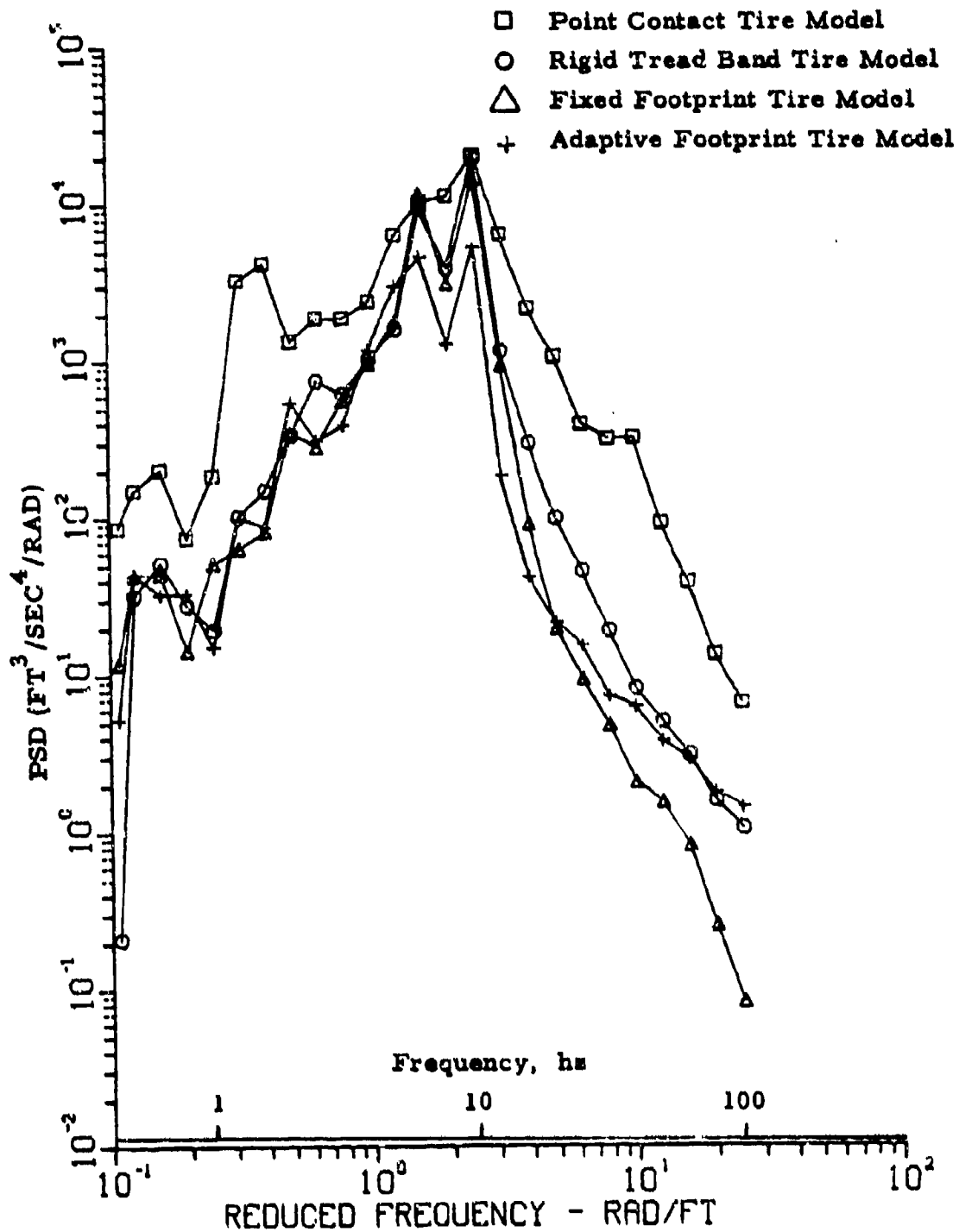


Figure C-3. Simulated Response - Rear Wheel Acceleration

FRONT AXLE DISPLN

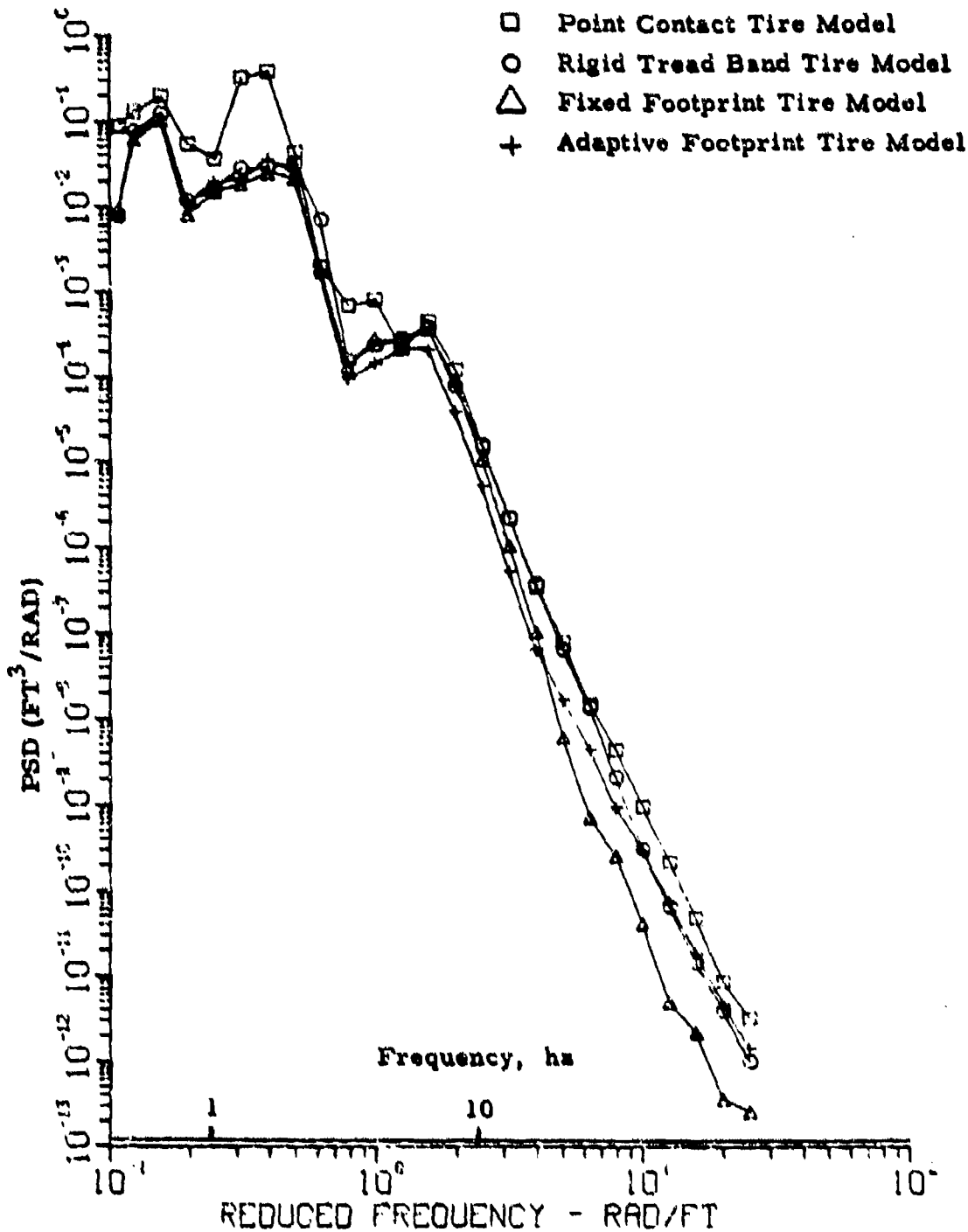


Figure C-4. Simulated Response - Front Wheel Displacement

MIDDLE AXLE DISPLN

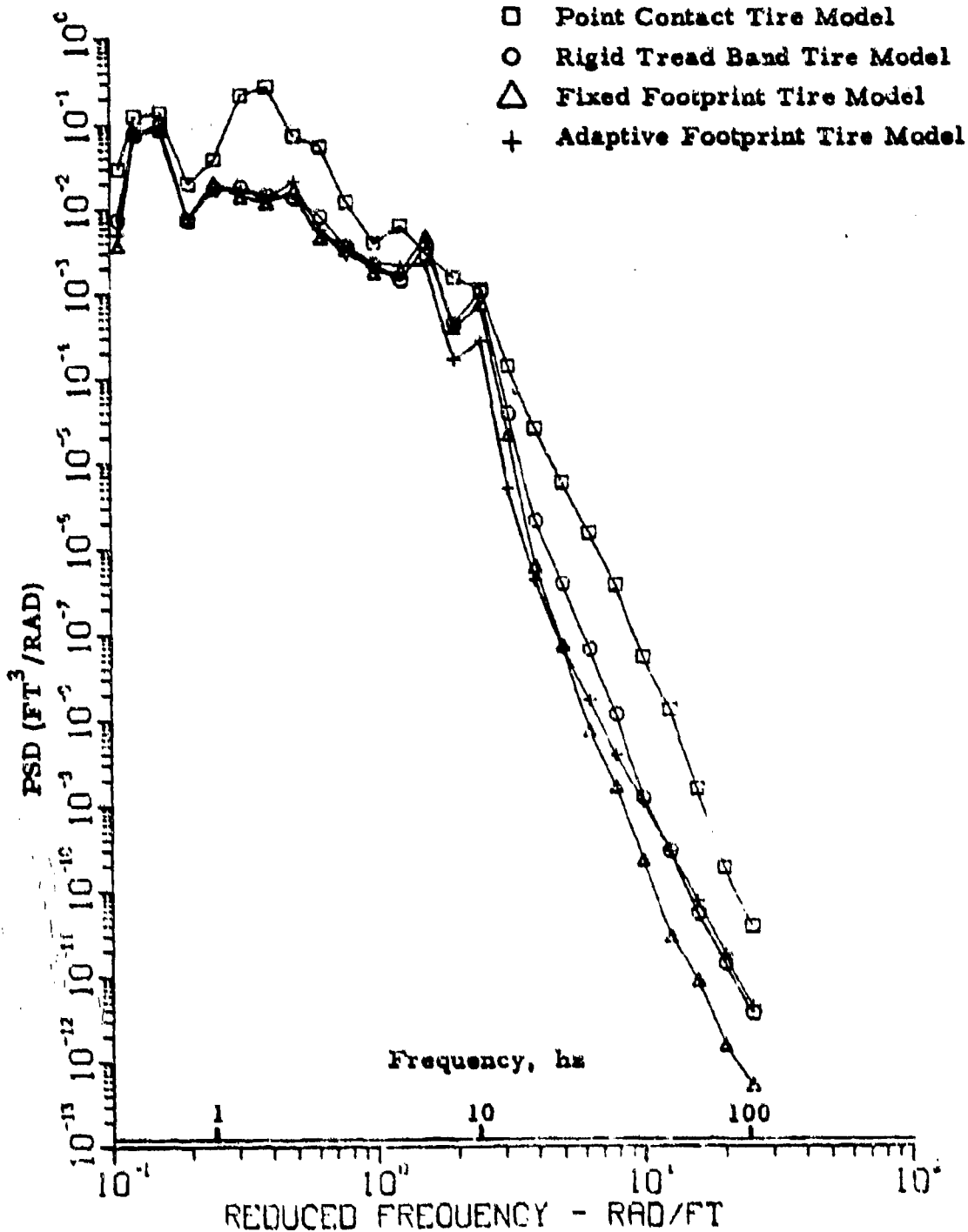


Figure C-5. Simulated Response - Middle Wheel Displacement

REAR AXLE DISPLN

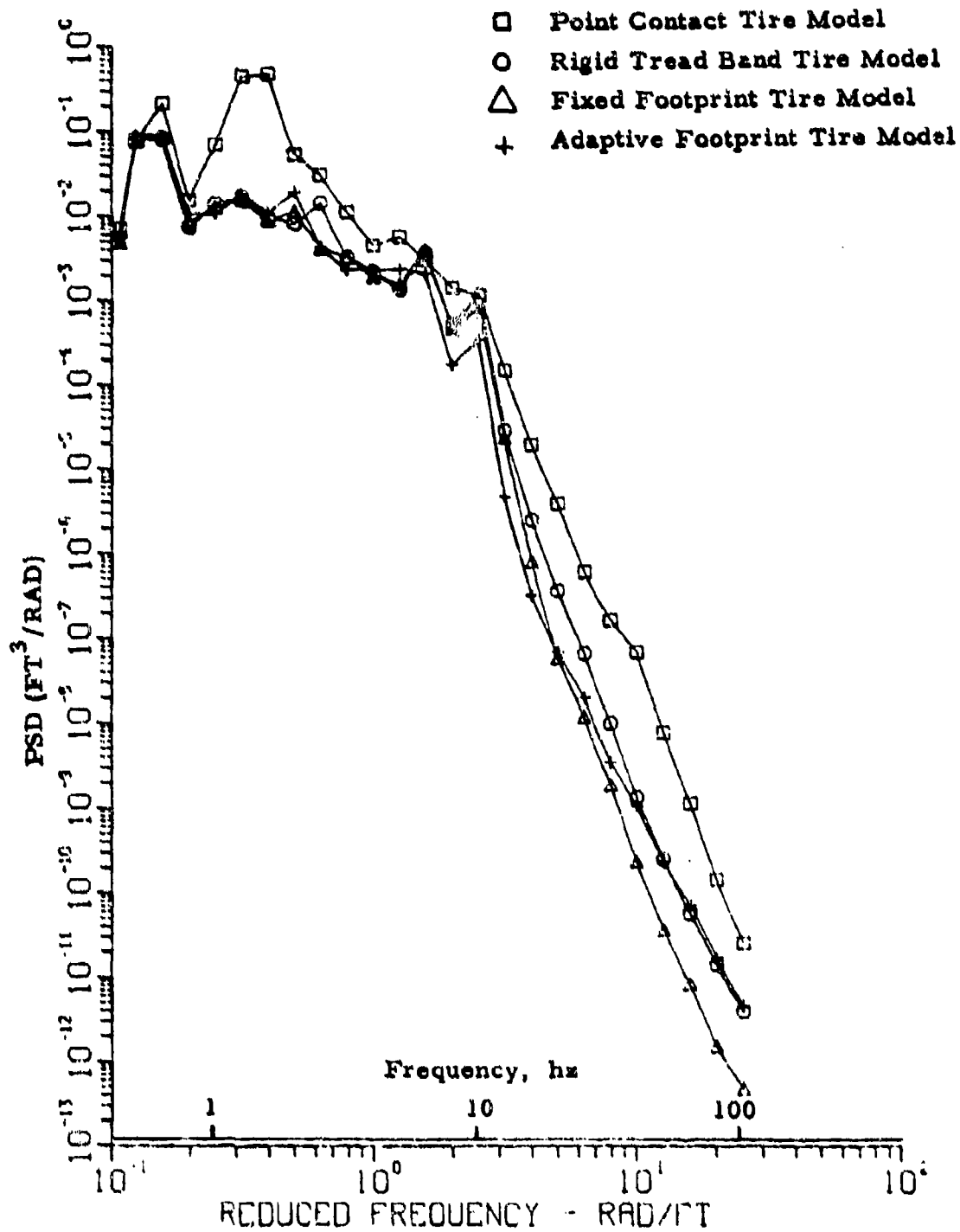


Figure C-6. Simulated Response - Rear Wheel Displacement

FRONT TIRE FORCE (VERTICAL)

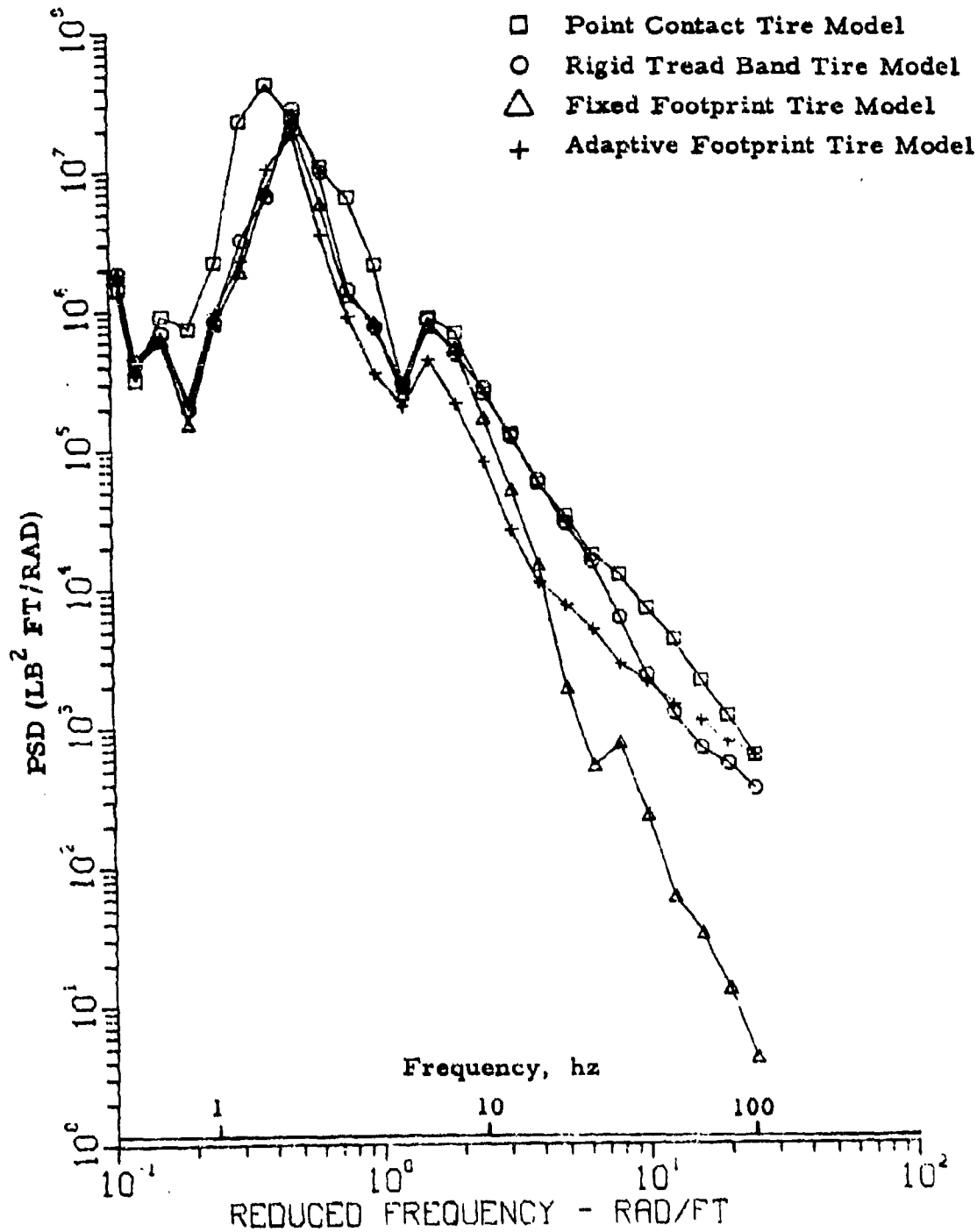


Figure C-7. Simulated Response - Vertical Tire Force (Front)

REAR TIRE FORCE (VERTICAL)

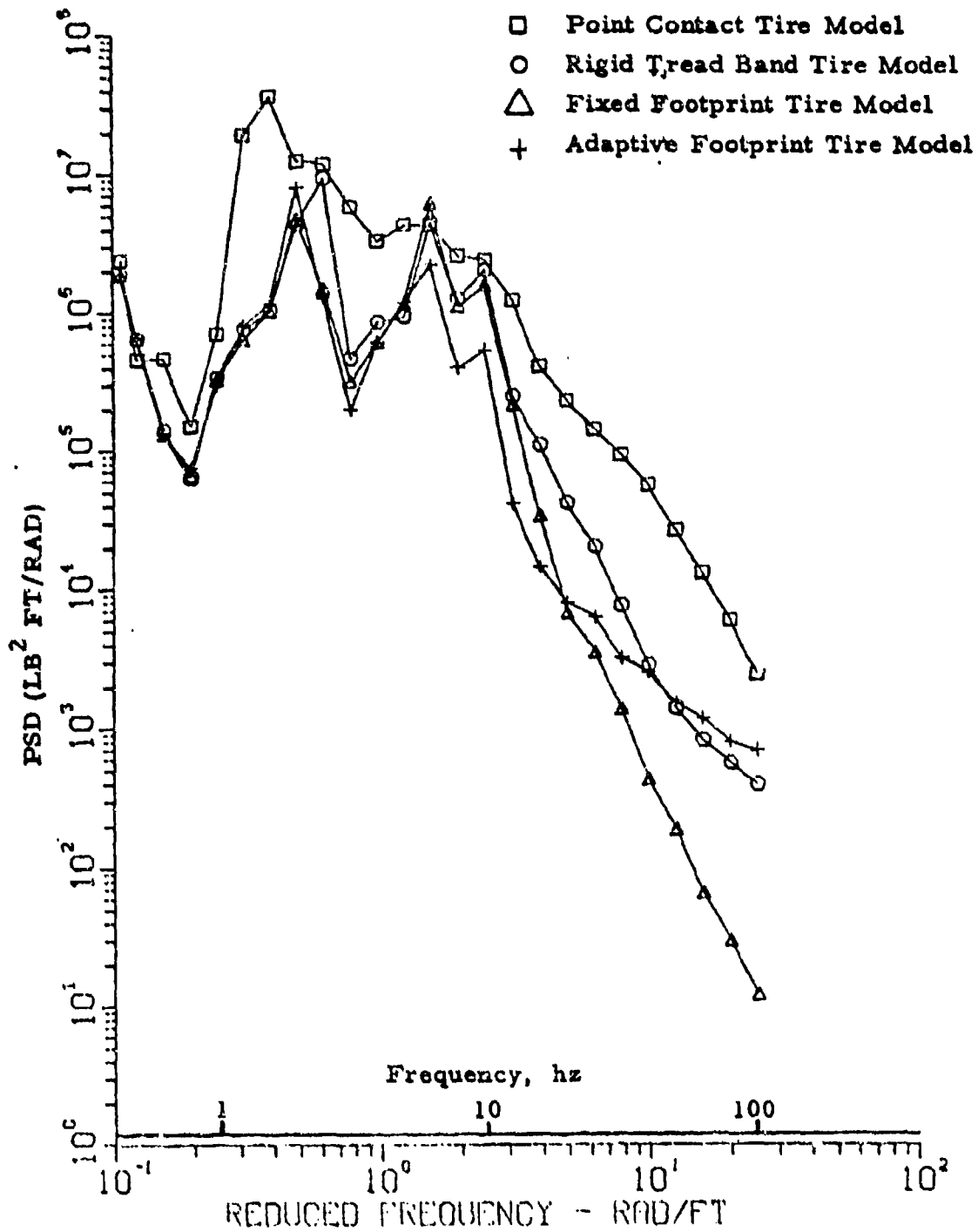


Figure C-8. Simulated Response - Vertical Tire Force (Rear)

FRONT TIRE FORCE (FORE-AND-AFT)

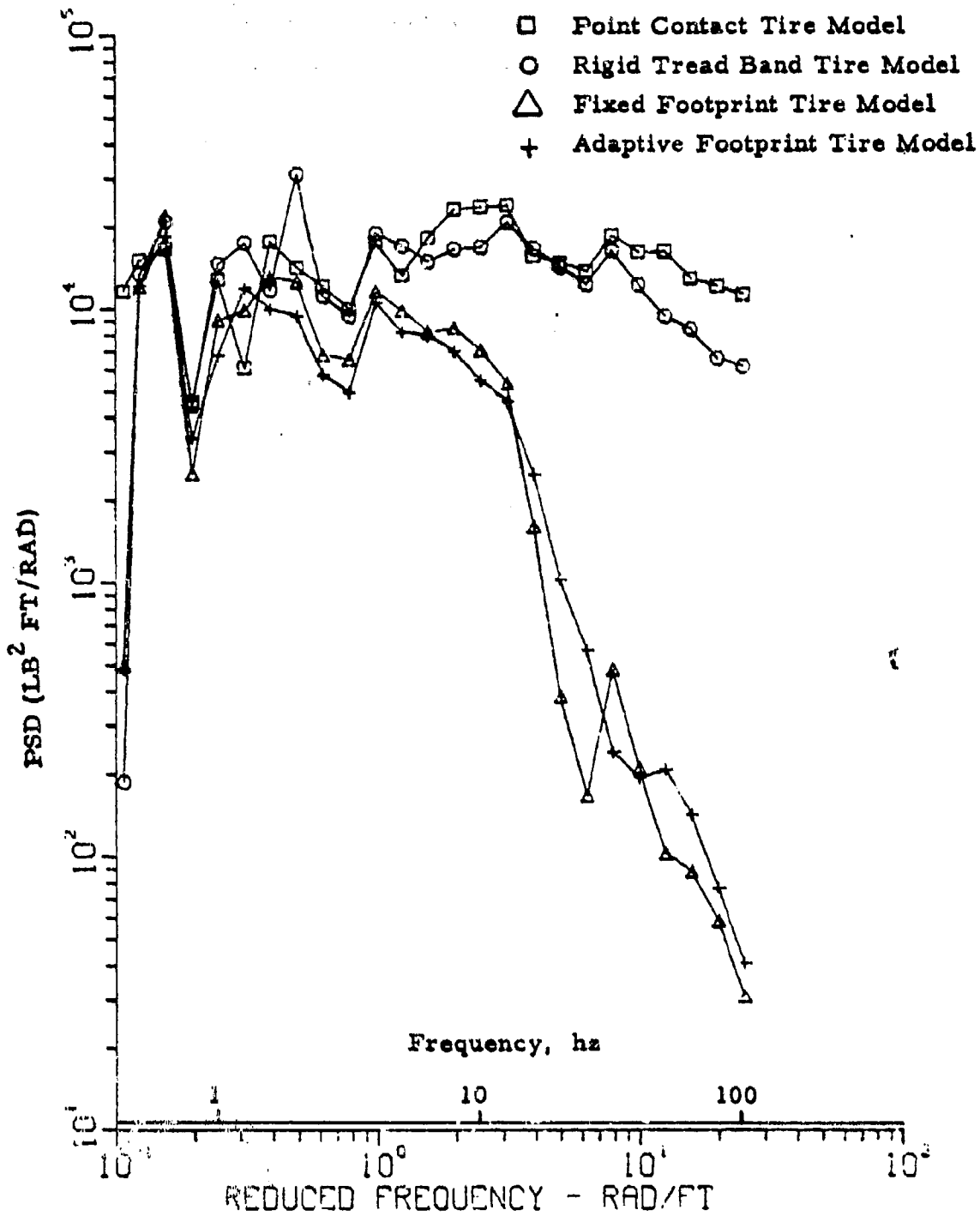


Figure C-9. Simulated Response - Fore-and-Aft Tire Force (Front)

REAR TIRE FORCE (FORE-AND-AFT)

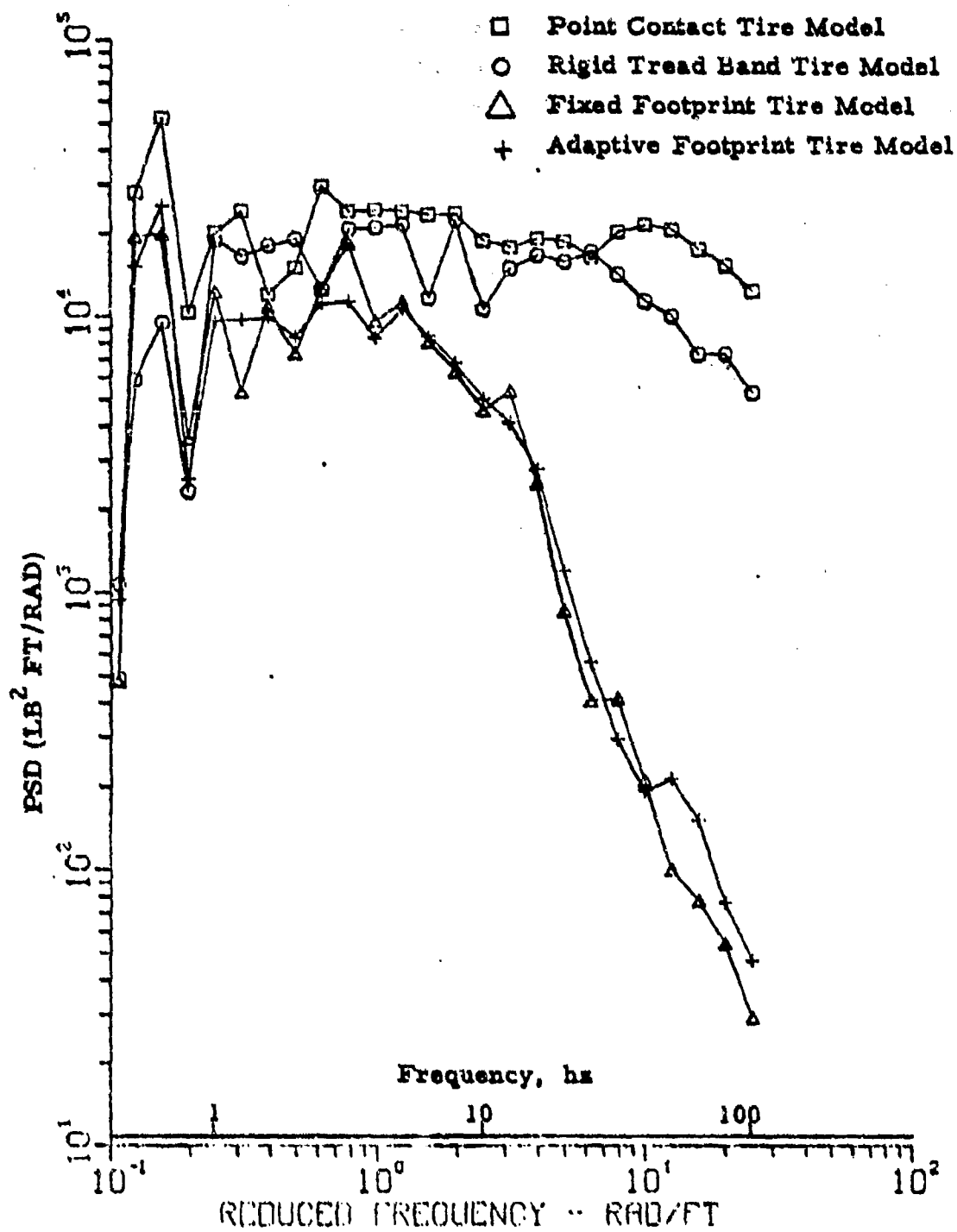


Figure C-10. Simulated Response - Fore-and-Aft Tire Force (Rear)

REFERENCES

1. Grant, J. W., "MB17 5-Ton 6 x 6 Dump Truck, Laboratory Road Simulator Test," Technical Report No. 11430, Mobility Systems Laboratory, USATACOM, Warren, Michigan, October 1971.
2. Captain, K. M., Wormley, D. N. and Grande, E., "The Development and Comparative Evaluation of Analytical Tire Models for Dynamic Vehicle Simulation," Technical Report No. 11877, Mobility Systems Laboratory, USATACOM, Warren, Michigan, May 1974.
3. Unpublished Data, USATACOM, Warren. Michigan
4. Boghani, A. B., and Fish, R. B., "Recorded Simulation Control Scheme : User's Manual, Volume II", Technical Report No. 12347, TARADCOM R&D Laboratory, Warren, MI January 1978.

DISTRIBUTION LIST

	<u>No. of Copies</u>
Commander	
U.S. Army Tank-Automotive Research and Development Command	
ATTN: Chief Scientist, DRDTA-NS	1
Dir, TASL, DRDTA-R	1
Dir, TAFL, DRDTA-Z	1
Foreign Intelligence Office, DRDTA-NF	1
Technical Library, DRDTA-UL	2
Simulation & Technology Exchange Office, DRDTA-RR	1
Computer Simulation & Test Methodology Func, DRDTA-RRS	10
Tactical Sys Div, DRDTA-RT	1
Combat Sys Div, DRDTA-RC	1
Track & Suspension Sub-Func, DRDTA-RCKT	1
Project Manager, Improved Tow Vehicle, DRCPM-ITV	1
Armored Combat Vehicle Tech, DRDTA-CVT	1
Warren, MI 48090	
U.S. Army Tank-Automotive Material Readiness Command	
ATTN: Commanding General, DRSTA-CG	1
Project Manager, Fighting Vehicle Sys, DRCPM-FVS	1
Project Manager, M-60 Tank Dev, DRCPM-MGOTD	1
Project Manager, XM1 Tank System, DRCPM-GCM	1
Federal Republic of Germany Liaison Office, FRG-LNO	1
Product Manager, M113/M113A1, Family of Vehicles, DRCPM-M113	1
Directorate for Weapons Sys Management, DRSTA-W	1
Product Manager, Heavy Equipment Transporter Sys, DRCPM-HT	1
Product Manager, 1 1/4 Ton Commercial Truck Sys, XM880, DRCPM-CT	1
U.S. Marine Corps Liaison Office, USMC-LNO	1
Canadian Forces Liaison Office, CDLS-(D)	1
Warren, MI 48090	

	<u>No. of Copies</u>
Commanding Officer U.S. Army Foreign Science & Technical Center Munitions Building, AMSTA-CR-ME Washington, DC 20315	1
Commander U.S. Army Materiel Development & Readiness Command ATTN: DRCRD-DN-G 5001 Eisenhower Avenue Alexandria, VA 22333	2
Commander Defense Documentation Center Cameron Station Alexandria, VA 22314	10
Harry Diamond Laboratories ATTN: Technical Reports Group Washington, DC 21438	1
U.S. Naval Civil Engineer Research & Engineering Lab Construction Battalion Center Port Hueneme, CA 93041	1
Commanding General U.S. Army Test and Evaluation Command Aberdeen Proving Ground, MD 21005	2
Commanding Officer Yuma Proving Ground ATTN: STEYP-TE Yuma, AZ 85364	2
Commander National Defense Headquarters ATTN: Scientific Advisor Ottawa, Ontario Canada KIA 0K2	1
Naval Research Office Washington, DC 20390	1

	<u>No. of Copies</u>
Superintendent U.S. Military Academy ATTN: Professor of Ordnance West Point, NY 10996	3
Superintendent U.S. Naval Academy Annapolis, MD 21402	1
U.S. Army Natick Laboratories Technical Library Natick, MA 01760	1
U.S. Army Deputy Chief of Staff for Operations Washington, DC 20310	2
National Tillage Machinery Laboratory U.S. Department of Agriculture Auburn, AL 36830	1
Commander Naval Ship Systems Command PHS 384-2, DWA Washington, DC 20360	1
Commanding General U.S. Army Engineer Research and Development Center Fort Belvoir, VA 22060	1
President U.S. Army Armor Board Fort Knox, KY 40121	1
President U.S. Army Artillery Board Fort Sill, OK 73503	1
President U.S. Army Infantry Board Fort Benning, GA 31905	1

	<u>No. of Copies</u>
President U.S. Army Airborne Electronic and Special Warfare Board Fort Bragg, NC 26307	1
President U.S. Army Arctic Test Center APO Seattle, WA 98733	1
President U.S. Army Maintenance Board Fort Knox, KY 40121	1
Commanding General U.S. Marine Corps Landing Forces Development Center Quantico, VA 22134	2
Commanding General Headquarters USARAL ATTN: ARAOD Seattle, WA 98749	2
Commanding General U.S. Army Supply and Maintenance Command ATTN: AMSSM-MR Washington, DC 20310	1
Commanding General U.S. Army Alaska APO 409 Seattle, WA 98749	1
Office, Chief of Research & Development Department of the Army Washington, DC 20310	2
U.S. Army Deputy Chief of Staff for Logistics Washington, DC 20310	2

	<u>No. of Copies</u>
Commanding General U.S. Army Weapons Command ATTN: AMSWE Rock Island, IL 61201	1
Commandant of the Marines U.S. Marine Corps ATTN: AD-4H Washington, DC 20380	1
Commanding Officer U.S. Army Aviation Material Lab Fort Eustis, VA 23604	1
Commanding Officer U.S. Army General Equipment Test Activity ATTN: Transportation Logistics Test Dir Fort Lee, VA 23801	1
Commanding Officer ATTN: STEAP-TL Aberdeen Proving Ground, MD 21005	1
Commanding General U.S. Army Aviation School Office of the Librarian ATTN: AASPI-L Fort Rucker, AL 36360	1
Canadian Army Staff 2450 Massachusetts Avenue Washington, DC 20008	4
Commanding General Office of the Chief of Research and Development Department of the Army Washington, DC 20310	1
Director U.S. Army Engineer Waterways Experiment Station Corps of Engineers P.O. Box 631 Vicksburg, MS 39181	3

	<u>No. of Copies</u>
U.S. Navy Industrial College of the Armed Forces ATTN: Vice Deputy Commandant Washington, DC 20315	2
HQ Department of the Army Office, Director of Defense Res & Engr ATTN: OSD/ODDR&E, Dr. D. Charvonie Washington, DC 20301	1
HQ Department of the Army Deputy Chief of Staff for Research Development & Acquisition ATTN: DAMA-ARZ-E, Dr. C. Church DAMA-CSS, LTC Hadjis DAMA-CSZ, Dr. R. L. Haley Washington, DC 20310	1 1 1

Unclassified

SECURITY CLASSIFICATION OF THIS PAGE (When Data Entered)

REPORT DOCUMENTATION PAGE		HEAD INSTRUCTIONS BEFORE COMPLETING FORM
1. REPORT NUMBER 12347	2. AUTHOR(s) (Last, First, Middle Initial) (18) TARADCOM	3. REPORT TYPE AND PERIOD COVERED (19) TR-22347-VOL-2
4. TITLE (and Subtitle) (6) Shake Testing of Vehicles Through Recorded Simulation Control Scheme, Volume 1	5. TYPE OF REPORT & PERIOD COVERED Final Report (Sept 1976 through Feb 1978)	6. PERFORMING ORGANIZATION NUMBER (17) DTAC-76224-VOL-2
7. AUTHOR(s) (10) A. B. Boghani K. M. Captain R. B. Fish	8. PERFORMING ORGANIZATION NAME AND ADDRESS Foster-Miller Associates, Inc. 135 Second Avenue Waltham, MA 02154	9. CONTRACT OR GRANT NUMBER(s) (5) DAAK30-76-C-0004
11. CONTROLLING OFFICE NAME AND ADDRESS U.S. Army Tank Automotive Research & Development Command Attn: DRDTA-RR, Warren, MI 48090	10. PROGRAM ELEMENT, PROJECT, TASK AREA & WORK UNIT NUMBERS	12. REPORT DATE (11) January 78
14. MONITORING AGENCY NAME & ADDRESS (if different from Controlling Office) (12) Y Y 3 P	13. NUMBER OF PAGES 116	15. SECURITY CLASS. (of this report) Unclassified
16. DISTRIBUTION STATEMENT (of this Report) Approved for public release; distribution unlimited.	15a. DECLASSIFICATION/DOWNGRADING SCHEDULE	
17. DISTRIBUTION STATEMENT (of the abstract entered in Block 20, if different from Report) (9) Final Rept. Sep 76-Feb 78		
18. KEY WORDS (Continue on reverse side if necessary and identify by block number) Shake Testing Vehicle Simulation Tire Models		
20. ABSTRACT (Continue on reverse side if necessary and identify by block number) Recorded simulation control scheme described in this report is a method of providing realistic inputs to a vehicle shaker. The scheme involves generating axle displacement records by simulating motion of the vehicle operation on the specified terrain, storing the records in memory of a control system and using them to provide input signals to the vehicle shaker. to next page		(Continued)

Unclassified

SECURITY CLASSIFICATION OF THIS PAGE (When Data Entered)

A terrain-tire-vehicle model needed to simulate vehicle motion is developed. The vehicle selected for the model is a typical three axle military truck. The tires are represented by any of these independently developed models: point contact model, rigid tread band model, fixed footprint model and adaptive footprint model. A comparison of the analytical and the field test results demonstrates that the vehicle motion is adequately simulated, particularly when the adaptive footprint or the fixed footprint tire model is employed.

The control system developed for storing the axle displacement records and playing them back incorporates a minicomputer, disc memory and input-output peripherals. Spectral densities of the shaker input signals generated by the control system agree well with those obtained from the test results, thereby verifying ability of the recorded simulation control scheme.

Unclassified

SECURITY CLASSIFICATION OF THIS PAGE (When Data Entered)